GSBS Dissertations and Theses   Graduate School of Biomedical Sciences

2017-07-31

Regulation of Local Translation, Synaptic Plasticity, and Cognitive Function by CNOT7

Rhonda L. McFleder
University of Massachusetts Medical School

Let us know how access to this document benefits you.

Repository Citation

REGULATION OF LOCAL TRANSLATION, SYNAPTIC PLASTICITY, AND COGNITIVE FUNCTION BY CNOT7

A Dissertation Presented

By

Rhonda Leah McFleder

Submitted to the Faculty of the University of Massachusetts Graduate School of Biomedical Sciences, Worcester in partial fulfillment of the requirements for the degree of

DOCTOR OF PHILOSOPHY

July 31, 2017

Program in Molecular Medicine

ACKNOWLEDGEMENTS

This work would not have been made possible without the leadership and guidance I received from my mentor, Dr. Joel Richter. I was warned before joining Joel's lab that it would be "intense", however I accepted the challenge and feel I am stronger person and scientist because of it. Joel helped me grow a backbone, which not only assisted me in working with him, but also gave me the confidence to pursue things I am passionate about both in science and everyday life. I am thankful to have had the opportunity to train under such a terrific scientist, and look forward to us continuing to work together in the future. I would also like to thank the members of my TRAC committee: Dr. Andrew Tapper, Dr. Vivian Budnik, Dr. William Theurkauf, and Dr. Andrei Korostelev for their time, advice, and feedback over the past four years. I appreciate both Dr. Victor Ambros and Dr. Ray Kelleher III for stepping in when I needed them and taking the time to review my thesis and attend my defense.

I would especially like to thank Dr. Jihae Shin, who I had the pleasure of working with closely during my rotation and from whom I would always receive honest advice and necessary feedback. I would like to thank Drs. Lori Lorenz, Ki Young Paek, Botao Liu, Elisa Donnard, Huan Shu, Emily Stackpole, and Annie Hien for their technical expertise and for never turning me away when I asked them a question. I would like to thank Dr. Fernanda Mansur, who became my partner in crime this past year, and aided in publishing my research. Of course, I

must also acknowledge Dr. Maria Ivshina; without Maria the lab would surely shut down and I would have not accomplished anything.

In addition to the many people at UMass, I would like to thank my previous mentors Dr. Patricia Gearhart and Dr. Robert Maul. They helped me realize how much I truly enjoyed research and that it was something I needed to pursue. The RISE program in addition to my many mentors at UNCP including: Dr. Robert Poage and Dr. Meredith Storms, are responsible for initiating my love for science. I have had so many opportunities because of them, and I know without them I would have never made it to UMASS in the MD/PhD program.

I am nothing without my support system. In addition to all my amazing friends, I would like to thank my Mother, who is my personal cheerleader, and my Dad, who I look to as a role-model. They have always been there for me and supported me in all my endeavors. I would like to thank my three brothers for keeping me entertained all these years, and my sister for being my best friend. I should probably also thank my husband, Matthias McFleder, for following me to UMass, and reminding me there is more to life than CNOT7.

ABSTRACT

Local translation of mRNAs in dendrites is vital for synaptic plasticity and learning and memory. Tight regulation of this translation is key to preventing neurological disorders resulting from aberrant local translation. Here we find that CNOT7, the major deadenylase in eukaryotic cells, takes on the distinct role of regulating local translation in the hippocampus. Depletion of CNOT7 from cultured neurons affects the poly(A) state, localization, and translation of dendritic mRNAs while having little effect on the global neuronal mRNA population. Following synaptic activity, CNOT7 is rapidly degraded resulting in polyadenylation and a change in the localization of its target mRNAs. We find that this degradation of CNOT7 is essential for synaptic plasticity to occur as keeping CNOT7 levels high prevents these changes. This regulation of dendritic mRNAs by CNOT7 is necessary for normal neuronal function in vivo, as depletion of CNOT7 also disrupts learning and memory in mice. We utilized deep sequencing to identify the neuronal mRNAs whose poly(A) state is governed by CNOT7. Interestingly these mRNAs can be separated into two distinct populations: ones that gain a poly(A) tail following CNOT7 depletion and ones that surprisingly lose their poly(A) tail following CNOT7 depletion. These two populations are also distinct based on the lengths of their 3' UTRs and their codon usage, suggesting that these key features may dictate how CNOT7 acts on its target mRNAs. This work reveals a central role for CNOT7 in the hippocampus where it governs local translation and higher cognitive function.

TABLE OF CONTENTS

LIST OF TABLES

LIST OF FIGURES

LIST OF COPYRIGHTED MATERIAL

CHAPTER II is reprinted from a work submitted and accepted at *Cell Reports* (permission not required).

CHAPTER I

Introduction

Rhonda L. McFleder

Program in Molecular Medicine, University of Massachusetts Medical School,
Worcester, Ma 01605, USA

Local Translation and Memory

How does a single experience result in the long-lasting changes in the brain that we call memory? This question has consumed the lives of researchers for centuries, and answering it may be key to treating the numerous neurological disorders that disrupt this important process including Huntington's Disease (Butters et al., 1985), Dementia (Reisberg et al., 1982), and certain autistic disorders (Bennetto et al., 1996). Most of the work to address this question has focused on the synapse, the structure mediating communication between two different neurons. In response to stimulation, synapses can undergo modifications such as an increase or decrease in pre-synaptic inputs (Bailey and Chen, 1988a), increase in post-synaptic surface area (Bailey and Chen, 1988b), and increase or decrease in number of synaptic receptors present at the surface of membranes (Lee et al., 2000); which corresponds to altered synaptic efficacy (Bliss and Lomo, 1973). This unique capability of the synapse to change in response to different stimuli, termed synaptic plasticity, may aid in differentiating a "learned" synapse from the potentially thousands of other naïve synapses present on individual neurons (Martin et al., 1997).

The initial work elucidating synaptic plasticity was focused on synaptic changes in response to electrical stimuli (Bliss and Lomo, 1973); however, it was unclear if this process occurred physiologically. Subsequent studies have demonstrated that various types of learning elicit similar changes in a variety of

different model organisms including: Aplysia neurons (Bailey and Chen, 1988a), honeybees (Brandon and Coss, 1982), and mice (Clarke et al., 2010, Gruart et al., 2006, Whitlock et al., 2006, Matsuo et al., 2008, Mitsushima et al., 2011). In mice, a linear relationship between maintenance of synaptic plasticity and retention of memories has also been demonstrated (Doyere and Laroche, 1992), suggesting their formation and decay are intertwined mechanistically. These studies, among others, have led to the hypothesis that learning-induced changes at the synapse are the basis of memory formation, and therefore the molecular events underlying these changes would be crucial to the development of memory (Kandel, 2001a, Costa-Mattioli et al., 2009).

To understand the processes responsible for memory formation, researchers focused on the hippocampus, a region of the brain essential for several types of memory such as short-term, long-term, and spatial memory (Scoville and Milner, 1957). Injection of translation inhibitors directly into the hippocampus prior to different learning paradigms, demonstrated that certain types of long-term memory depend on protein synthesis (Bourtchouladze et al., 1998, Quevedo et al., 1999, Wanisch et al., 2005, Artinian et al., 2007, Rossato et al., 2007). This dependence on translation extends to long-term potentiation (LTP) and long-term depression (LTD), two types of synaptic plasticity that result in an increase or decrease, respectively, in synaptic efficacy (Stanton and Sarvey, 1984, Otani et al., 1989, Krug et al., 1984, Fazeli et al., 1993, Kauderer and Kandel, 2000). A hypothesis arose amidst these experiments, that perhaps

this translation was occurring locally at/or near synapses enabling new proteins to "tag" stimulated synapses differentiating them from their neighboring naïve synapse. Single cell assays focusing on the synapse between an Aplysia sensory neuron and a motor neuron, demonstrated that chemical stimulation results in translation-dependent plasticity at only the stimulated synapse and not neighboring synapses on the same cell. By applying the inhibitor locally, it became clear that this form of synaptic plasticity required local translation (Martin et al., 1997). Is this dependence on local translation also true in the intact hippocampus?

Kang and Schuman set out to answer this question by focusing on the well described CA1 region of the hippocampus; a region essential for several types of learning and memory in mice. In this study, the cell body-containing region (soma) of the CA1 hippocampus was mechanically separated from the neuropil, a region enriched with synapses (Figure 1.1). Brain-derived neurotrophic factor (BDNF)-induced synaptic plasticity could still be elicited in the synapses separated from their cell bodies, indicating that factors transported from the cell soma are not necessary. Moreover, application of a translation inhibitor abrogated this synaptic plasticity, suggesting that local translation is essential for at least this form of synaptic plasticity (Kang and Schuman, 1996). Subsequent studies have used similar approaches to confirm the dependence of other forms of synaptic plasticity such as LTP and metabotrophic glutamate receptor (mGluR)-dependent LTD on local translation. These studies have resulted in a

widely-accepted model that synaptic plasticity, and likely learning and memory, requires new protein synthesis locally at or near synapses (Huber et al., 2000, Bradshaw et al., 2003b, Sutton and Schuman, 2006b). Indeed, thousands of mRNAs localize to hippocampal dendrites or axons and code for protein products that could "tag" the synapse such as synaptic receptors, cytoskeleton proteins, and kinases (Poon et al., 2006, Cajigas et al., 2012). mRNAs are not alone as tRNAs, ribosomes, and components of the endoplasmic reticulum have also been identified in both dendrites at post-synaptic sites and axons at presynaptic sites (Steward and Levy, 1982, Tiedge and Brosius, 1996, Steward and Ribak, 1986, Koenig, 1979, Merianda et al., 2009). The presence of these components indicates a vast transcriptome localized to synapses, where they can be potentially translated at a moment's notice.

Translation Regulation
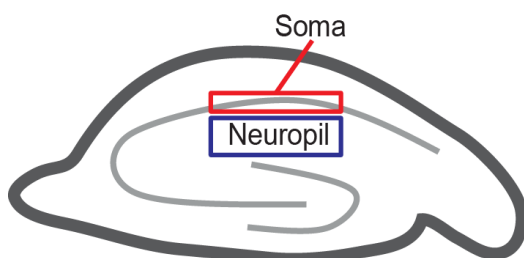
Figure 1.1 Diagram of the mouse hippocampus with the CA1 soma outlined in red and the CA1 neuropil outlined in blue.

Proper neuronal function appears to be hinged on tight regulation of protein synthesis, as mutations in known translational regulators underlie several neurological disorders (Kelleher and Bear, 2008). One well-known example is the Fragile X syndrome (FXS), the most common single gene cause of autism spectrum disorders (ASD). FXS results from a CGG repeat expansion in the

Fragile X Mental Retardation 1 gene (FMR1) and subsequent loss of the gene

product, Fragile X mental retardation Protein (FMRP) (Verkerk et al., 1991,

Pieretti et al., 1991). FMRP is an RNA-binding protein that appears to play an

important role in repressing translation of specific mRNAs (Schaeffer et al.,

2001). Loss of FMRP in mouse models of the disease, results in an >20%

increase in translation in the hippocampus, as assayed using radiolabeled

leucine (Qin et al., 2005). At least part of this excess translation may be occurring

directly at synapses as several FMRP targets experience increased association

with polyribosomes, an indicator of increased translation, in synaptic

compartments of FMR1 knockout mice (Zalfa et al., 2003). Many molecular,

synaptic, and behavioral phenotypes present in the FMRPKO mice can be

ameliorated by targeting other known regulators of translation such as p70 S6

kinase 1 (S6K1), MAP kinase-interacting serine/threonine-protein kinase 1

(MNK1), and cytoplasmic polyadenylation element binding protein (CPEB1)

(Udagawa et al., 2013, Gkogkas et al., 2014, Bhattacharya et al., 2012). These

data suggest that at least some of the neurological deficits in FXS are a result of

increased translation, and therefore restoring translational levels would likely be

vital for treatment.

The mammalian target of rapamycin-raptor complex 1 (mTORC1)

represents another translation regulator linked to neurological dysfunction.

Although mTORC1 has numerous functions, perhaps the best-characterized is its

role in cap-dependent translation initiation. mTORC1 carries out this role by

targeting the eukaryotic initiation factor 4E binding protein (4E-BP), a factor that

sequesters the eukaryotic initiation factor 4E (eIF4E) and inhibits translation

initiation (Haghighat et al., 1995). Phosphorylation by mTORC1 disrupts 4E-BP

binding to eIF4E and thus activates translation (Heesom and Denton, 1999,

Gingras et al., 2001, Mothe-Satney et al., 2000). Mutations in negative regulators

of mTORC1, and therefore translation, such as (PTEN) or tuberous sclerosis

complex proteins are associated with the development of autism (Butler et al.,

2005, Zori et al., 1998, Goffin et al., 2001, O'Roak et al., 2012, Jeste et al.,

2008). Interestingly, the ASD-like phenotypes in models of both of these

mutations can be abolished with the application of mTORC1 inhibitors,

demonstrating the contribution of aberrant mTORC1 activity to neurological

dysfunction (Ehninger et al., 2008, Zhou et al., 2009a, Meikle et al., 2008). These

examples highlight the importance of translational repression for proper neuronal

function; elucidating the mechanisms underlying such repression is therefore

critical to understanding and treating disorders such as ASD.
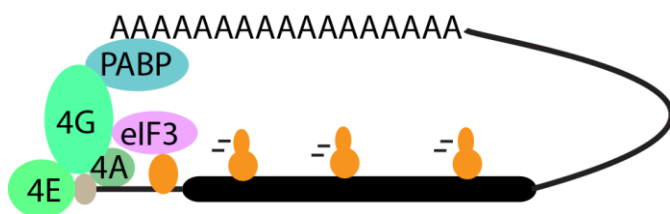
Figure 1.2 Model of mRNA circularization. On the 3'
end, long poly(A) tails recruit poly(A) binding protein
(PABP), which can in turn stabilize the eIF4F complex
onto 5' cap. PABP performs this action by binding to
the scaffolding protein, eIF4G, which binds to the RNA
helicase, eIF4A, and the cap-binding factor, eIF4E. eIF3

binds the now stabilized eIF4F complex and recruits the small ribosomal subunit (40S) which scans the mRNA until it reaches a start codon and can recruit the large ribosomal subunit and initiate translation (Grifo et al., 1983, Lamphear et al., 1995, Deo et al., 1999, Tarun and Sachs, 1995, De Gregorio et al., 1999, Wells et al., 1998, Weill et al., 2012, Preiss and M, 2003). The poly(A) tail appears to play a central role in translation initiation, and is therefore the target of tight regulation (Munroe and Jacobson, 1990). In the nucleus, nearly all eukaryotic mRNAs gain a non-templated, ~200 adenosine long tail on their 3' end (Sheets and Wickens, 1989, Gilmartin, 2005). The length of this poly(A) tail is further regulated in the cytoplasm where it is thought to mediate translation and stability of the mRNA (Shyu et al., 1991, Beilharz and Preiss, 2007). Although conflicting reports exist on the global level, the use of reporter mRNAs has demonstrated that longer poly(A) tail are correlated with increased translation of specific mRNAs (Beilharz and Preiss, 2007, Lim et al., 2016, Subtelny et al., 2014, Barkoff et al., 1998). This correlation is thought to be mediated by increased recruitment of the poly(A) binding protein (PABP) which, in addition to binding the poly(A) tail, binds and stabilizes the eukaryotic initiation factor 4F complex onto the 5' cap of the mRNAs, circularizing the mRNA (Deo et al., 1999, Tarun and Sachs, 1995). This circularized mRNA is thought to recruit the ribosome and initiate translation (Wells et al., 1998, Beilharz and Preiss, 2007, McGrew et al., 1989) (Figure 1.2). This complex process makes the poly(A) tail crucial for cap-dependent translation initiation, the rate-limiting step for translation (Weill et al., 2012) .

Cytoplasmic polyadenylation element binding protein (CPEB) is one well-characterized regulator of both poly(A) tail length and translation. In *Xenopus* oocytes, CPEB recognizes the cytoplasmic polyadenylation element (CPE; UUUUUAU) in the 3' untranslated region of mRNAs (Paris et al., 1991), and recruits both a poly(A) polymerase, germ-line-development factor 2 (Gld2), and a deadenylase, poly(A) ribonuclease (PARN). PARN is more active in this complex, resulting in short poly(A) tails and translational repression (Kim and Richter, 2006). A progesterone signal results in phosphorylation of CPEB, impeding its interaction with PARN. In the absence of PARN, Gld2 can lengthen the poly(A) tails resulting in increased translation of these mRNAs and oocyte maturation (Sarkissian et al., 2004, Richter, 2007). CPEB appears to play a similar role in neurons where it mediates dendritic transport and stimulation-induced polyadenylation and translation of mRNAs at post-synaptic sites (Huang et al., 2003, Udagawa et al., 2012). This function is critical for both synaptic plasticity and learning in mice, and may have relevance to disorders such as FXS, as CPEB and FMRP share the same neuronal targets (Udagawa et al., 2012, Alarcon et al., 2004, Berger-Sweeney et al., 2006, Zearfoss et al., 2008, Udagawa et al., 2013). Unlike Gld2 and CPEB, PARN did not seem to be important for dendritic poly(A) or synaptic plasticity suggesting that CPEB recruits a different deadenylase to mediate translational repression of mRNAs in neurons (Udagawa et al., 2012).

Pumilio and fem-3 binding proteins (PUF) represent a separate family of RNA-binding proteins that mediates translation of specific mRNAs by regulating their poly(A) tails. Human PUF proteins recognize a UGARAUA motif in the 3'UTR of mRNAs, and recruit deadenylases to shorten their poly(A) tail and repress translation (Wang et al., 2002, Van Etten et al., 2012, Wreden et al., 1997, Goldstrohm et al., 2007). This action may be important for global translation at the synapse as a *Drosophila* homologue represses the translation of eIF4E, an essential factor for translation initiation, specifically at post-synaptic sites (Menon et al., 2004). Deletion of PUF proteins disrupts normal synaptic function, local translation, and learning in various model organisms (Vessey et al., 2010, Dubnau et al., 2003, Ye et al., 2004), and demonstrate phenotypes reminiscent of those present in autistic models (Siemen et al., 2011).

Autism is not the only neurological disorder seemingly resulting from aberrant translational repression. Myotonic Dystrophy 1 (DM1), characterized by muscle wasting, results from a CUG repeat expansion in the 3'UTR of the dystrophia myotonica protein kinase (DMPK gene) (Brook et al., 1992). This expansion is thought to sequester the muscleblind-like family members (MBNL) in distinct nuclear foci, therefore hindering their normal splicing function on other mRNAs (Goodwin et al., 2015). Although mis-splicing has been the focus of study in DM1, MBNL proteins play other cytoplasmic roles including translation repression and RNA localization (Masuda et al., 2012, Wang et al., 2012, Wang et al., 2015). Indeed most neurite-localized mRNAs contain the CUGCUG motif

that MBNL proteins recognize. This localization is impaired in MBNL knockout mice, likely resulting in disrupted local translation, and could therefore also be impaired in diseased patients (Taliaferro et al., 2016). How MBNL proteins repress translation and mediate localization is unclear but deadenylation may play a role, as MBNL1 has been shown to interact with deadenylation complexes (Lau et al., 2009).

These examples build the case for deadenylation as a key step in repressing translation at synapses; as all of these proteins have been demonstrated to regulate mRNAs at post-synaptic sites (Udagawa et al., 2012, Taliaferro et al., 2016, Menon et al., 2004, Wang et al., 2017). The deadenylase or deadenylases involved would likely associate with several different complexes to oversee the dynamic translational landscape present in neuronal dendrites.

Deadenylases

There are nine known cytoplasmic deadenylases currently described in mammals: Angel1, Angel2, CNOT6, CNOT6L, CNOT7, CNOT8, Nocturnin, PARN, and PAN2 (Yan, 2014). Although these deadenylases carry out the same enzymatic function, they form different complexes within the cell to carry out a variety of different roles. For example, PARN associates with the CPEB complex in *Xenopus* oocytes to deadenylate and therefore silence mRNAs prior to fertilization (Kim and Richter, 2006). This interaction is conserved in neurons, however unlike CPEB, PARN is not vital for synaptic plasticity (Udagawa et al.,

2012). Nocturnin is a rhythmically expressed gene whose expression peaks in the early night, and is therefore thought to deadenylate mRNAs to regulate circadian processes (Baggs and Green, 2003, Nagoshi et al., 2010, Kojima et al., 2015). The deadenylase activity for Angel1 and Angel2 has not yet been validated and their activity is inferred based on sequence homology to other deadenylases (Wagner et al., 2007), however Angel1 appears to carry out targeted regulation of translation through an interaction with eIF4E (Gosselin et al., 2013). Most of the work on deadenylases has focused on the CNOT and PAN2 enzymes, which are thought to be responsible for deadenylation of most cellular mRNAs (Brown et al., 1996, Tucker et al., 2001). The model of how these two deadenylases carry out this function is based on experiments performed in a mouse fibroblast cell line looking at a beta globin reporter mRNA. This reporter appeared to be deadenylated in two steps: during the first step its tail was shortened to ~110nt with no effect on stability, the second step removed the tail entirely and resulted in degradation of the mRNA (Yamashita et al., 2005, Chen et al., 2009). Using RNAi and enzymatically-dead mutants, the authors determined that the PAN2-PAN3 complex was responsible for the initial shortening of the poly(A) tail and the CNOT complex subsequently removed the entire tail, triggering mRNA decay (Zheng et al., 2008, Yamashita et al., 2005, Chen et al., 2009). This consecutive function of these two complexes may differ depending on cell type however, as the CNOT deadenylases play a larger role in

global deadenylation in *Drosophila* and yeast cells compared to PAN2 (Tucker et al., 2001, Bonisch et al., 2007).

The CNOT complex

The human Carbon catabolite repression 4-negative on TATA-less (CNOT) complex is a heterogeneous ~1.2 MDa complex, involved in various cellular processes including: transcription, mRNA degradation, and protein modification. It contains 7 core subunits: CNOT1, CNOT2, CNOT3, CNOT9, CNOT10, TAB182 (tankyrase binding protein of 182 kDa), and CNOT11, in addition to two of four different deadenylases: CNOT7 or CNOT8 and CNOT6 or CNOT6L (Mauxion et al., 2013, Lau et al., 2009, Boland et al., 2013, Ito et al., 2011). Most subunits bind directly to the scaffolding protein CNOT1, except for CNOT3 which binds CNOT2, CNOT6 and 6L which bind to CNOT7 or CNOT8 (Ito et al., 2011), and CNOT10 which binds through CNOT11 (Bawankar et al., 2013, Boland et al., 2013)(Figure1.3). CNOT4 is capable of binding to CNOT1 in yeast two-hybrid assays, however it does not appear to be a stable component of the complex in human cells as measured via immunoprecipitation and mass spectrometry (Lau et al., 2009). Initial work on the CNOT complex focused on its role in transcription as several of its subunits regulate this process. For instance, CNOT2 and CNOT9 appear to repress transcription by regulating promoter activity through an interaction with a histone deacetylase (Zwartjes et al., 2004, Zheng et al., 2012, Rodriguez-Gil et al., 2017). CNOT3 contains a similar domain

necessary for this repression and therefore may have a similar function (Cejas et al., 2017, Zwartjes et al., 2004, Zheng et al., 2012). As work continued on this complex, its enzymatic activities became apparent such as ubiquitination by the E3 ligase, CNOT4 (Albert et al., 2002), and deadenylation by the deadenylase subunits (Tucker et al., 2001). It is now widely accepted that the CNOT complex functions as the major deadenylase in cells and this function is critical for development, cancer progression, and stress response (Nousch et al., 2013, Schwede et al., 2008, Faraji et al., 2016, Tucker et al., 2001, Hilgers et al., 2006).
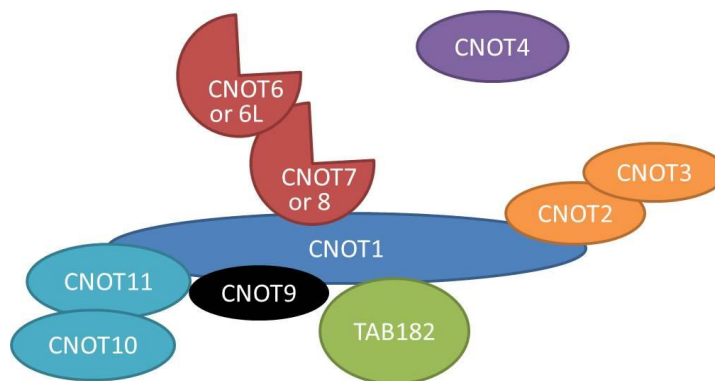
Figure 1.3 Model depicting the structure of the human CNOT complex (Lau et al., 2009, Bawankar et al., 2013) (Ito et al., 2011, Costa-Mattioli et al., 2009).

As mentioned above the human CNOT complex contains four deadenylases: CNOT6, 6L, 7, and 8 (Lau et al., 2009). CNOT6 and CNOT6L are paralogues of each other and are seemingly never present in the same complex, and the same is true of CNOT7 and CNOT8 (Lau et al., 2009). The presence of two functional deadenylases within the same CNOT complex is a characteristic conserved all the way down to yeast where only one homologue of each pair exist: Ccr4 for CNOT6 and 6L, and Caf1 for CNOT7 and CNOT8 (Lau et al., 2009). The advantage of this redundancy is unclear, but it appears that

these enzymes may contribute differently to deadenylation of their substrate. In yeast, although the presence of both proteins is necessary for deadenylation, only the enzymatic activity of Ccr4 is required (Viswanathan et al., 2004, Goldstrohm et al., 2007). In contrast, depletion of Caf1 but not Ccr4 in *Drosophila* cells resulted in a dramatic lengthening of bulk poly(A) (Temme et al., 2010, Temme et al., 2004). The observation that Caf1, and its homologues, regulate bulk poly(A) is also true in trypanosomes and human fibrosarcoma cells, which lead to the generally accepted conclusion that CNOT7 and CNOT8 (Caf1 homologues) are the major deadenylases in mammalian cells (Schwede et al., 2008). The predominant deadenylase may differ, however, depending on the cell type tested as CNOT6 and CNOT6L appear to regulate more mRNAs than CNOT7 and CNOT8 in human breast cancer cells (Mittal et al., 2011). The integrity of the complex is also key, as depletion of non-enzymatic subunits such as CNOT3 and CNOT10 disrupts the deadenylation and degradation of mRNAs (Zheng et al., 2016, Zhou et al., 2017, Inoue et al., 2015, Takahashi et al., 2012, Farber et al., 2013).Taken together this data suggest that the CNOT complex is heterogenous and constitutes the major deadenylase in cells, although its subunits have differing specificity in different cell types.

There are many scenarios that could result in one deadenylase dominating over the others in various cell types, with the most obvious being differential expression of the subunits. One study tested the levels of the different members of the CNOT complex in various tissues from the adult mouse and

found widely distinct expression patterns. CNOT6L appeared to be expressed ubiquitiously, while CNOT6 and 7 were enriched in reproductive organs such as the ovary and testis, and CNOT8 in immune organs such as the spleen and thymus (Chen et al., 2011). Even within one cell, the deadenylases could have differential localization, as demonstrated by Cajigas et al 2012 who sequenced mRNAs from the neuropil in the CA1 region of the hippocampus, and from the corresponding soma region (Figure 1.1). CNOT7 mRNA levels were at least 2.5x more abundant in the neuropil area compared to the other CNOT deadenylase, indicating its protein may also predominate in this region (Cajigas et al., 2012).

RNA-binding proteins are another mechanism that can provide specificity to the heterogenous CNOT complex. Several RNA-binding proteins have been shown to associate with the complex to target it to specific mRNAs (Table 1.1). These RNA-binding proteins link the complex to a multitude of functions such as inflammatory response, miRNA induced-silencing, and potentially learning and memory through the RNA-binding protein CPEB. Most of these interactions occur directly with the scaffolding subunit, CNOT1; however some are mediated through the other subunits. TNRC6/GW182, for instance, binds to CNOT9 in order to recruit the complex to miRNA targets (Chen et al., 2014, Mathys et al., 2014). Tob1 binds directly to CNOT7 and mediates its interaction with CPEB1 and Poly(A) Binding Protein (PABP) (Ogami et al., 2014). Even certain subunits appear to contain specificity, such as CNOT3 which targets mRNAs important for cell death in mouse embryonic fibroblasts (Suzuki et al., 2015), and CNOT4

which contains a RNA recognition motif domain and appears to target mRNAs with a CACACA motif (Ray et al., 2013). These various interactions allow this ubiquitiously expressed complex to play a refined role in different cell types by deadenylating specific subsets of mRNAs.

Table 1.1: Well described interacting proteins of the CNOT complex

Interacting Protein	Motif	Cell type	reference	RBP Function
Tristetrapolin (TTP) & BRF1	AU rich elements (ARE)	HEK293T cells	(Lykke-Andersen and Wagner, 2005, Fabian et al., 2013)	Inflammatory response and cancer
Nanos	Non-specific	Drosophila, mouse	(Raisch et al., 2016, Suzuki et al., 2012, Kadyrova et al., 2007)	Embryonic germline development
Pumilio (Puf proteins)	UGUARAUA	Drosophila, yeast, hek 293t	(Goldstrohm et al., 2007, Van Etten et al., 2012, Miller and Olivas, 2011)	Development
GW182/TNRC6	Multiple	Hek293t, drosophila	(Braun et al., 2011)	microRNA-induced silencing complex
Tob1	Interacts with PABPc1	Human, Mouse	(Horiuchi et al., 2009, Ezzeddine et al., 2007)	Anti-proliferative
CPEB1	UUUUUAUU	HeLa cells	(Ogami et al., 2014)	Learning memory, development
CPEB3	U-rich hairpin structure	Cos7 cells (monkey)	(Hosoda et al., 2011)	Glur2 mRNA regulation

How or if the CNOT complex functions in neuronal cells has not been studied, however several of the subunits are expressed in the brain and this expression is modulated during development (Chen et al., 2011). Numerous interactions have also been described between the CNOT complex and factors that regulate post-synaptic local translation, synaptic plasticity, and learning such as: CPEB, MBNL1, PUF, and GW182 (Ogami et al., 2014, Lau et al., 2009, Goldstrohm et al., 2007, Braun et al., 2011). Many of these interactions are mediated by CNOT1, however a few (CPEB & MBNL1) are direct interactions with CNOT7 (Ogami et al., 2014, Lau et al., 2009). In addition to these interactions, CNOT7 mRNA levels are enriched in the CA1 hippocampal neuropil compared to any other known deadenylase (Cajigas et al., 2012). These data indicate that the CNOT complex, specifically CNOT7, may constitute the major deadenylase at synapses and therefore a key factor governing local translation.

CHAPTER II

Dynamic Control of Dendritic mRNA Expression by CNOT7 Regulates Synaptic Efficacy and Higher Cognitive Function

Rhonda L. McFleder, Fernanda Mansur, and Joel D. Richter

Program in Molecular Medicine, University of Massachusetts Medical School,

Worcester, Ma 01605, USA

Abstract

Translation of mRNAs in dendrites mediates synaptic plasticity, the probable cellular basis of learning and memory. Coordination of translational inhibitory and stimulatory mechanisms as well as dendritic transport of mRNA is necessary to ensure proper control of this local translation. Here, we find that the deadenylase CNOT7 dynamically regulates dendritic mRNA translation and transport as well as synaptic plasticity and higher cognitive function. In cultured hippocampal neurons, synaptic stimulation induces a rapid decrease in CNOT7 which in the short-term results in poly(A) tail lengthening of target mRNAs. However, at later times following stimulation, decreased poly(A) and dendritic localization of mRNA take place, similar to what is observed when CNOT7 is depleted over several days. In mice, CNOT7 is essential for hippocampal-dependent learning and memory. This study identifies CNOT7 as an important regulator of RNA transport and translation in dendrites as well as higher cognitive function.

Introduction

Experience-induced modifications of synapses are thought to serve as the molecular basis of learning and memory (Kandel, 2001b). Synaptic plasticity provides long-lasting alterations in neuronal communication that allows memories to be retained for many years (Costa-Mattioli et al., 2009). Of the several forms of synaptic plasticity, at least three are dependent on protein synthesis: long-lasting neurotrophin-induced enhancement of synaptic efficacy (Kang H, 1996), metabotropic glutamate receptor long-term depression (mGluR-LTD) (Huber KM, 2000), and N-methyl-D-aspartate late-phase long-term potentiation (L-LTP) (Bradshaw et al., 2003a, Miller et al., 2002). The necessity for new protein production in synaptic plasticity is independent of transcription and relies upon mRNAs and translation factors in dendrites (Bradshaw et al., 2003a, Kang H, 1996, Martin and Kandel, 1996). Following synaptic stimulation, dendritic mRNAs are translated at postsynaptic sites where their protein products modify synapse structure and function (Sutton and Schuman, 2006a). Based on sequence analysis of RNAs in the mammalian hippocampal neuropil, a region rich in axons and dendrites, there are >2,500 mRNAs localized to neurites (Cajigas et al., 2012). It is almost axiomatic that regulation of these mRNAs is necessary to ensure localized translation in response to synaptic activity (Buxbaum et al., 2015); when this regulation goes awry, autism and other neurological disorders can ensue (Kelleher and Bear, 2008).

Repression of translation is necessary during mRNA transport to dendrites, but even when localized, silencing must continue until synaptic activity occurs (Costa-Mattioli et al., 2009). This mRNA masking takes multiple forms and involves repression at initiation (Krichevsky and Kosik, 2001) and elongation (Sutton et al., 2007, Richter, 2015). Although the mechanism(s) and/or factors by which these and other processes control mRNA expression in dendrites is often unclear, it is evident that they frequently involve miRNAs (Ashraf et al., 2006, Bicker et al., 2013, Schratt, 2009) or RNA binding proteins (Darnell, 2013, Eom et al., 2013, Udagawa et al., 2015). Many of these trans-acting factors utilize deadenylation as an initiation step to silence mRNAs (Ashraf et al., 2006, Giorgi et al., 2007, Richter, 2007). Mechanistically, deadenylases repress translation by shortening poly(A) tails and thereby abrogate association of poly(A) binding protein (PABP), which is important for circularizing mRNA and recruiting the 40S ribosomal subunit (Richter, 2007). The deadenylase PARN (poly(A) ribonuclease) was presumed to be the enzyme responsible for initiating repression for at least a subset of dendritic mRNAs because it interacts with the RNA-binding protein CPEB1 (Richter, 2007, Udagawa et al., 2012). In oocytes, CPEB1 regulates translation by recruiting both Gld2, a non-canonical poly(A) polymerase, and PARN to specific mRNAs (Richter, 2007). Upon phosphorylation of CPEB, PARN is expelled from the ribonucleoprotein complex, which results in polyadenylation and subsequently translation of target mRNAs. In the brain, CPEB1 and Gld2 mediate translation in dendrites in response to

synaptic stimulation (Wu et al., 1998, Zearfoss et al., 2008, Udagawa et al., 2012). However, because depletion of PARN had no discernable effect on synaptic plasticity, the deadenylase essential for repressing translation was unclear (Udagawa et al., 2012). We surmised that one or perhaps multiple deadenylases would likely govern poly(A) tail length of several different populations of dendritic mRNAs to impact learning and memory.

The carbon catabolite repression 4 negative on TATA-less (CNOT) is a conserved, multisubunit complex that functions as the major deadenylase in yeast to humans (Tucker et al., 2001, Temme et al., 2004, Schwede et al., 2008). The mammalian CNOT complex consists of four functional deadenylase enzymes: CNOT6, CNOT6L, CNOT7, and CNOT8 (Lau et al., 2009). Of these, CNOT7 and CNOT8 regulate poly(A) tail length on the majority of mRNAs (Schwede et al., 2008). Although CNOT7 and CNOT8 are 75% homologous, they have distinct targets, probably because they are differentially expressed and associate with different complexes (Lau et al., 2009). CNOT7 levels are enriched in neurons relative to CNOT8 (Chen et al., 2011); CNOT7 also associates with both the microRNA machinery (Fabian et al., 2009, Piao et al., 2010) and CPEB1 (Ogami et al., 2014). These data suggest that CNOT7 might influence translation in dendrites, and as a consequence modify synaptic transmission and higher cognitive function.

Here we identify CNOT7 as an important enzyme that regulates local translation, synapse efficacy, and learning and memory. Within 3 minutes following induction of synaptic plasticity *in vitro* by glycine-induced LTP, CNOT7 levels begin to decrease, which is necessary for the immediate increase in total dendritic poly(A) occurring at this time. Interestingly twenty minutes following stimulation, when CNOT7 levels are low, total dendritic poly(A) is decreased. We found that these different effects are due to short-term versus long-term depletion of CNOT7. Paradoxically, poly(A) tails are lengthened following both short-term ($\leq$ 10 min) and long-term CNOT7 depletion ($\geq$ 20 min), but long-term depletion induced by stimulation of LTP or knockdown of the enzyme also impairs dendritic localization of CNOT7 target mRNAs resulting in reduced dendritic poly(A). These observations indicate a critical role for CNOT7 in localization and deadenylation of dendritic mRNAs. The effect of long-term CNOT7 depletion is most apparent after four days, which in addition to the effects stated above, also resulted in reduced local translation as well as impaired synaptic plasticity. Depletion of CNOT7 in the hippocampus over several weeks following injection of AAV-expressed shRNA resulted in reduced poly(A) in the CA1 neuropil and impaired learning and memory in several cognitive tests. These and other data demonstrate that CNOT7 governs the localization, polyadenylation, and translation of specific dendritic mRNAs and that it has a key role in synaptic plasticity, learning, and memory.

Results

Depletion of CNOT7 decreases dendritic poly(A) and local protein synthesis
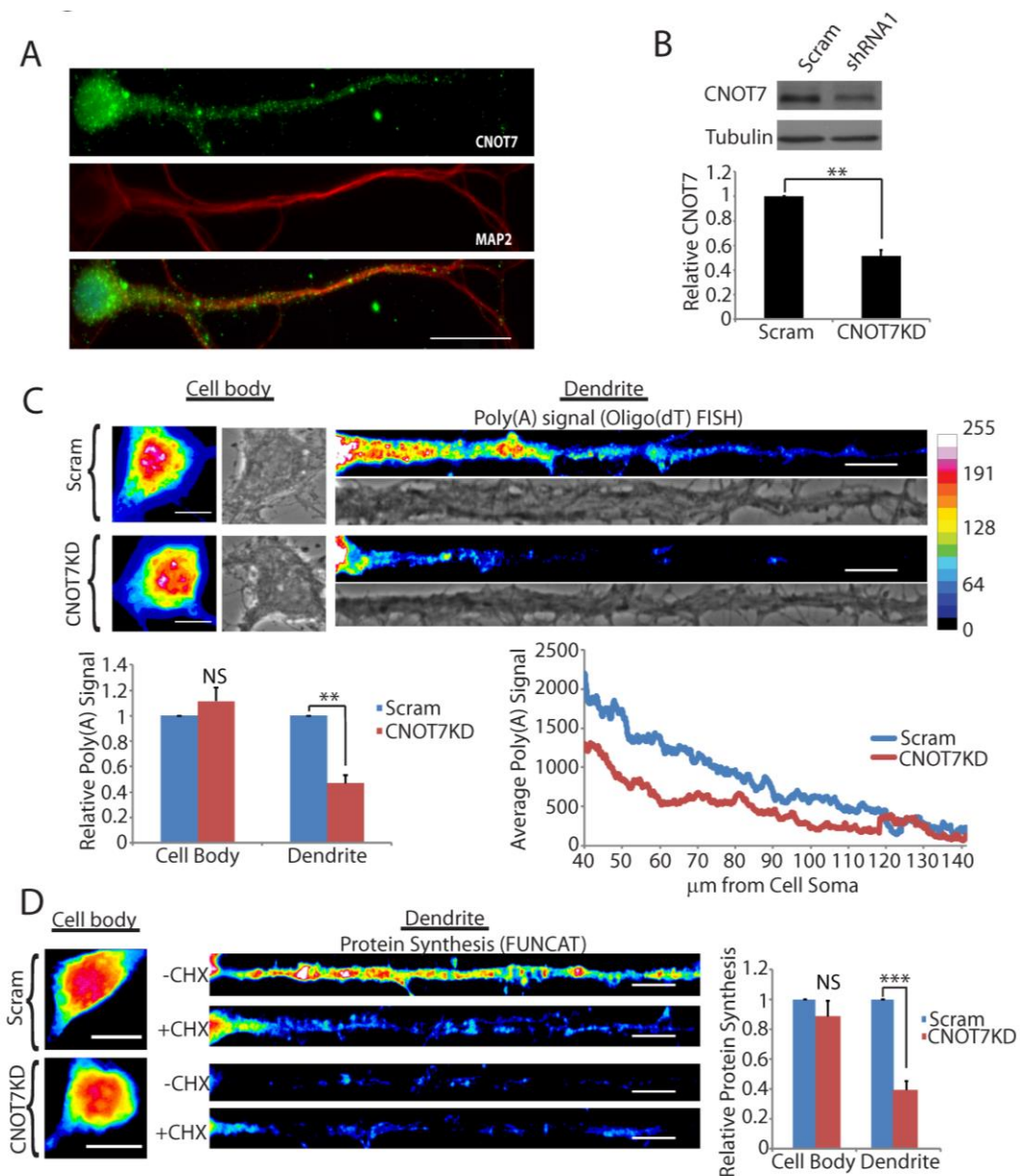
Figure 2.1. CNOT7 regulates dendritic poly(A). (A) Immunocytochemistry of cultured hippocampal neurons DIV 17 for CNOT7 (green), MAP2 (red), and DAPI (Blue). Scale bar represents 20μm (B) Representative western blot of CNOT7 (top) and tubulin (bottom). Histogram represents the average of three experiments. (C) (Top) Representative brightfield and

oligo(dT) fluorescent in situ hybridization (FISH) images from the cell body (left) and dendrites (right) of scrambled (Scram) or CNOT7 knockdown (CNOT7KD) neurons. Scale bar represents 10μm. (Bottom) Bar and line graph are averages of the oligo(dT) FISH signal in ≥60 neurons/condition from three experimental replicates. (D) FUNCAT analysis of scrambled and CNOT7 knockdown neurons in the presence (+CHX) or absence (-CHX) of cycloheximide. Bar graph is the average of ≥40 neurons/condition from three experimental replicates. In these and all subsequent figures, the error bars represent SEM, *p<0.05, **p<0.01, ***p<0.001. NS, not significant.

We analyzed the mRNA levels of all nine known cytoplasmic deadenylases (Angel1, Angel2, CNOT6, CNOT6L, CNOT7, CNOT8, Nocturnin, Pan2, and PARN) in the liver, cerebellum, hippocampus, and cortex from 40 day old mice. CNOT7 and CNOT8 were enriched in the hippocampus compared to the other enzymes (Figure 2.2A). CNOT7 RNA also exceeds the levels of all other deadenylases in the hippocampal CA1 neuropil, an area enriched for dendrites (Figure 2.2B) (Cajigas et al., 2012). Immuno-staining of cultured hippocampal neurons (DIV17) showed that CNOT7 is present throughout the cells including dendrites (Figure 2.1A), and is significantly reduced upon shRNA-mediated depletion (Figure 2.2C). Western blot analysis of mouse brain lysates revealed CNOT7 to be present in synaptosomes (Figure 2.2D), suggesting that it may have a synaptic function.
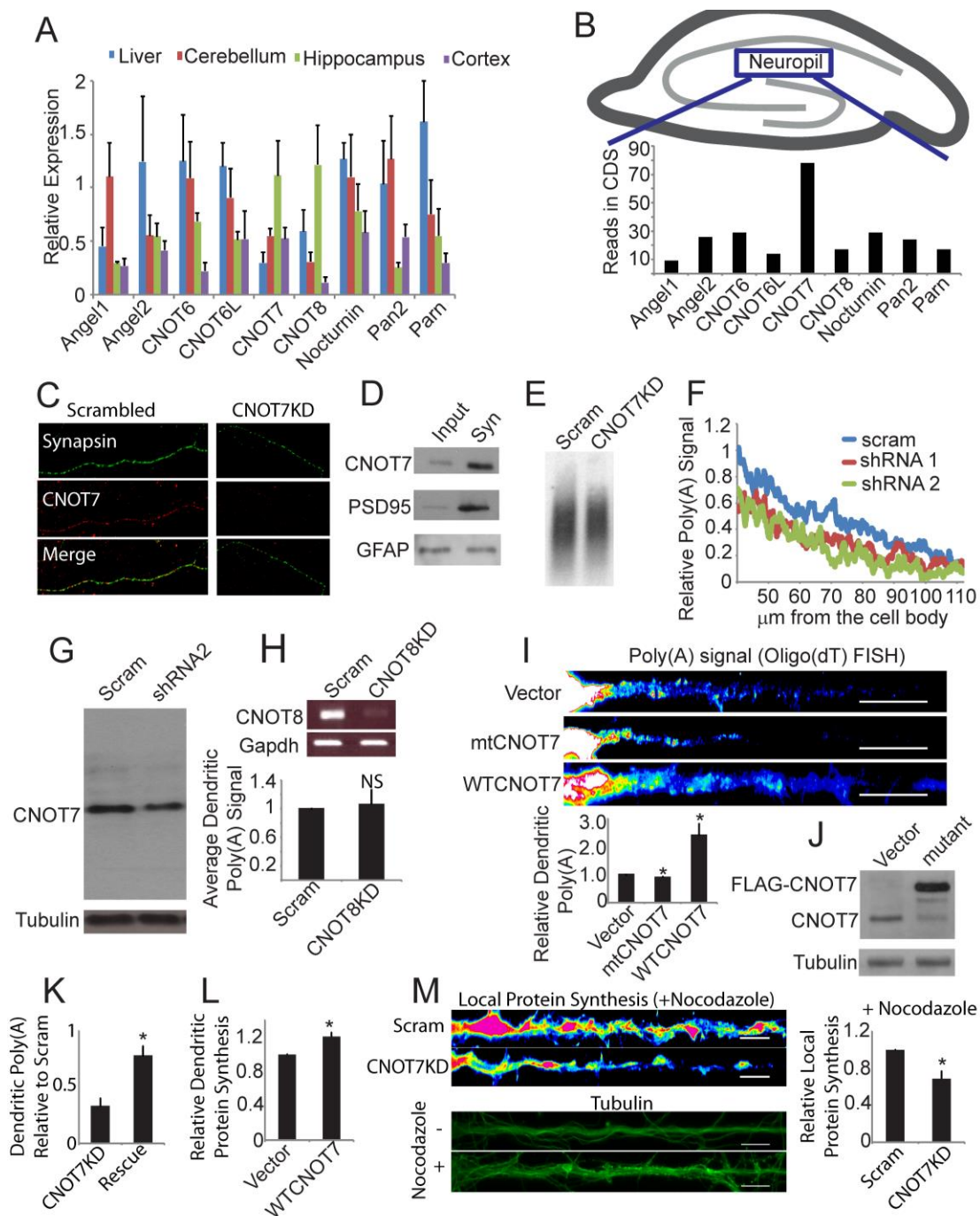
Figure 2.2. CNOT7 is the major deadenylase regulating dendritic poly(A) tails. (A) Bar graph represents the quantification of the relative amount of the nine different deadenylases in four different mouse tissues: liver (blue), cerebellum (red), hippocampus (green), and cortex (purple). Quantification of each deadenylase is plotted relative to GAPDH and is the average mRNA levels from tissues from four forty day old female mice. (B) Schematic of the

hippocampus (top) with a box surrounding the CA1 neuropil. Bar graph (bottom) represents quantification of the mRNA levels of the nine deadenylase measured in the CA1 neuropil by Cajigas et al 2012. (C) Representative images of dendrites from either scrambled or CNOT7 shRNA-expressing neurons showing CNOT7 (red) or synapsin (green). (D) Western blot of CNOT7 in total hippocampus or the hippocampal synaptoneurosomes (Syn). PSD95 and GFAP are shown as positive and negative controls for synaptoneurosome enrichment. (E) Oligo(dT) northern blot depicting total poly(A) in neurons infected with either scrambled or CNOT7 targeting shRNA. (F) Line graph depicts the average poly(A) signal in the distal dendrites in ≥40neurons/condition infected with either a scrambled shRNA (blue) or two different shRNAs targeting CNOT7 (red and green). Poly(A) signals are plotted relative to the Scrambled control. (G) Western blot depicting CNOT7 (top) or tubulin (bottom) in either scrambled or CNOT7 shRNA infected neurons (shRNA2). (H) RT-PCR of CNOT8 and GAPDH RNAs in scrambled or CNOT8 shRNA-expressing neurons (top). Bar graph represents the average poly(A) signal from dendrites of ≥ 30 neurons/condition from three biological replicates. (I) Oligo(dT) FISH analysis of neurons ectopically-expressing either empty vector, D40A mutant CNOT7 (mtCNOT7), or wild-type CNOT7. Bar graph represents the average of ≥28 neurons/condition from three experimental replicates. Scale bar represents 20μm. (J) Representative western blot of CNOT7 (top) and tubulin (bottom) from cells expressing either an empty vector control (vector) or a FLAG-tagged catalytically-inactive D40A mutant CNOT7 (mtCNOT7). (K) Histogram represents the average oligo(dT) FISH signal from ≥ 24 neurons/condition from three experimental replicates relative to control neurons infected with Scrambled shRNA. Rescue neurons are ectopically expressing CNOT7 in addition to the CNOT7 shRNA. (L) FUNCAT analysis of dendrites from neurons ectopically expressing empty vector or CNOT7. Histogram represents the average dendritic FUNCAT signal from ≥ 30 neurons/condition. (M) (top) FUNCAT analysis of dendrites from either scrambled or CNOT7KD neurons treated with 30μM nocodazole to inhibit protein transport. (bottom) Tubulin staining of dendrites with (+) or without (-) nocodazole treatment. Histogram represents the average FUNCAT signal in the distal dendrites following nocodazole treatment from 30 neurons/condition. *P≤0.05, NS = not significant.

Using fluorescence in situ hybridization (FISH) with labeled oligo(dT), we analyzed poly(A) in cultured hippocampal neurons four days after infection with a lentivirus expressing either a CNOT7-specific shRNA or a scrambled control (Figure 2.1B). Surprisingly, CNOT7 knockdown (CNOT7KD) resulted in an ~50% decrease in dendritic poly(A), not the expected increase. This result occurred mostly on dendritic mRNA because the cell body poly(A) FISH signal (Figure 2.1C) as well as total cellular poly(A) (Figure 2.2E), was not significantly affected.

The decrease in dendritic poly(A) signal was replicated with a second shRNA targeting CNOT7 (Figure 2.2F & G). Knockdown of CNOT8, the CNOT7 paralogue, had no effect on dendritic poly(A) (Figure 2.2H). We ectopically expressed a catalytically-inactive form of the enzyme (D40A, mtCNOT7) as well as the wild-type enzyme (WTCNOT7) and performed oligo(dT) FISH. Neurons expressing mtCNOT7 had decreased dendritic poly(A) signal similar to the CNOT7KD neurons, while ectopic expression of WTCNOT7 produced the opposite effect (Figure 2.2I & J). Ectopic expression of wildtype CNOT7 was able to rescue the reduced dendritic poly(A), indicating that this dramatic effect was due to the loss of CNOT7 and not non-specific effects (Figure 2.2K). Newly synthesized proteins, as measured by Fluorescent Non-Canonical Amino Acid Tagging (FUNCAT), decreased by ~60% in dendrites of CNOT7KD neurons but only modestly in their cell bodies (Figure 2.1D), similar to the observations of poly(A). Ectopic expression of WTCNOT7 resulted in increased dendritic FUNCAT signal (Figure 2.2L). We also treated neurons with nocodazole, a microtubule depolymerizing agent that disrupts microtubules and inhibits protein transport to dendrites (Cid-Arregui et al., 1995, Kohrmann et al., 1999, Yuen et al., 2005). This procedure distorted tubulin staining (Figure 2.2M), and is admittedly quite stressful to the neurons however the neurons still produced protein as shown by FUNCAT labeling and this labeling was reduced in distal dendrites of CNOT7KD neurons relative to control shRNA-expressing neurons by

32% (Figure 2.2M). These data indicate that CNOT7 mediates dendritic

translation.
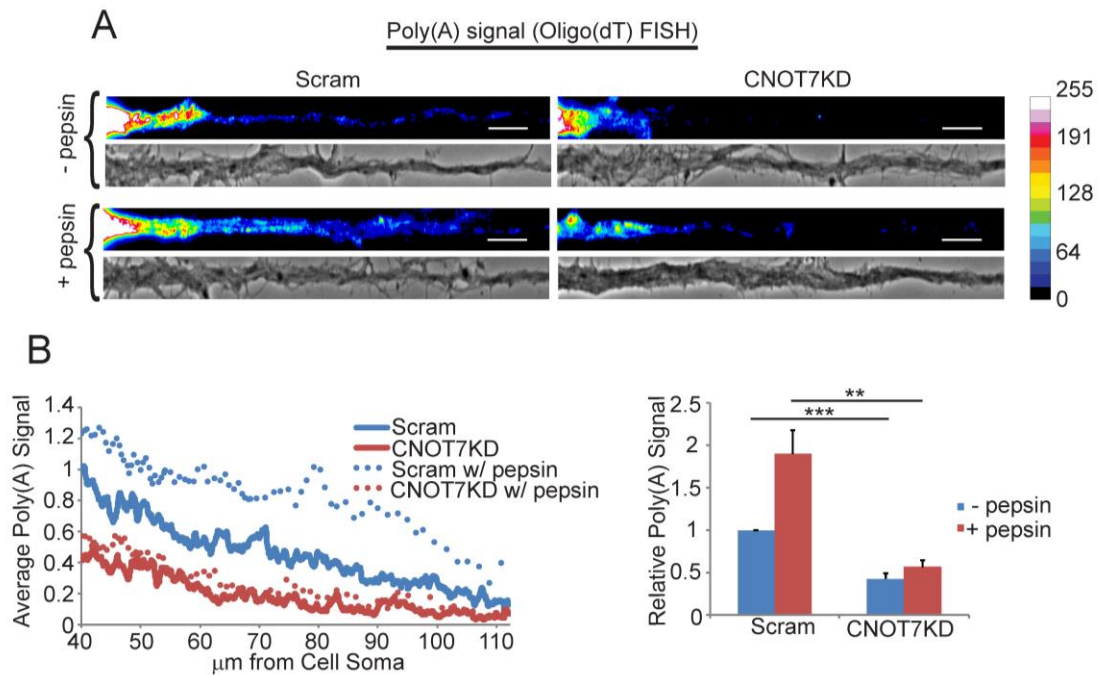
Figure 2.3. CNOT7 does not regulate masking of dendritic mRNAs. (A) Representative images and (B) quantification of oligo(dT) FISH signal in scrambled or CNOT7KD dendrites with (+) or without (-) pepsin. Scale bars represent 10μm. Bar and line graphs are the average oligo(dT) FISH signal in ≥60 dendrites/condition from 3 experimental replicates

It was possible that that the decrease in dendritic poly(A) signal following

CNOT7KD could be due to increased protein binding to mRNA and not reduced

poly(A) (Buxbaum et al., 2014). Consequently, we treated cultured neurons with

pepsin prior to FISH, which caused an ~2 fold increase in poly(A) signal in the

control neurons, indicating that proteins do obscure probe hybridization to poly(A)

(Figure 2.3A & B). CNOT7KD neurons, however, did not display an increased

poly(A) signal following pepsin digestion, indicating that in dendrites, there is

reduced poly(A) following CNOT7 depletion.

Knockdown of CNOT7 decreases synaptic plasticity *in vitro*
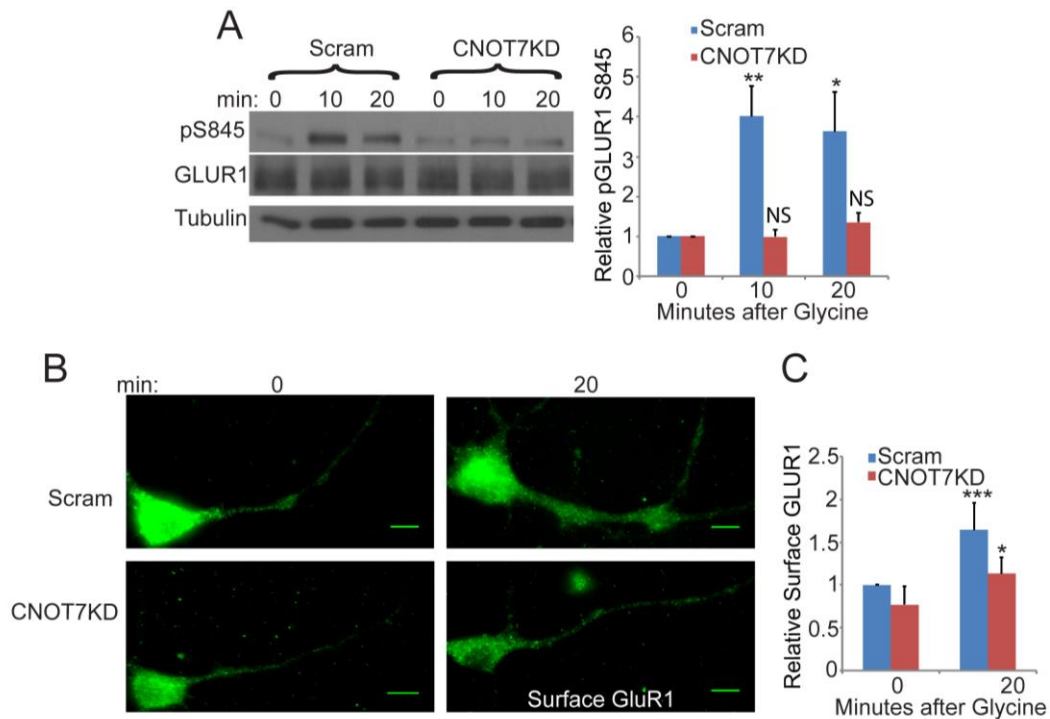
Figure 2.4. CNOT7KD inhibits long term potentiation. (A) Western blot analysis of S845 GluR1 phosphorylation in scrambled or CNOT7KD neurons at different time points following glycine stimulation. Phospho-GluR1 was normalized to total GluR1 and the bar graphs represent the average of three experiments. Time points are plotted relative to the 0 time point. (B) Representative images and (C) quantification of surface GluR1 in scrambled and CNOT7KD neurons fixed at 0 or 20 minutes following glycine stimulation. Scale bars represent 10μm. (C) Bar graph represents the average surface GluR1 in ≥50 dendrites/condition from three experimental replicates relative to the scrambled control.

Because poly(A) regulation in dendrites is correlated with alterations in

synaptic plasticity (Udagawa et al., 2012), we tested whether CNOT7 modulates

synapse function. We evoked one form of synaptic plasticity, glycine-induced

LTP (also referred to as chem-LTP), in CNOT7 depleted or control neurons.

Twenty minutes after glycine treatment, phosphorylation of GluR1 at S831 and

S845 increased 3-4 fold in control neurons, indicating successful induction of

LTP (Figure 2.4A & 2.5A) (Lee H, 2000). In CNOT7KD neurons, S831

phosphorylation modestly increased ~1.5 fold while S845 phosphorylation was

virtually unchanged (Figure 2.4A, 2.5A, and 2.5B). Depletion of CNOT8 did not

impede the increase in S845 phosphorylation following stimulation (Figure 2.5B),

indicating that the inhibition of GluR1 phosphorylation was specific to CNOT7.

Recycling of GluR1 to the membrane surface of dendrites was also impaired in

CNOT7KD neurons (Figure 2.4B & C). This impairment was not due to

decreased GluR1 because the level of this protein was unchanged between

scrambled or CNOT7KD neurons (Figures 2.4A & 2.5C). These data suggest that

CNOT7KD neurons have impairment in LTP induction.
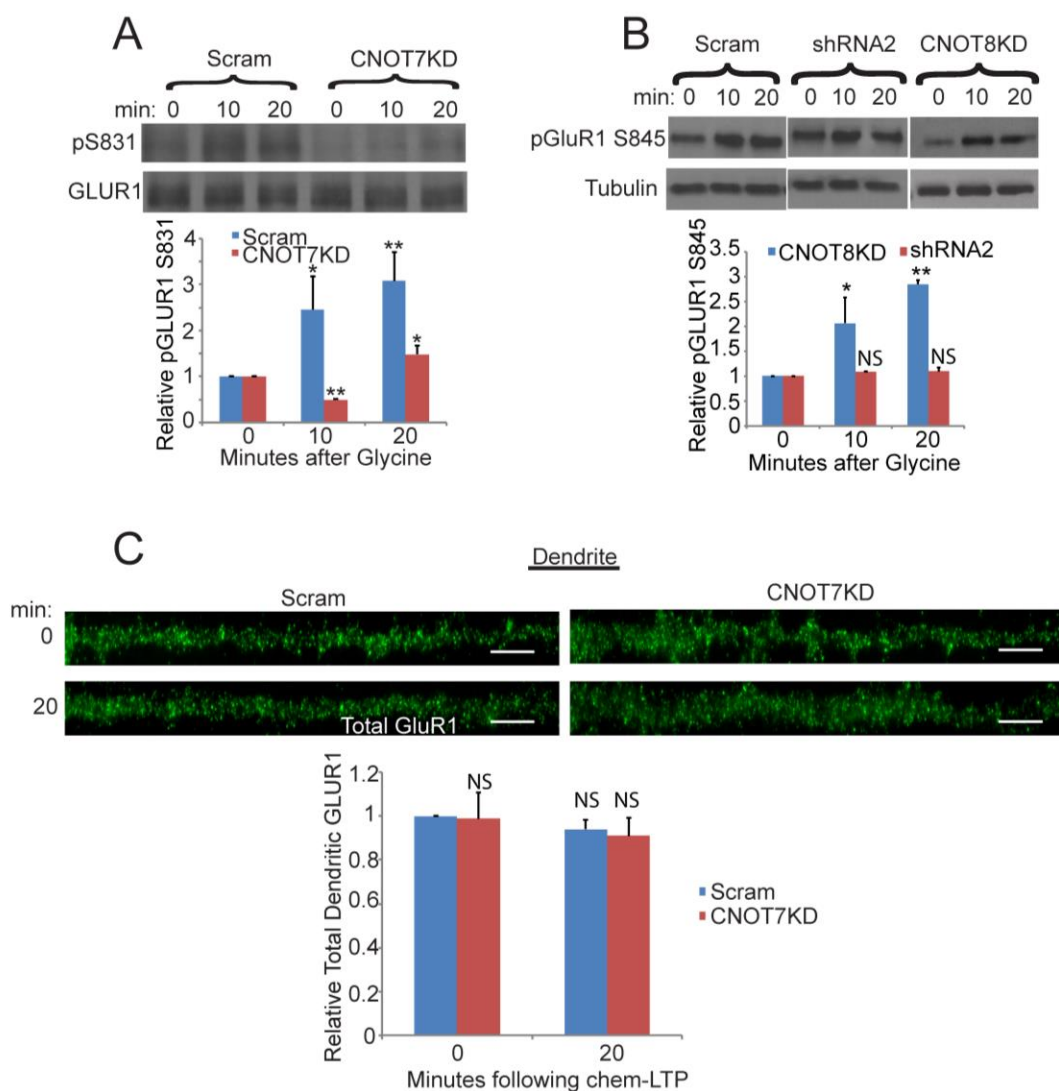
Figure 2.5. CNOT7KD inhibits chem-LTP. (A) Western blot analysis of S831 GluR1 phosphorylation in scrambled or CNOT7KD neurons at different time points following glycine stimulation. Phospho-GluR1 was normalized to total GluR1 (same from Figure 2.4A) and the bar graphs represent the average of three experiments. Time points are plotted relative to the 0 time point. (B) Western blot analysis of phosphor-Glur1 S845 and tubulin in neurons infected with either scrambled (Scram), CNOT7 targeting (shRNA2), or CNOT8 targeting (CNOT8KD) shRNAs. Neurons were stimulated and protein collected at either 0, 10, or 20 minutes following stimulation. Histogram (right) represents the average relative phospho-GluR1 S845 from three biological replicates. (C) Representative Images (top) and quantification (bottom) of total GluR1 in either Scrambled or CNOT7 shRNA infected neurons fixed at either 0 or 20 minutes following stimulation. Bar graph represents the average total GluR1 signal in the distal dendrite from ≥ 30 neurons/condition from three experimental replicates. *p≤0.05, **p≤0.01, NS = not significant.

CNOT7 regulates LTP induced changes in polyadenylation
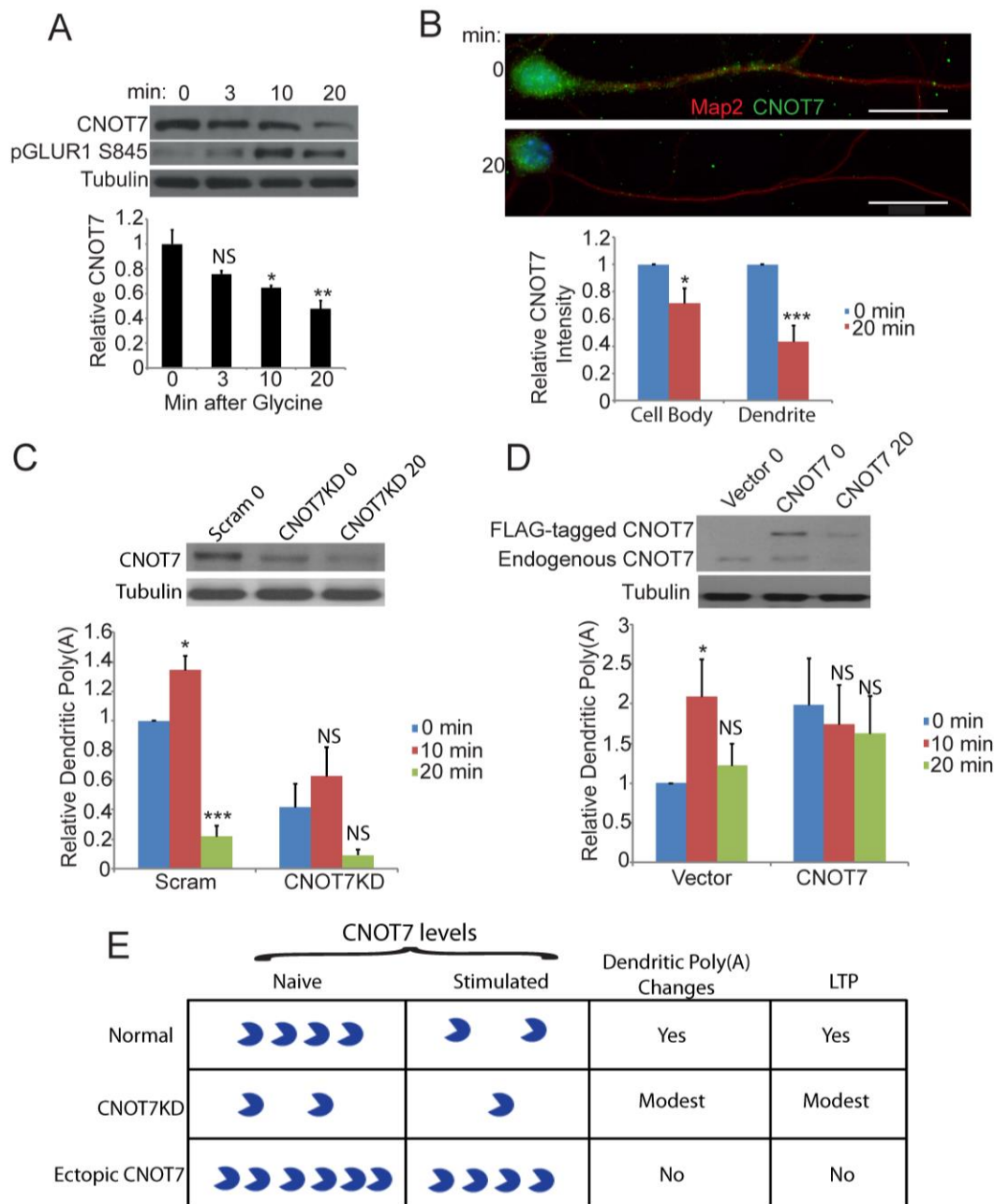
Figure 2.6. CNOT7 regulates dendritic poly(A) following synaptic plasticity. (A) Western blot analysis of CNOT7 (top), pGluR1 S845 (middle), and tubulin (bottom) at different time points following glycine stimulation. CNOT7 was normalized to tubulin and the bar graph represents the average of three experiments. Time points are plotted relative to the 0 time point. (B) Representative images of CNOT7 immunofluorescence at different time points following

stimulation. Bar graphs represent the average relative CNOT7 intensity in either the soma (left) or dendrites (right) from ≥40 neurons/condition from three experimental replicates. (C) (Top) Western blot depicts CNOT7 and tubulin levels in neurons infected with scrambled shRNA (scram) 0 minutes after glycine treatment, or CNOT7 shRNA 0 or 20 min following glycine treatment. The histogram depicts average relative dendritic poly(A) signal in stimulated cells infected with either a scrambled or CNOT7 targeting shRNA from ≥24 neurons/condition from three experimental replicates. All conditions are plotted relative to the scrambled control 0 time point. (D) (Top) Western blot depicts CNOT7 and tubulin levels in neurons expressing empty vector (vector) 0 minutes following glycine stimulation, or expressing ectopic FLAG-CNOT7 at 0 or 20 min following glycine stimulation. The histogram depicts average relative dendritic poly(A) signal in stimulated cells infected with either empty vector or CNOT7-expressing lentivirus. Data are from ≥26 neurons/condition from three experimental replicates. All conditions are plotted relative to the vector control 0 time point. (E) Summary diagram showing that in normal neurons, glycine stimulation causes an ~50% decrease in CNOT7, which is correlated with a change in dendritic poly(A) and LTP induction. In CNOT7KD neurons, ~50% of normal CNOT7 is present, which decreases by an additional 50% 20 min after glycine stimulation. These CNOT7 levels are correlated with modest changes in dendritic poly(A) changes and LTP induction. Ectopic expression of FLAG-CNOT7 in neurons results in about a doubling of this protein. Twenty minutes after glycine treatment, CNOT7 levels fall to about the same level as in control (vector) neurons at time 0. Consequently, there are no changes in dendritic poly(A) and LTP is not induced.

We induced chem-LTP in cultured hippocampal neurons and collected protein 0, 3, 10, and 20 minutes later. Twenty minutes was chosen as the final time point because that is when both the amplitude and frequency of miniature excitatory post-synaptic currents (mEPSCs) are at their peaks (Lu et al., 2001). Western blotting revealed that CNOT7 decreased in the neurons to ~50% of pre-stimulation levels (Figure 2.6A). Immunocytochemistry of neurons fixed at 0 or 20 minutes post-glycine, revealed that the decrease in CNOT7 was more substantial in dendrites relative to cell bodies, 53% versus 29%, respectively (Figure 2.6B). The NMDA receptor antagonist MK801 prevented this in both the cell body and dendrites (Figure 2.7A).
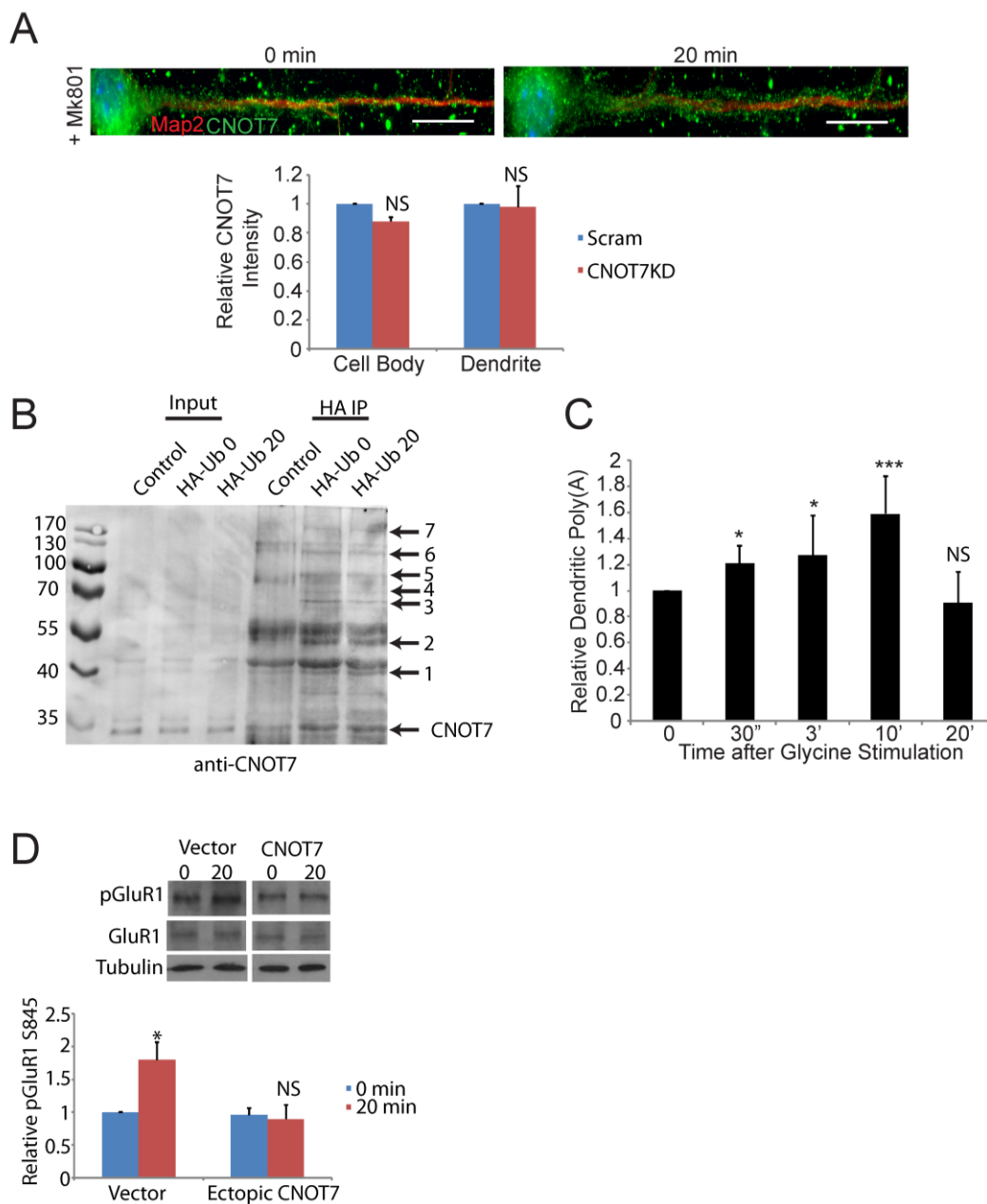
Figure 2.7. CNOT7 controls stimulation-induced changes in dendritic poly(A). (A) Representative images (top) and quantification (bottom) of CNOT7 (green) and Map2 (red) in neurons stimulated in the presence of MK801, an inhibitor of the NMDA receptor. The histogram shows the mean of ≥30 neurons/condition from 3 experimental replicates. (B) Western blot analysis of CNOT7 following HA immunoprecipitation from neurons expressing HA-tagged Ubiqutin, 0 (HA-Ub 0) or 20 minutes (HA-Ub 20) following glycine stimulation. Control lanes represent neurons not expressing HA-Ub. MG132 was added to all neurons for the same period of time. Arrow denotes expected size of CNOT7. Numbers denote putative CNOT7-ubiquitin conjugates. Band 1

size=37.8kDa (CNOT7-1Ub predicted size=41.5kDa), Band 2 size=49.2kDa (CNOT7-2Ub conjugate predicted size=50 kDa), Band 3 size=62.5kDa (CNOT7-3Ub predicted size=58.5kDa), Band 4 size=68.5kDa (CNOT7-4Ub predicted size=67kDa), Band 5 size=76kDa (CNOT7-5Ub predicted size=75.5kDA), Band 6 size=118kDa (CNOT7-10Ub predicted size=118kDa), Band 7 size=171kDa (CNOT7-16Ub predicted size=169kDa). Note that because both the HA and the CNOT7 antibodies are both mouse, the IgG band is present in all immunoprecipitate samples. (C) Bar graph representing the relative dendritic poly(A) signal in ≥ 30 neurons/condition from 3 experimental replicates stimulated and fixed at either 0, 0.5, 3, 10, and 20 minutes. All time points are plotted relative to the 0 time point. (D) Representative western blot images of phospho-GluR1 S845 (pGluR1), GluR1, and tubulin from neurons ectopically expressing either empty vector or CNOT7 0 min or 20 min following glycine stimulation. The histogram represents the average relative pGluR1 from three biological replicates. Error bars represent the standard error of the experimental replicates. *p≤0.05, **p≤0.01, ***p≤0.001, NS = not significant.

To determine whether this decrease in CNOT7 was due to ubiquitination, we expressed hemagglutinin-tagged ubiquitin (HA-Ub) in neurons, immunoprecipitated for HA, and western blotted for CNOT7. MG132 was added to all cells to inhibit the degradation of ubiquitinated proteins. Several CNOT7-ubiquitin conjugates were identified in the HA-Ub expressing cells (denoted with numbers in the figure) that were absent from control cells not expressing HA-Ub, indicating that CNOT7 is ubiquitinated in neurons (Figure 2.7B). Stimulation did not increase the abundance or number of these CNOT7-ubiquitin conjugates, however, this could be due to the presence of MG132 which inhibits the proteasomal machinery, vital for LTP induction (Alvarez-Castelao and Schuman, 2015).

Oligo(dT) FISH on neurons fixed at various times following stimulation, demonstrated that dendritic poly(A) increases to ~160% of pre-stimulation levels 10 min after glycine treatment (Figure 2.7C). Surprisingly, dendritic poly(A) then

decreases to pre-stimulation levels at the 20 minute time point, which coincides with when CNOT7 levels are at 50% of their pre-stimulation levels and when mEPSCs are at their peak (Lu et al., 2001) (Figure 2.7C).

The effect of glycine stimulation on dendritic poly(A) under normal conditions or upon CNOT7 depletion was examined. Figure 2.6C demonstrates that shRNA treatment resulted in a ~50% knockdown of CNOT7, which declined by an additional 50% upon glycine stimulation. In control (scrambled shRNA-infected) neurons, dendritic poly(A) increased at 10 minutes post-glycine but fell dramatically at 20 minutes. This same biphasic trend also occurred in CNOT7KD neurons, although the differences were not statistically different. This result is not surprising because the ~50% of control levels of CNOT7 present in these cells, is still under stimulation-induced regulation and sufficient to elicit mild changes in dendritic poly(A). Moreover, these reduced levels of CNOT7 are still adequate for glycine to promote modest LTP as assessed by phosphorylation of GluR1 and surface GluR1 immuno-staining (Figure 2.4).

To further investigate the importance of CNOT7 in stimulation-induced biphasic changes in dendritic poly(A), we ectopically expressed FLAG-tagged CNOT7 in neurons followed by glycine treatment (Figure 2.6D). CNOT7 levels were approximately double relative to those expressing only the vector (compare vector 0 and CNOT7 0). This high level of CNOT7 results in increased dendritic poly(A) (Figure 2.6D, Figure 2.2J). Glycine treatment caused destruction of

exogenous and endogenous CNOT7, but the total amount of CNOT7 remaining

was nearly identical to that observed in naïve (vector only expressing) cells.

Maintenance of this near-control level of CNOT7 inhibited the increase and

decrease in dendritic poly(A) at 10 and 20 min post-glycine treatment (Figure

2.6D). This near-control level of CNOT7 also impaired LTP induction as

measured by pGluR1 S845 (Figure 2.7D). These data indicate that rapid

stimulation-induced depletion of CNOT7 is necessary for stimulation-induced

changes in dendritic poly(A) and induction of LTP (Figure 2.6E).

CNOT7 regulates polyadenylation and stability of specific neuronal mRNAs
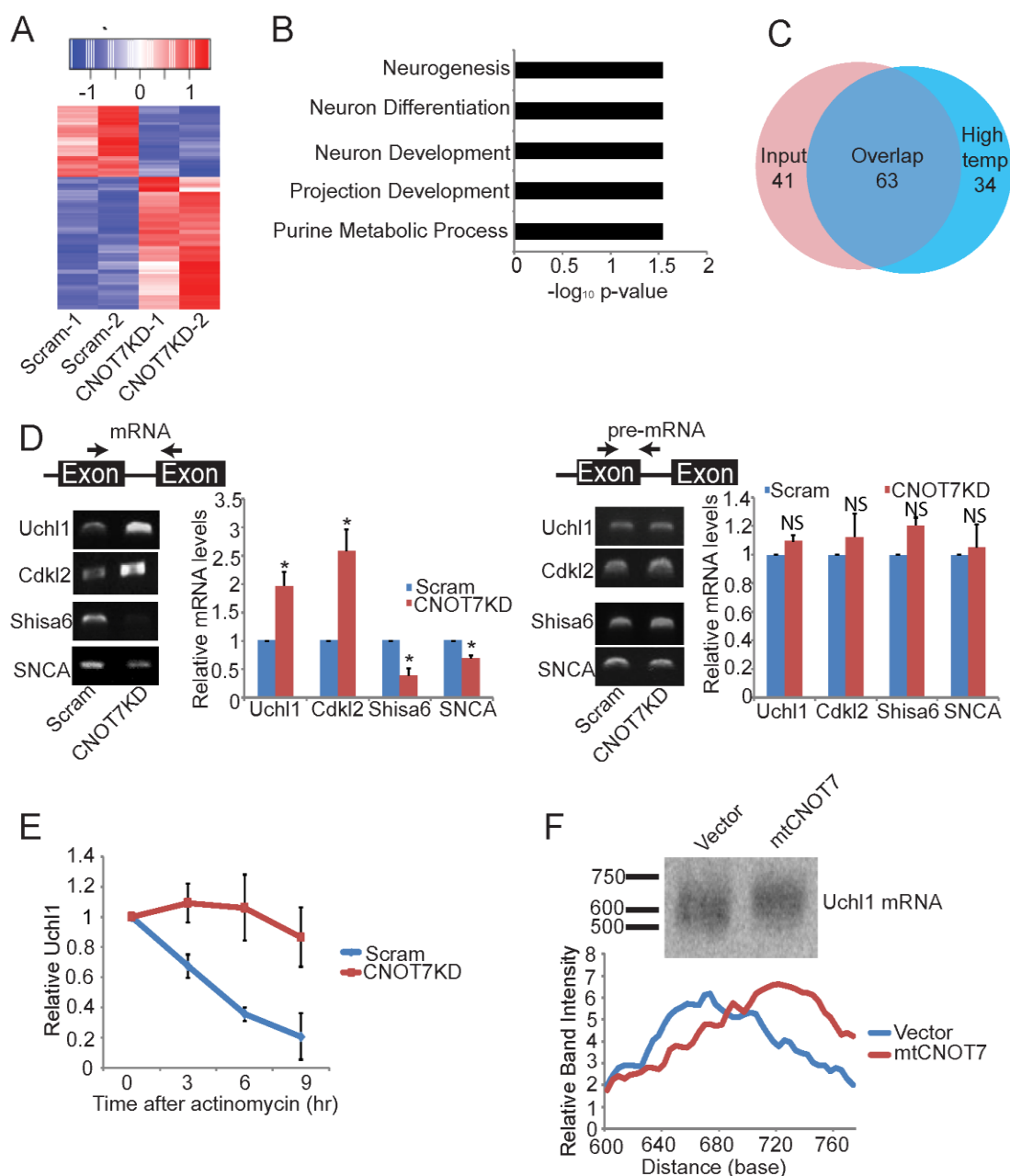
Figure 2.8. CNOT7 regulates poly(A) tail length and stability of specific mRNAs. (A) Heatmap of the 97 differentially expressed mRNAs eluted from poly(U) agarose at 75˚ (high temp)following CNOT7KD. (B) Bar graph representing the top 5 GO terms for the 63 mRNAs enriched in the high temperature samples following CNOT7KD. (C) Venn diagram of genes differentially expressed in either the input samples (pink) or the high temperature (blue) samples. (D) (Top) Diagram depicts placement of primers (arrows) to detect mature mRNA or pre-mRNA; black boxes represent the exons and lines represent the introns. (bottom) Representative gel images and quantification of 4 different mature mRNAs (Uchl1, Cdkl2, Shisa6, or SNCA) and their

corresponding pre-mRNAs in scrambled and CNOT7KD neurons. Bar graph depicts the average of three different experiments. (E) Quantification of Uchl1 mRNA in either scrambled or CNOT7KD neurons at the indicated time points following the addition of actinomycin D. The graph represents the average of two different experiments. (F) Representative northern blot analysis of Uchl1 in neurons ectopically expressing either empty vector or catalytically-inactive mutant CNOT7 (mtCNOT7). Line graph represents the Uchl1 band intensity relative to the intensity of each respective band at the 600 base mark.

We sought to identify specific CNOT7 target mRNAs. RNA from control or CNOT7KD neurons was incubated with poly(U) agarose; washed at 50˚C to elutes mRNAs with short (< 50 nucleotides) poly(A) tails (Du and Richter, 2005) (Figure 2.9A); and eluted mRNAs with longer poly(A) tails (>50 nucleotides) at 75˚C. Sequencing of the mRNAs with long poly(A) tails identified 97 that were differentially distributed between the scrambled and CNOT7KD samples (Figure 2.8A). Most of these (~65%) were enriched in the long tailed sample following CNOT7KD, suggesting that they could be direct targets of CNOT7. Gene Ontology term analysis (GO terms) indicated that many are involved in neural development and function (Figure 2.8B).

Many mRNAs from neurons depleted of CNOT7 that were disproportionately eluted from poly(U) at 75° also underwent alterations in their steady state levels as assessed by RNA-seq and RT-PCR (Figure 2.8C & D). We examined four RNAs that increased (Uchl1 & Cdkl2) or decreased (SNCA & Shisa6) in the poly(U) 75° elution fraction in CNOT7KD neurons. RT-PCR with primers spanning an exon-exon junction was used to assess predominantly cytoplasmic RNA, and primers spanning an exon-intron junction were used to

detect pre-mRNA, which serves as a proxy for transcription (Figure 2.8D).

Because RNA levels increased in CNOT7KD cells only when analyzed with

exon-exon primers, we infer that enhanced RNA stability was likely the cause of

the changes in transcript levels upon CNOT7 depletion (Figure 2.8D). To confirm

this, we examined Uchl1 (ubiquitin C-terminal hydrolase L1) RNA because

CNOT7 depletion elicited a large change in the apparent poly(A) tail size as well

its steady state RNA levels. Moreover, Uchl1 is an abundant mRNA that encodes

a protein involved in synaptic plasticity (Gong et al., 2006, Hegde et al., 1997).

To measure the decay rate of Uchl1 mRNA, control or CNOT7KD neurons were

treated with actinomycin D to inhibit transcription and cells were collected 0-9

hours later. Figure 2.8E shows that although there was little change in the Uchl1

RNA in CNOT7KD cells, the transcript underwent a steady decline in control

cells, confirming that this deadenylating enzyme mediates RNA instability.

Furthermore, ectopic expression of CNOT7 in CNOT7KD cells appeared to

partially rescue the increase in both Uchl1 and Cdkl2 mRNA, indicating that this

increased stability was due to CNOT7 depletion (Figure 2.9B).
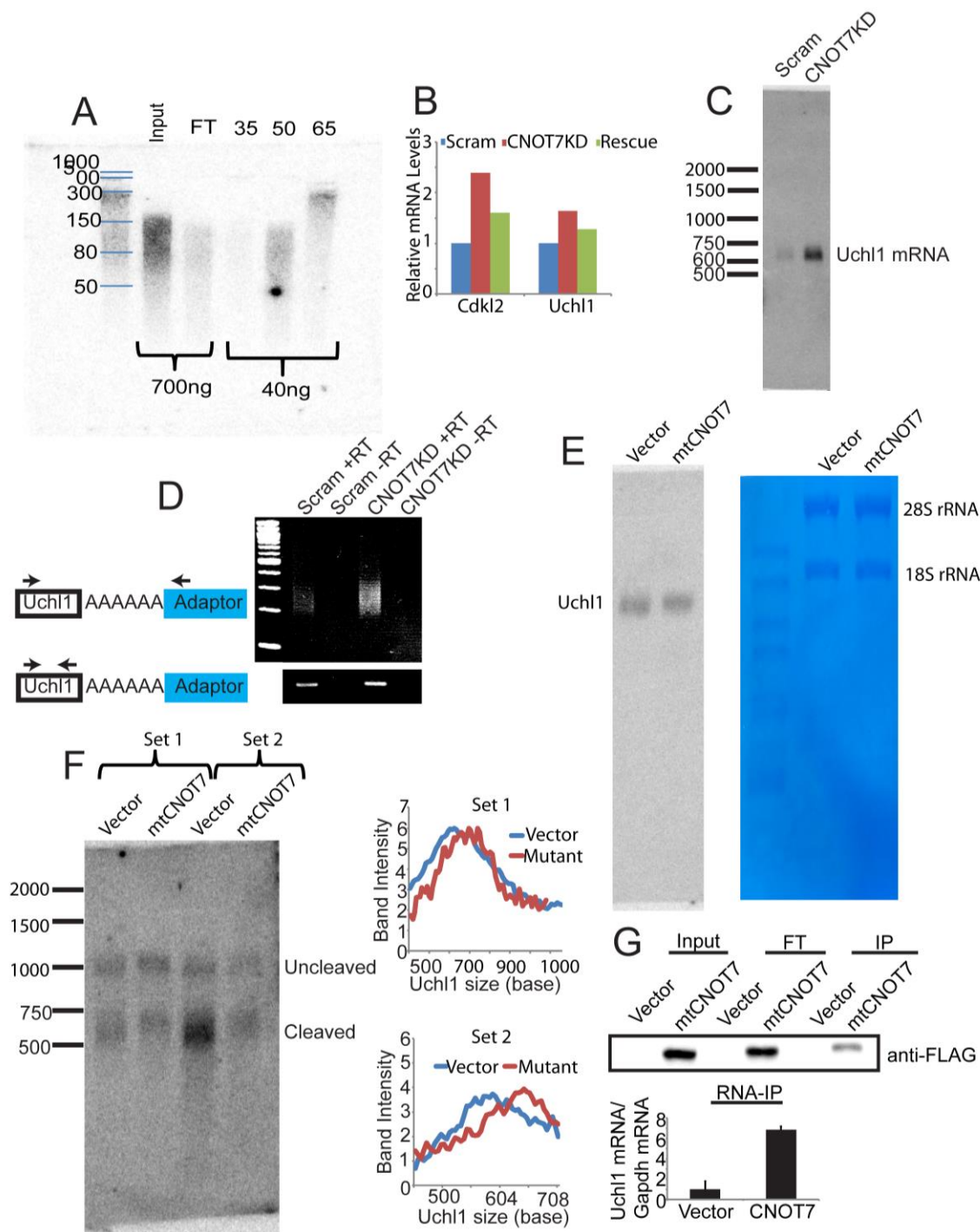
Figure 2.9. CNOT7 regulates the poly(A) tails of specific neuronal mRNAs. (A) Oligo(dT) northern blot of thermal elution samples collected at different temperatures. Seven hundred ng of input and flow-through (FT) and 40 ng of material eluted from the poly(U) agarose at either 35˚, 50˚, or 60˚ were analyzed by gel electrophoresis. (B) Histogram representing the relative mRNA levels of Uchl1 or Cdkl2 in either Scrambled, CNOT7KD, or Rescue (expressing both CNOT7

shRNA and ectopic CNOT7) neurons. (C) Northern blot analysis of Uchl1 mRNA in either scrambled (Scram) or CNOT7KD neurons. (D) PAT assay for Uchl1 in neurons expressing either scrambled control or CNOT7KD negative controls are included for each sample where no RT was added. A reverse primer in the adaptor was used to detect the polyadenylated Uchl1 (top blot), and for a control a separate PCR was performed to detect the Uchl1 3' UTR by using a reverse primer in the UTR (bottom). (E) Full length blot from Figure 2.8F (left) and methylene blue staining depicting the ribosomal RNAs (right) that display no shift in their band migration. (F) Blots represent Uchl1 mRNA in neurons ectopically expressing either empty vector or mutant CNOT7 (mtCNOT7) from two different sets of neurons. Both the cleaved and full length Uchl1 display shifts in their migration. Line graphs represent cleaved Uchl1 band intensity versus size. (G) (top) Western blot analysis of FLAG in cells expressing either empty vector (Vector) or FLAG-tagged mutant CNOT7 (mtCNOT7). Lanes 1 and 2 are input of each condition, 3 and 4 are flow-through (FT), and 5 and 6 are after immunoprecipitation and reversal of the crosslinking. (bottom). Histogram represents Uchl1 mRNA relative to GAPDH mRNA present in the RNA-IP from each condition. Error bars represent SEM from two separate experiments.

We attempted to assess Uchl1 RNA poly(A) tail size by northern blotting (Figure 2.9C) or with a RT-PCR based poly(A) tail-length assay (Figure 2.9D). The large increase in Uchl1 mRNA following CNOT7KD obscured any tail size changes. Because of the slower kinetics involved in ectopic expression of a dominant-negative catalytically-inactive form of CNOT7 (D40A), we suspected this method would allow us to detect Uchl1 after it gained a poly(A) tail but before it had time to accumulate due to increased stability (Figure 2.8E). Because Uchl1 is a large transcript (1156 bases), we annealed RNA from control and CNOT7 D40A-expressing neurons with an antisense oligonucleotide positioned 606 nucleotides from the 3' end, which was followed by RNAse H cleavage and northern analysis. Figures 2.8F, 2.9E, and 2.9F show that the Uchl1 median tail size lengthened from ~49nt to ~118nt following the D40A mutant expression. We also demonstrated that FLAG-mtCNOT7 interacts directly with Uchl1 mRNA by formaldehyde crosslinking, FLAG immunopecipitation, and RT-PCR for Uclhl1

and GAPDH mRNAs (Figure 2.9G). Wild-type CNOT7 was not used, because it

would increase deadenylation and likely degradation of Uchl1 RNA. These

results indicate that CNOT7 directly regulates the poly(A) tail length and overall

stability of Uchl1 and likely many other RNAs identified in Figure 2.8.

Differential localization and polyadenylation of CNOT7 targets following

long-term CNOT7 depletion
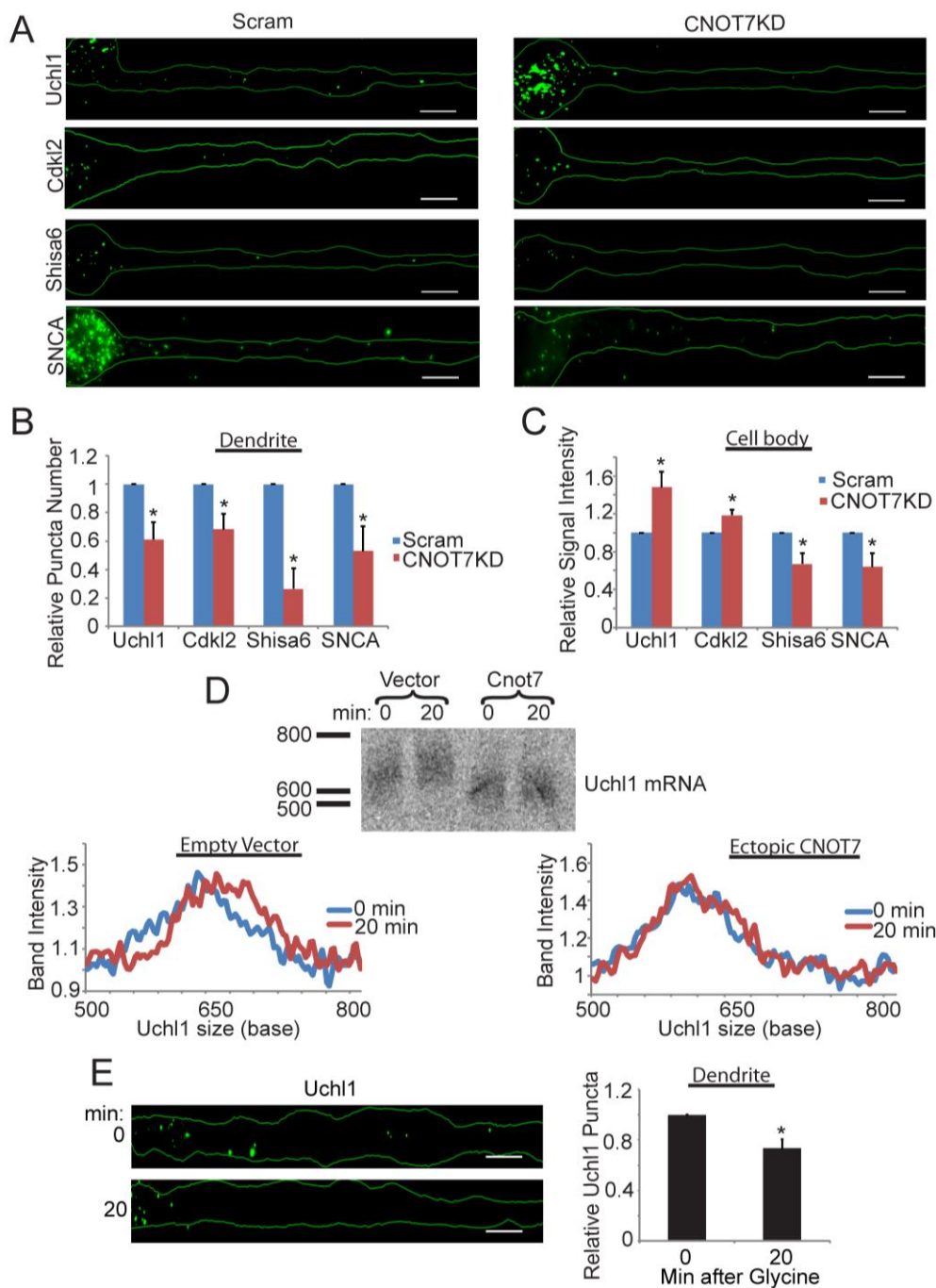
Figure 2.10. CNOT7 regulates its target's localization and poly(A) tail length. (A) Representative images of FISH for specific targets (Uchl1, Cdkl2, Shisa6, or SNCA) in scrambled or CNOT7KD neurons. Scale bars represent 10µm. Bar graphs represent the average quantification of either the relative number of dendritic puncta (B) or relative cell body signal intensity (C) for the specific targets in either scrambled (blue) or CNOT7KD (red) neurons. Bar graphs represent the average signal from ≥40 neurons/condition plotted relative to the scrambled control. (D) (top)

Northern blot of Uchl1 zero or twenty minutes following stimulation in either vector or CNOT7 expressing neurons. (bottom) Line graph represents the Uchl1 band intensity relative to the intensity of each respective band at the 500 base mark. (E) (left) Representative images for Uchl1 mRNA FISH in dendrites of neurons fixed either 0 minutes or 20 minutes following stimulation. (right) Bar graphs represent the average signal from ≥30 neurons/condition plotted relative to the 0 minute control.

Our data seem paradoxical: CNOT7 knockdown or ectopic expression of a catalytically-inactive protein causes a reduction in dendritic poly(A) when analyzed by oligo(dT) FISH (Figures 2.1 and 2.3), yet also results in increased poly(A) tail size and/or stability of specific RNAs (Figure 2.8). To resolve this issue, we repeated the FISH experiments but examined specific mRNAs whose poly(A) and/or stability is regulated by CNOT7 (Figure 2.8). Our reasoning was that a possible differential localization of specific RNAs would not be discernable by oligo(dT) FISH, yet could at least partially explain the loss of dendritic poly(A) upon CNOT7 knockdown. For these experiments we utilized the ViewRNA ISH kit, which utilizes ~20 oligonucleotide pairs/target and only when the oligo pairs bind side by side is there fluorescent signal. This provides high specificity to this technique. FISH for Uchl1 RNA in control and CNOT7KD neurons shows that CNOT7 depletion resulted in decreased Uchl1 puncta in dendrites but increased signal in the cell body (Figure 2.10 A, B, and C). The RNA encoding Cdkl2 (cyclin dependent kinase like 2) also shifted from a dendritic to a cell body localization following CNOT7 knockdown. Thus, RNAs that gain poly(A) and/or are stabilized by CNOT7 knockdown also accumulate in the cell body over the four days of knockdown, at the expense of decreased localization to dendrites. On the other

hand, SNCA (α–synuclein and Shisa6, two RNAs that had reduced poly(A) and/or steady state levels following CNOT7 knockdown, displayed decreased FISH signals in both dendrites and cell bodies (Figure 2.10A-C). We are confident these signals are specific, as they matched perfectly the changes we observed via qPCR (Figure 2.8C). CaMKIIα, (calmodulin-dependent kinase IIα) and PPIB (peptidylprolyl isomerase B) RNAs, whose poly(A) tail length and stability were not altered by CNOT7, exhibited no change in their localization upon CNOT7 depletion(Figure 2.11A). Control cells treated with all FISH reagents except for the targeting probe resulted in no detectable fluorescence (Figure 2.11B). Importantly, ectopic expression of CNOT7 caused an increase in dendritic localization of Uchl1 RNA (Figure 2.11C), opposite from what was observed in CNOT7 knockdown neurons. These data indicate that CNOT7 regulates dendritic localization of specific target RNAs.
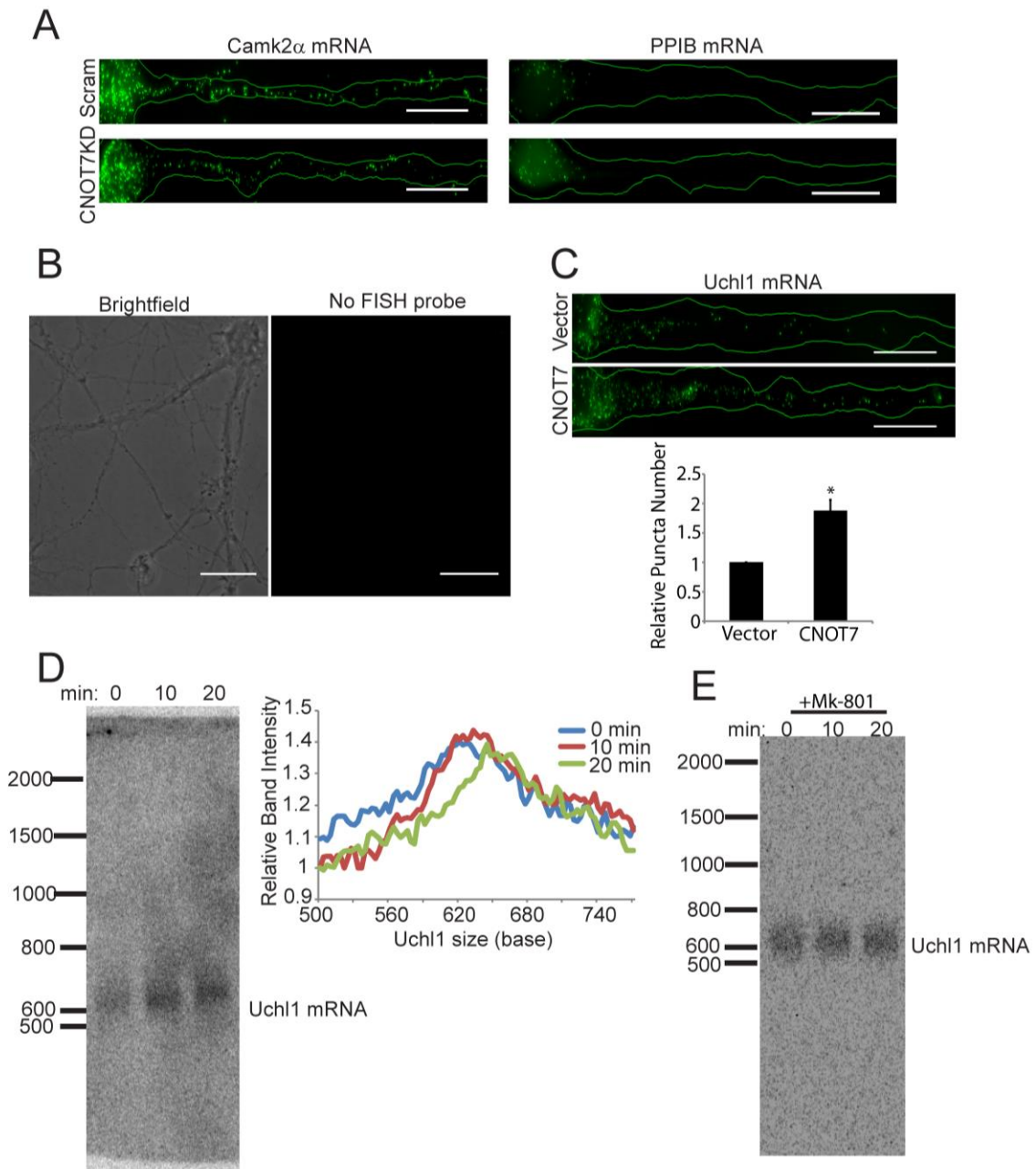
Figure 2.11. CNOT7 regulates dendritic localization and stimulation-induced changes in poly(A) for specific target RNAs. (A) Representative images of FISH analysis of CaMK2α (left) or PPIB (right) mRNA in either control (Scram) or CNOT7KD neurons. Scale bar represents 20μm. (B) Representative image of control FISH with no targeting probe added. Scale bar represents 20μm. (C) (top) Representative images of Uchl1 mRNA in neurons ectopically expressing either empty vector control or CNOT7. (bottom). The histogram represents the average relative number of dendritically localized Uchl1 mRNA puncta in neurons ectopically expressing either empty vector or CNOT7 (D) Northern blot analysis of Uchl1 mRNA collected either 0, 10, or 20

minutes following stimulation. Line graph represents the Uchl1 band intensity relative to the intensity of each respective band at the 500 base mark. Error bars represent SEM, *p≤0.05. (E) Northern blot analysis of Uchl1 mRNA collected either 0, 10, or 20 minutes following stimulation in the presence of a NMDA inhibitor Mk-801.

RNA from neurons (DIV17-19) collected 0-20 minutes following chem-LTP was used for northern analysis of Uchl1. Chem-LTP induced a gradual, NMDA-dependent increase in Uchl1 RNA poly(A) over the 20 minutes following stimulation (Figure 2.11D & E). To determine whether this polyadenylation is mediated by the rapid depletion of CNOT7 as suggested by the data in Figure 2.6, wild type CNOT7 was ectopically expressed in cultured neurons followed by chem-LTP. Ectopic CNOT7 prevented the glycine-induced increase in Uchl1 poly(A) (Figure 2.10D). We conclude that rapid destruction of CNOT7 is essential for stimulation-induced polyadenylation of target mRNAs. We next performed FISH for Uchl1 RNA in dendrites fixed at 0 or 20 minutes post-stimulation. Uchl1 RNA exhibited decreased dendritic localization in response to stimulation (Figure 2.10E). These data indicate that depletion of CNOT7 following stimulation could activate translation through lengthening of dendritic mRNA poly(A) tails and, over time (i.e. long-term depletion), inhibit translation by impairing localization of new mRNAs to dendrites. Because both long-term stimulation-induced depletion and CNOT7 knockdown have similar effects, we consider long-term depletion of CNOT7 to be 20 minutes to several days.

Depletion of CNOT7 in the hippocampus decreases poly(A) in the neuropil and impairs cognitive function
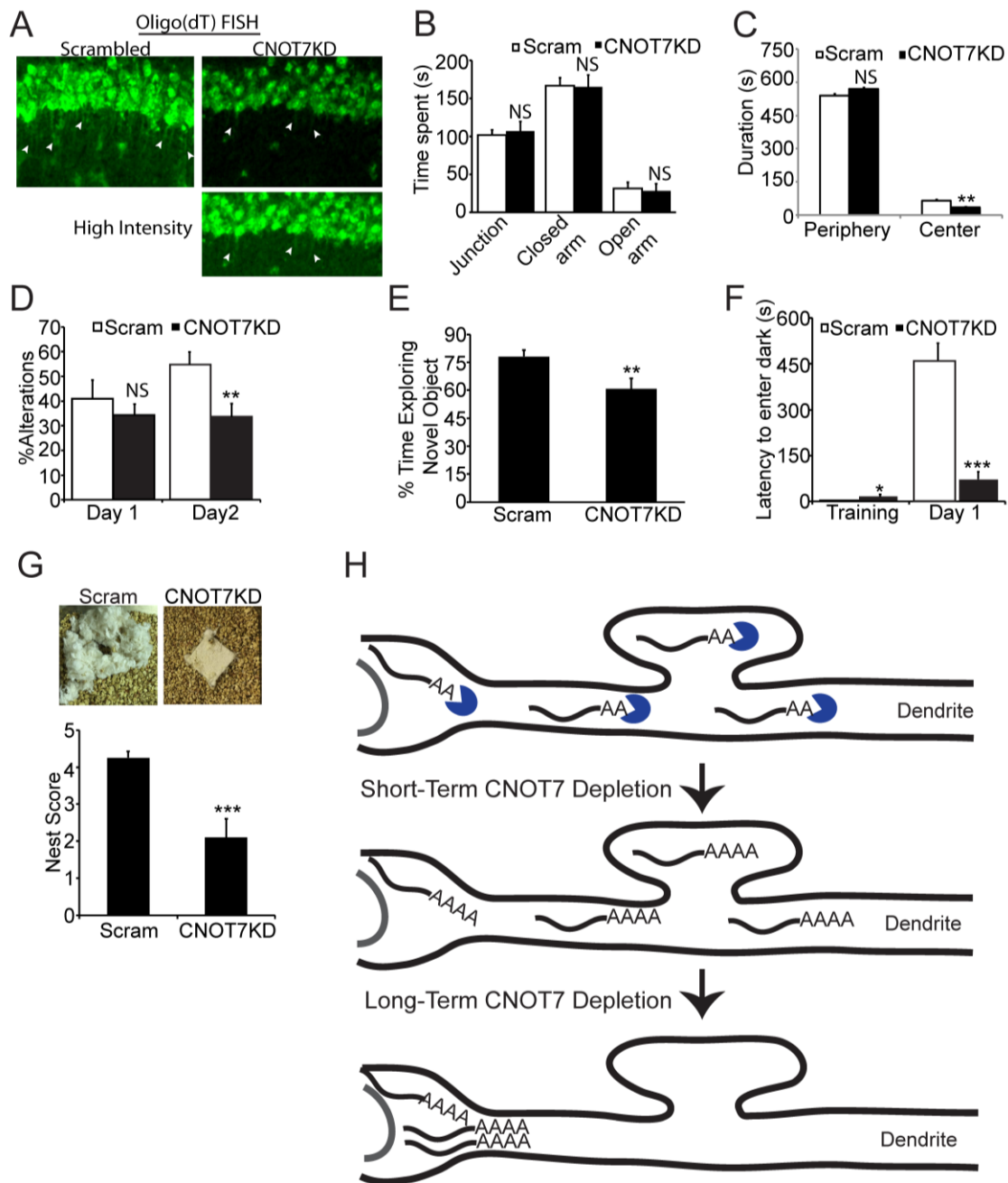
Figure 2.12. CNOT7KD in the hippocampus decreases poly(A) localization and impairs cognitive function. (A) Magnified images of oligo(dT) FISH signal in the CA1 neuropil of set 1 mice (Figure 2.13C) injected with either scrambled or CNOT7 targeting shRNA. White arrows show examples of neurite-localized signal. Bottom right image is the CNOT7KD image with brightness level

increased. (B) Bar graphs represent the average time (seconds) spent in the junction, closed, or open arms of an elevated plus maze (14 mice per condition). (C) Bar graph represents the average time in seconds spent in either the periphery or the center of an open field (14 mice/ condition). (D) Bar graph represents the percent alterations performed in a T-maze (8-10 mice/ condition). (E) Bar graph represents the percent time animals spent exploring a novel object (12-14 mice/ condition). (F) Bar graph represents the latency to enter the dark compartment either on a training day or 24 hours after a foot shock in the dark (10-12 mice/ condition). (G) Representative images (top) of nestlets from either scrambled or CNOT7KD mice. Bar graph (bottom) represents the average nest scores (10 mice/ condition). (H) Model of major CNOT7 activities in neurons. The top diagram depicts mRNAs throughout a dendrite and cell body whose poly(A) tails are shortened by CNOT7 (blue). The middle diagram depicts a dendrite shortly after CNOT7 depletion, which occurs during glycine-induced LTP. Dendritic mRNAs have lengthened poly(A) tails. The bottom diagram depicts a dendrite after long-term CNOT7 depletion, such as by shRNA-mediated knockdown or ≥ 20min following stimulation. CNOT7 target RNAs retain long poly(A) tails but transport to dendrites is impeded; RNAs extant in dendrites are likely degraded.

We injected AAV expressing either CNOT7-targeting or scrambled shRNAs into the hippocampus of wild type mice (Figure 2.13A). The CNOT7KD mice exhibited significantly reduced CNOT7 in the CA1 region (Figure 2.13B). Two CNOT7 target RNAs, Uchl1 and Cdkl2, were increased in CA1 of these mice (Figure 2.13B), indicating that *in vivo*, CNOT7 activity is similar to that observed in cultured neurons. Oligo(dT) FISH signal was detected in hippocampal CA1 dendritic projections emanating from the cell body of scrambled shRNA-injected mice (Figure 2.12A, arrows). However, there was a strong reduction in FISH signal in these projections in CA1 from the CNOT7 shRNA-injected mice (Figure 2.12A). The average oligo(dT) signal in the neuropil relative to the corresponding somatic region was reduced by ~40%, indicating impaired dendritically localized poly(A) *in vivo* (Figure 2.13C).
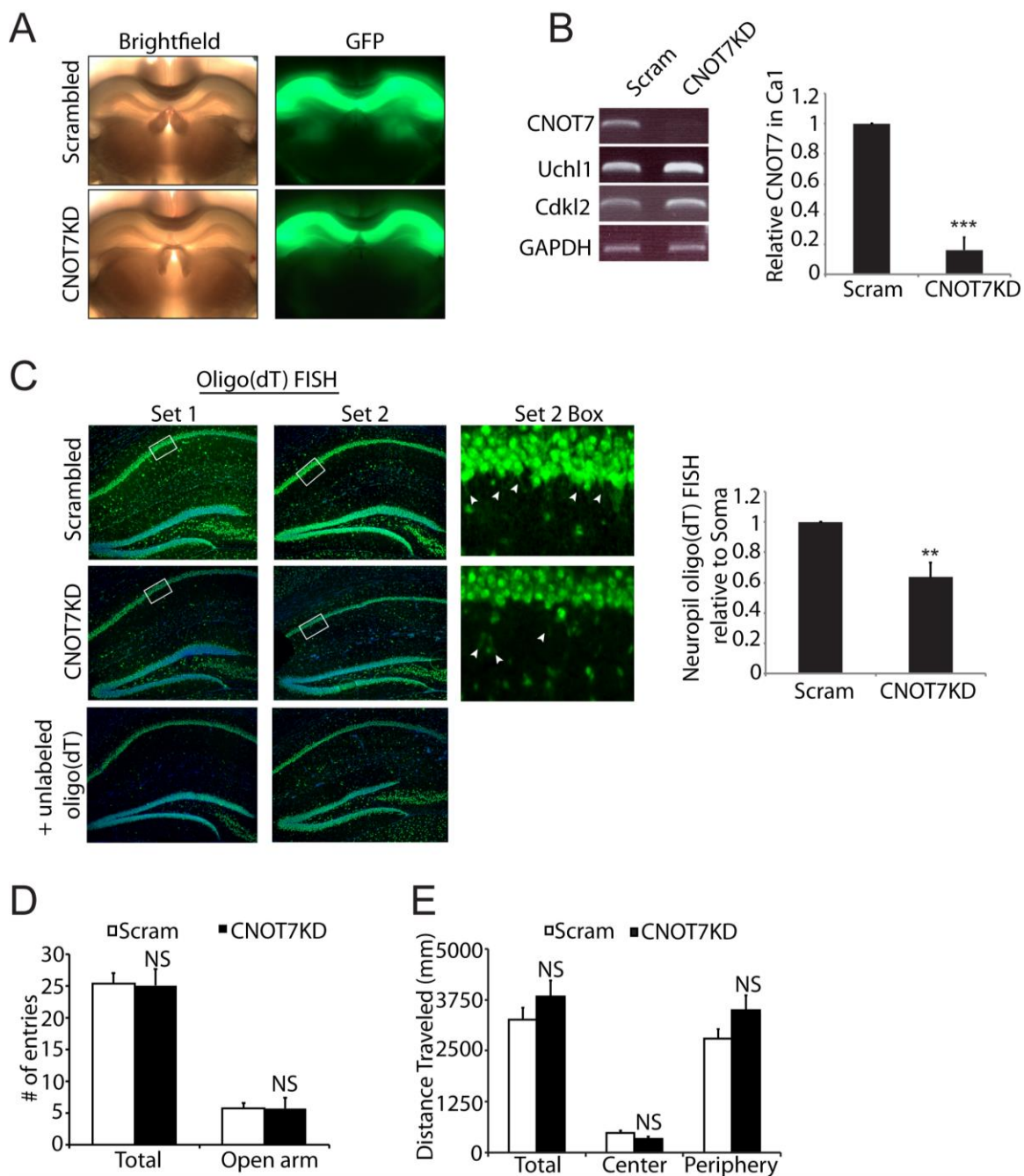
Figure 2.13. CNOT7KD in the hippocampus decreases neuropil-localized oligo(dT) FISH signal without altering locomotor activity. (A) Brightfield and GFP images from scrambled or CNOT7KD mice depicting the region of the brain injected with virus. (B) RT-PCR analysis of CNOT7, Uchl1, Cdkl2, and GAPDH RNAs from control and CNOTKD hippocampus. The histogram represents the average CNOT7 levels in the CA1 region from mice injected with scrambled or CNOT7 targeting shRNA, n=3. (C) 10X images of oligo(dT) FISH (green) and DAPI (blue) signal in the CA1 region from two different sets of injected mice. Images on the far right are highly magnified images of

the boxed area depicted in set 2 images. White arrows show examples oligo(dT) FISH signal in neurites. Bar graph represents the average intensity of oligo(dT) FISH signal in the neuropil relative to the soma area (n=2). (D) Bar graph depicting the average number of total entries or entries into the open arm CNOT7KD and Scrambled control mice made in an elevated plus maze. (E) Bar depicting the average distance traveled in an open field by CNOT7KD or scrambled control mice. n=14 for each test. Bars represent mean $\pm$ SEM. Error bars represent SEM, **$p \leq 0.01$, ***$p \leq 0.001$, NS = not significant.

We next tested the AAV-injected mice for anxiety by the elevated plus maze (EPM) and the open field test (OFT). For the EPM, mice choose to spend time in the closed or open arms of an elevated platform. More time spent in the closed arms indicates increased anxiety. CNOT7KD mice spent equal time in the closed arms as the scrambled controls (Figure 2.12B). The OFT, which measures the time mice spend in the center of an open field, showed that CNOT7KD mice spent 50% less time (31s vs 62s) in the center compared to control mice (Figure 2.12C). These results are not due to decreased locomotor activity as distance traveled in the open field test and the total number of entries into the arms of the elevated plus maze were comparable between groups (Figure 2.13D & E).

We used several assays to measure working (short term) and long-term memory. Working memory was assessed using the T-maze, where the spontaneous alternations of mice are measured in a T-shaped apparatus. On the habituation day one, the percent alternations were comparable between both sets of mice. On day 2, CNOT7KD mice had significantly decreased alterations compared to controls (33.6% vs 54.7%), indicating impaired working memory

(Figure 2.12D). Long-term memory was assessed using two assays: novel object recognition and passive avoidance. In novel object recognition, mice were placed in an arena with a novel object and a familiar object. Mice that remember the familiar object spend more time with the novel object. CNOT7KD mice spent 61% of their time exploring the novel object compared to 78% for the control animals (Figure 2.12E). In the passive avoidance assay, mice were placed in a light chamber connected to a dark chamber by a door. The mice prefer the dark and immediately enter the dark chamber, after which the door closes and the mice were given a mild foot shock. Twenty-four hours later the mice were placed back in the light chamber and the latency to enter the dark was measured, with a longer latency indicating memory of the foot shock. Control animals had an average latency of 459 seconds while CNOT7KD animal latency was only 72 seconds (Figure 2.12F). Nest building was also impaired in CNOT7KD animals (Figure 2.12G). Increased anxiety, impaired learning and memory, and impaired nest building are shared features of various autistic models, which could suggest a role for CNOT7 in this disorder.

Discussion

This study identifies CNOT7 as a coordinator of mRNA transport and translation in dendrites and does so by modulating RNA poly(A) tail length and stability. Figure 2.12H shows a model that depicts some of the most salient activities of this enzyme in neurons. Although it is expressed throughout the cells,

CNOT7 has a particularly important function in dendrites. In response to synaptic stimulation, it is gradually destroyed. This leads to polyadenylation of specific dendritic mRNAs and is likely followed by a burst of translation in dendrites (Udagawa et al., 2012). Twenty minutes after stimulation, the localization of these specific polyadenylated mRNAs are decreased in dendrites resulting in reduced overall dendritic poly(A), which is caused by the destruction of CNOT7. This event is recapitulated when CNOT7 is knocked down for 4 days, indicating stimulation-induced long-term (20 minutes) depletion of CNOT7 and shRNA-mediated knockdown *in vivo* for several days result in similar outcomes. When CNOT7 is depleted for 4 days, the enzyme's target RNAs become more stable and are mostly confined to the cell body. The dendritic RNAs, at least in part, are then destroyed, resulting in decreased protein synthesis. Two additional events occur upon prolonged CNOT7 knockdown *in vivo*: reduction of poly(A) in CA1 dendrites and a decline in the performance in several cognitive tasks, indicating impaired learning and memory.

We were unable to confirm a physical link between CPEB1 and CNOT7 as shown by Ogamai et al (2014), and consequently surmise that these proteins act independently, probably on unique sets of mRNAs to control poly(A) tail length and translation in dendrites. CPEB1 requires a 3' UTR cytoplasmic polyadenylation element (CPE) to affect polyadenylation. The RNAs whose poly(A) tails are controlled by CNOT7, at least as identified by differential thermal elution from poly(U) beads, are not enriched for this element relative to total

RNA. How CNOT7 might be tethered to specific RNAs such as Uchl1 is unknown but it may involve RNA binding proteins. These RNA binding proteins are likely unique to CNOT7 because depletion of CNOT8, the CNOT7 paralogue, has no obvious effect on dendritic poly(A) or chem-LTP. In non-neuronal cells, CNOT8 apparently compensates for the loss of CNOT7 (Aslam et al., 2009, Doidge et al., 2012a), which we do not observe. Of course, CNOT8 or other deadenylating enzymes such as PARN or PAN2 (Udagawa et al., 2015) could modulate poly (A) tail length in dendrites, but a consequential change in synaptic efficacy may not necessarily occur.

CNOT7 regulates a dynamic translational landscape in neurons and thus has multiple roles in RNA expression and consequent changes in synaptic function. For example, soon after glycine activation of LTP (≤10 min), CNOT7 levels are moderately reduced, resulting in polyadenylation of target RNAs in dendrites. At longer times (≥20 min) after treatment with glycine, substantial CNOT7 destruction takes place, which evokes further polyadenylation and a reduction in transcript level in dendrites. This effect of long-term CNOT7 depletion is more dramatically evident when CNOT7 is depleted for 4 days by treatment of neurons with an shRNA. Such time-dependent effects of CNOT7 at least partially explain the bimodal changes in dendritic poly(A) and translation that occur after synaptic stimulation.

The key event that mediates this mRNA regulation is CNOT7 reduction within the twenty minutes following synaptic activity. The half-life of CNOT7 is greater than 6 hours, making it likely that this reduction is predominantly due to destruction of CNOT7 (Cano et al., 2015). Some evidence suggests that a reduction of CNOT7 takes place with other types of stimulation in cultured neurons (Schanzenbacher et al., 2016) and even during learning and memory in living animals (Cho et al., 2015). Although it is clear from our data that CNOT7 is rapidly destroyed upon LTP induction, reduced CNOT7 synthesis may also occur at this time. CNOT7 destruction is most likely mediated by the ubiquitin-proteasome system, which is known to regulate synaptic function and the dendritic proteome (Lee et al., 2012, Huang et al., 2015, Hegde, 2016, Alvarez-Castelao and Schuman, 2015).

Depletion of CNOT7 from the hippocampus results in deficient short and long term memory, which may be causally linked to the decreased poly(A) in the CA1 neuropil we observed following knockdown. It was recently demonstrated that contextual fear learning in mice correlated with a significant decrease in the translational efficiency of several mRNAs including that for CNOT7 (Cho et al., 2015). This decrease occurred within five minutes and was moderately maintained for up to four hours. However, the entire hippocampus was analyzed and not just the neurite-rich neuropil, which our data suggest would be the region where CNOT7 levels would decrease most dramatically. Taken together these data indicate that the changes we observed in cultured neurons may represent

similar events that occur during learning in the living animal, and that dynamic control of CNOT7 destruction may regulate dendritic translation and higher cognitive function.

Material and Methods

<u>Mouse Maintenance</u>

Mouse protocols were reviewed and approved by the institutional animal care and use committee (IACUC) and all colonies were maintained following animal research guidelines. Only C57Bl/6 wild-type mice were used in this study with the ages indicated for each experiment in the method details.

<u>Primary Hippocampal Neuron Culture</u>

For primary cultures, hippocampi from embryonic day 18.5 mice were dissected and dissociated with 0.25% trypsin for 15 min at 37°C. Neurons are plated on poly-L-lysine coated plates in plating media (Neurobasal media with 10% horse serum and 1% Antibiotic-Antimycotic). Plating media is changed to culture media (Neurobasal with 1% Glutamax, 1% Antibiotic-Antimycotic, and 2% B27 supplement) one hour after plating. Media was half changed every 3-5 days.

<u>Cell Culture</u>

HEK 293T cells were used for lentiviral production and RNA-IP. Cells were maintained in DMEM with 10% FBS and 1% Antibiotic-Antimycotic.

Method Details

Hippocampal Neuron Culture and Drug Treatments

Hippocampal neurons were cultured and maintained exactly as described in (Huang and Richter, 2007). For chem-LTP, 17-19 days *in vitro* (DIV) hippocampal neurons were incubated in pre-warmed ACSF (140mM NaCl, 1.3mM $CaCl_2$, 5mM KCl, 25mM HEPES, 33mM glucose, 0.5mM tetrodotoxin, 1μM strychnine, 20μM bicuculline) for 20 minutes at 37°C. For control cells, 1μM MK-801 (Sigma) was added to the ACSF for 20min prior to the addition of glycine. Artificial cerebrospinal fluid (ACSF) was removed by aspiration and replaced with pre-warmed ACSF plus 200μM glycine. After a 3 min incubation, the ACSF was replaced with fresh pre-warmed glycine-free ACSF and incubated for the indicated time points before the cells were either fixed for imaging or isolated for protein or RNA extraction (Lu et al., 2001). Fifty μM MG132 (Sigma) was added to neurons with the glycine in the experiments indicated. After glycine washout, MG132 remained in the ACSF for the indicated time points. For control cells, Mg132 was added for the same total amount of time as the longest time point following stimulation (23min). Actinomycin D (Sigma) was added to DIV 17-19 hippocampal neurons at a concentration of 2.5μg/mL. The neurons were collected for RNA extraction at the indicated time points after the addition of actinomycin.

Western Blotting

To collect total protein, hippocampal neurons were disrupted by sonication in RIPA buffer (50mM Tris-HCl pH 8.0, 1% NP-40, 1% sodium deoxycholate, 150mM NaCl, 1mM EDTA, 1mM NaF, 1mM DTT, 1mM phenylmethylsulfonyl fluoride (PMSF), and 1mM Na_3VO_4). To isolate synaptosomal protein, hippocampi were isolated from 10, 40 day-old mice and homogenized in 3mL of homogenizing buffer (0.32M sucrose, 1mM EDTA, 1mg/mL BSA, 5mM HEPES pH 7.4). The homogenate was centrifuged for 10 min at 4°C at 3000g. 50μL of the supernatant was collected and saved to represent input protein. The supernatant was transferred to two microcentrifuge tubes and centrifuged again at 14000g for 12min at 4°C. Each pellet was resuspended in 110μL of Kreb's Ringer Buffer (14mM NaCl, 3mM KCl, 5mM glucose, 1mM EDTA, 10mM HEPES pH 7.4) and 90μL of Percol (Sigma) was added to each tube. The mixture was centrifuged for 2 min at 14000g and 4°C and the bottom Percol layer was removed and replaced with 200μL of Kreb's Ringer Buffer. The mixture was centrifuged for 30 seconds at 14000g and 4°C; the pellet comprises the synaptoneurosome. All liquid was removed and the pellet was resuspended in 200μL of HEPES-Kreb's Buffer (147mM NaCl, 3mM KCl, 10mM glucose, 2mM $MgSO_4$, 2mM $CaCl_2$, 20mM HEPES pH 7.4).

Five (to detect CNOT7, PSD95 and pGluR1) or 14 (to detect GluR1) μg of protein was loaded onto a 6 or 12% gel, depending on the protein of interest. Western blotting was carried out using standard procedures with the following antibodies:

CNOT7 1:500 (Novus), GluR1 1:500 (Calbiochem), pGluR1 S831 1:500 (Millipore), pGluR1 S845 1:500 (Millipore), PSD-95 1:1000(Transduction Laboratories), GFAP 1:10,000 (Cell Signaling), tubulin 1:100,000 (Sigma), anti-HA.11 monoclonal 1:500 (Biolegend).

Immunocytochemistry

Hippocampal neurons were grown on coverslips, permeabilized with 0.1% Triton-X-100, fixed with 4% paraformaldehyde (PFA)/4% sucrose, blocked with 10% bovine serum albumin, and immunostained for CNOT7 1:100, Map2 1:500 (Millipore), tubulin 1:1000 or GluR1 1:10. Surface staining of GluR1 was performed as described above except without permeabilization. Images were acquired with a Zeiss Axiovert 200M microscope and a Hammatsu ORCA-ER camera using a 100X oil objective. The Z stack maximum projection images as well as the straightened dendrites were obtained using Image J software. To quantify fluorescence intensity, a 20 pixel wide line that was either 100 pixels long (cell body) or 1800 pixels long (dendrite) was drawn over the desired cell region and the fluorescence intensity under this line quantified.

shRNA design, Site-directed Mutagenesis, and Lentivirus production

Plasmids and lentiviruses were made using standard procedures with custom designed oligonucleotides described below. To generate mRNA-specific shRNAs, a CNOT8-specific oligonucleotide (GAGGAGGAAGGGATCGATA) or CNOT7-specific oligonucleotides (shRNA 1: GGATCTGACTCACTGCTTA or

shRNA 2: GGAGAATACCCTCCAGGAA) were annealed and ligated into the pll3.7-Syn vector. For ectopic expression assays, full length mouse CNOT7 was ligated into the FUGW lentiviral vector. Site-directed mutagenesis of CNOT7 was carried out using the Phusion High-Fidelity PCR Mastermix (NEB) and two specific primers (GTTGCTATGGCCACCGAGTTTCC, GGAAACTCGGTGGCCATAGCAAC) with an annealing temperature of 60° and an extension time of five minutes. Viral plasmids in addition to an envelope and empty backbone packaging vector (pMD2.G and psPAX2) were transfected into HEK cells using calcium phosphate precipitation and the virus containing media collected three days later. 1x10^5 TU/mL pLenti puro HA-ubiquitin lentiviral prepreparation (Addgene) was added to neurons. Neurons were infected with virus at DIV 13-15.

Fluorescent In-Situ Hybridization (FISH)

Oligo(dT) FISH was performed as described in Swanger et al 2011 (Swanger et al., 2011) with a 50-mer oligo(dT) probe labeled with Cy5 using the Cy5 Mono-Reactive Dye Pack (GE) according to the manufacturer's instructions. 20μg of Salmon Sperm DNA and 20μg of tRNA were speed vacuumed and resuspended in 15μL of 30% formamide/2X Sodium Citrate Buffer (SSC). Probe mixture was heated to 90°C for 5 min and placed on ice to cool. 15μL of hybridization buffer (10mg dextran sulfate, 5mg Bovine Serum Albumin, 100μL ribonucleoside vanadyl complexes, 2X SSC, and 1mM Phosphate Buffer) is added to make pre-

hybridization solution. Neurons are fixed in 4%PFA/4% Sucrose for 20min and

washed with 1X PBS/5mM $MgCl_2$. Coverslips with neurons are placed in 1X SSC

for 10min and equilibrated for 5 min in 15% formamide/1X SSC. 30μL of pre-

hybridization solution is placed on each coverslip and incubated at 37°C for 1

hour. Hybridization solution is prepared exactly like prehybridization solution

except with the addition of 25ng of the Fluorophore labeled Oligo(dT) probe.

Hybridization solution is added to coverslips and incubated for 3 hours at 37°C in

the dark. Coverslips are washed twice in prewarmed 15% formamide/1X SSC for

20 min. Coverslips are then washed five times in 1X SSC and once with 1X

PBS/5mM $MgCl_2$. Coverslips are post-fixed with 4%PFA\4% Sucrose for 5 min

then washed 3 times in 1X PBS. Coverslips are mounted to slides with 10μL of

Prolong Gold with Dapi. Pepsin digestion was performed as described in

(Buxbaum et al., 2014) except with 0.05mg/mL pepsin for 45sec on ice. Pepsin

treatment was performed after fixation step in the FISH protocol. To perform

oligo(dT) FISH on hippocampal slices, mouse brains were flash frozen in OCT

and placed into -80°C. Twenty-five μm sections were taken throughout the

hippocampus and kept at -20°C until staining. Sections were fixed in 4%PFA/4%

Sucrose for 15min at room temperature then washed twice with 2X SSC for 5

min each. Slices were then equilibrated in 0.1M Triethanolamine-HCl pH 8.0 for

5min, followed by a 10min incubation with and Acetic anhydride mixture (50mL

0.1 Triethanolamine-HCl, 750μL Acetic Anhydride). Sections were washed with

ice cold water and incubated with an ice cold methanol/acetone mixture (50%

methanol, 50% acetone). Sections were washed twice with ice cold 2X SSC

before being placed in a moisture chamber and incubated with Hybridization

buffer (4X SSC, 1X Denhardts, 10% Dextran Sulfate, 0.5μg/mL Sperm DNA,

0.25μg/mL tRNA) for 2 hours at 37˚C. Five hundred nanograms of labeled

oligo(dT) is added to 1mL of hybridization buffer and incubated with the slices

overnight at 37˚C. For a negative control 100X more unlabeled oligo(dT) is added

to the slices to compete out the labeled oligo(dT) and reduce the signal. The next

day slices are washed twice with 2X SSC at room temperature and mounted with

Prolong Gold with Dapi. For FISH of specific targets, the ViewRNA ISH

(Affymetrix) kit was used according to manufacturer's instructions except the

protease step was omitted and the working probe sets were incubated for four

hours instead of three. All solutions used RNAse-free water. Pixel intensity or

number of punctate in the cell body or the distal dendrite (40-100μm from cell

soma) was measured from the combined maximum projection Z stack images

using Image J as described above. All microscope and brightness settings were

kept constant for all images taken in one experiment using the same microscope

setup described above. Fluorescence intensity in both the cell body and the

dendrites were maintained within the linear range of the Hammatsu ORCA-ER

camera.

Fluorescent Non-Canonical Amino Acid Tagging (FUNCAT)

FUNCAT was performed as described in Dietrich et al, 2010 (Dietrich et al., 2010) using the Click-iT kit (ThermoFisher). Briefly, hippocampal neurons were incubated for 30 minutes at 37° in methionine-free DMEM supplemented with 2% B27, 1% Glutamax, and 1% antibiotic/antimycotic to deplete methionine stores. L-azidohomoalanine (AHA) was then added to a final concentration of 25 μM and cells were incubated for an additional hour. For control cells, cycloheximide was added 15 minutes prior to the addition of AHA to a final concentration of 100μg/mL. Cells were then fixed with 4% PFA and the FUNCAT reaction was carried out according to the manufacturer's protocol. For nocodazole treatment, 30μM nocodazole was added to the neurons one hour prior to the addition of AHA. Images were obtained and fluorescent intensity analyzed as described above.

Poly(U) Chromatography, Thermal Elution, and Sequencing

RNA was extracted from cultured neurons with Trizol and denatured in CSB Buffer (25% formamide, 700mM NaCl, 50mM Tris-Cl pH 7.5, and 1mM EDTA). Forty micrograms of total RNA was incubated with 0.025g of poly(U) agarose (Sigma) for 1-2hrs. The agarose was then washed with room temperature LSB buffer (25% formamide, 0.1M NaCl, 50mM Tris-Cl pH 7.5, 10mM EDTA) which should leave only polyadenylated mRNA bound to the beads. To elute mRNAs with poly(A) tails shorter than 50nt (Du and Richter, 2005, Udagawa et al., 2012), the agarose was washed again with LSB buffer warmed to 50°C (this step was

omitted in the total RNA samples). mRNA was then eluted with LSB buffer warmed to 75°C. Sequencing libraries were prepared from 50 ng of polyadenylated mRNA using the NEXTflex qRNA-Seq Kit v2. Paired-end sequencing was performed using a HiSeq 2000 instrument. Sequences were mapped to the mm10 genome using Tophat, and to the transcriptome using RSEM. Differential expression was analyzed using DESeq2 in R (R Core Team, 2016) on transcripts with over 10 reads with an adjusted p-value cutoff of 0.01. The heatmap was made using R .The WebGestalt Analysis Toolkit (Zhang et al., 2005) was used to identify the Gene Ontology (GO) terms significantly enriched in differentially expressed genes.

Immunoprecipitation

For HA-ubiquitin immunoprecipitation, ~1.5 million neurons were collected/condition in 1mL of ice cold PBS-NaF (1mM) following the indicated treatments. Cells were centrifuged at 6000rpm for 3 min and resuspended in 250μL of NP40 IP Buffer (25mM HEPES-KOH pH 7.5, 150mM NaCl, 10% glycerol, 1mM $MgCl_2$, 1% NP-40, 1mM DTT, 100U/mL RNAseOut, 1mM NaF, 1mM PMSF, 1mM Na_3VO_4). Cells were incubated in NP40-IP buffer for 30 min on ice at 4°C, and 10% of the lysate was saved for input. Twenty-five μL of Dynabeads Sheep Anti-Mouse IgG were incubated with 2μg of anti-HA.11 antibody (Biolegend) and allowed to rotate at 4°C for 1 hour. Beads were washed with NP40 IP buffer and added to the cell lysate. Beads and lysate were rotated

overnight at 4°C. The beads were washed in low Triton wash buffer (25mM HEPES-KOH pH 7.5, 150mM NaCl, 10% Glycerol, 1mM MgCl2, 0.05% Triton) four times before being resuspended in 25μL of 1X SDS loading buffer. The beads were boiled at 95°C for 3 min and supernatant containing protein was collected.

For protein/RNA immunoprecipitation, HEK293T cells transduced with lentivirus expressing mtCNOT7-FLAG or empty plasmid were cross-linked with 0.5% formaldehyde for 10 minutes at room temperature. The formaldehyde cross-linking was stopped by adding 125mM glycine pH 7.0 for 5 minutes at room temperature. Cells were washed twice with ice-cold PBS, resuspended in RIPA buffer (50 mM Tris-HCl p 7.5, 1% (v/v) NP-40, 0.5% (w/v) sodium deoxycholate, 0.1% (w/v) SDS, 1 mM EDTA, 150 mM NaCl, cocktail of protease inhibitors and RNase OUT), and disrupted by sonication on ice 4 times for 15 seconds with amplitude 7. The insoluble fraction was removed by centrifugation at 16,000 x g for 10 minutes at 4C and the supernatant was pre cleared with anti-mouse IgG Dynabeads for one hour at 4°C supplemented with 200μg of tRNA and 40 μg/mL of salmon sperm DNA. After that the pre-cleared extract was incubated with 5μg of anti-FLAG antibody overnight a 4°C. The antibody-bound complexes were recovered using anti-mouse IgG Dynabeads, previously blocked with 0.5% BSA, 0.1 mg/mL tRNA and 0.1 mg/mL glycogen, and washed 5 times with RIPA buffer supplemented with 1M urea. The cross-linking was reversed by resuspending the

beads in 130 uL of reversal buffer (50mM Tris-HCl pH 6.8, 5 mM EDTA, 10 mM DTT and 1% SDS) and incubating at 70°C for 2 hours. The RNA was then extracted with Trizol and used for cDNA synthesis followed by RT-PCR.

RNA Collection and RT- PCR

All RNA was collected using Trizol (Life Technologies). The Quantitect Reverse Transcription Kit (Qiagen) was then used to synthesize cDNA. All primer sets were tested by comparing the PCR product after at least three different number of amplification cycles to identify which cycle number was in the linear range and should therefore be used for experiments. All primer sets targeting mature mRNAs were designed to span an exon-exon junction. To identify pre-mRNA semiquantitave PCR was performed exactly as above except with primer sets spanning an exon-intron junction.

RNAse H and Oligo(dT) Northern Blotting

For the RNAse H northern blotting, 2-5 μg of total neuronal RNA and 600ng of an Uchl1 specific oligonucleotide (CGAAACACTTGGCTCTATCT) were denatured at 75°C for 5 min in a 19 μL reaction containing 2μL of RNAse H 10X buffer (NEB). 0.5μL of RNAse H (NEB) and RNAseOUT (Invitrogen) were added and the 20μL reaction was incubated at 37° for one hour.

For the oligo(dT) northern, 3μg of total neuronal RNA was digested with 150U of RNAse T1 (ThermoScientific) in a 80μL reaction with 10mM Tris-Cl pH7.5 and

0.3M NaCl for one hour at 37 degrees. The reaction was stopped by adding 20uL of stop buffer (2mg/mL Proteinase K, 130mM EDTA, and 2.5% SDS) and incubating at 37° for an additional 30 minutes.

RNA was extracted after both reactions using phenol/chloroform and separated on a 1.8% agarose/formaldehyde gel. After transferring RNA to a charged nylon membrane, hybridization was carried out using the ExpressHyb hybridization solution (Clontech). Membranes were either probed with a radiolabeled Uchl1 specific probe made using the Random Primer DNA Labeling Kit (Takara) or a 5' end labeled oligo(dT)$_{40}$ probe made using T4 polynucleotide kinase (PNK) (NEB). ImageJ was used to quantify placement of the bands on the gel.

Poly(A) Tail-Length Assay (PAT Assay)

PAT assay was carried out using the USB Poly(A) Tail-Length Assay Kit (Affymetrix) according to the manufacturer's instructions. One μg of total RNA was used for each condition, and 30 cycles were used for the PCR amplification step.

Behavioral assays

Adult male wild type mice from the C56BL/6 background were used for all mouse studies. For AAV injections, 10-12 week old mice were injected bilaterally with 2 x 10^{11} viral particles in the hippocampus using the coordinates Anterior-Posterior: -1.75 mm, medial-lateral: ±1.30 mm, and dorsal-ventral: 1.65 mm. Animals were

allowed to recover and behavioral experiments were performed three weeks later. Behavioral assays were performed in the following order: elevated plus maze, open field test, novel object recognition, T-maze, passive avoidance, nest building. The elevated plus maze, open field test, novel object recognition, T-maze, and Passive avoidance were performed as described in (Mansur et al., 2016).

For the elevated plus maze mice were placed at the intersection of two open arms and two closed arms. The number of entries and the amount of time spent in each arm were recorded during a 5 min interval.

For the open field test, mice were placed in the center of an open field and allowed to explore for 10min. The distance traveled and the amount of time spent in either the center or periphery of the open field is recorded.

For the novel object recognition test, on the training day mice were placed in a field with two identical objects and allowed to explore these objects for 10min. Twenty-four hours later the mice were placed in the same field and allowed to explore one novel object and one familiar object that they explored the day before. The percentage of time the animals spent exploring the novel object is calculated relative to the total time spent exploring both objects.

For the T-maze, mice were placed in the start arm of a T shaped maze. Mice explored the maze and have to make a left-right choice at the T-intersection.

Mice were allowed to make 15 choices and the percentage of alternations between left and right is calculated.

For the passive avoidance, mice were placed in a light chamber that contains an open door to a dark chamber. The amount of time it takes the mice to enter the dark chamber is recorded. Once the mice enter the dark chamber the door closes and the mice were given a 0.25 mA foot shock for 2s. Mice remained in the dark chamber for 30 s after the foot shock before being removed from the apparatus. Twenty-four hours later, mice were placed back in the light chamber and the amount of time they took to enter the dark was again recorded. If the animals did not enter the dark chamber within 600s the experiment was terminated.

For the nest building assay, ~2.5g nestlets were placed in the cages of single housed animals one hour before the beginning of the dark cycle. Sixteen hours later the nestlets were photographed and weighed to determine a nest building score. Both the weight of the unshredded nestlet and the quality of the nest were used to determine a nest score (Deacon, 2006). Nests were scored blinded.

Table 2.1 Key Resources

Reagent or Resource	Source	Identifier
Antibodies		
CNOT7 Antibody (2F6)	Novus Biologicals	Cat#: H00029883-M01; RRID:AB_2082466
Anti-GluR1 Rabbit pAb	EMD Millipore	Cat#: PC246; RRID:AB_564636

Anti-phospho-GluR1 Ser831	Millipore	Cat#: AB5847; RRID:AB_11211981
Anti-phospho-GluR1 Ser845	Millipore	Cat#: AB5849; RRID:AB_92079
Anti-PSD-95	BD Biosciences	Cat#: 610496; RRID:AB_397862
Anti-GFAP	Cell Signaling	Cat#: 3670; RRID:AB_561049
Anti-α-Tubulin	Sigma	Cat#: T5168; RRID:AB_477579
Anti-HA.11	Biolegend	Cat#: 901501; RRID:AB_2565335
Anti-FLAG M2 monoclonal	Sigma	Cat#: F1804; RRID: AB_262044
Anti-Map2	Millipore	Cat#AB5622; RRID:AB_11213363
Polyuridic acid-agarose	Sigma	Cat#P8563
Alexa-Fluor 647 Alkyne	Life Technologies	Cat#A10278
Click-iT AHA	Invitrogen	Cat#C10102
Trizol	Life Technologies	Cat#15596018
Prolong Gold antifade reagent with Dapi	Invitrogen	Cat#p36931
ExpressHyb Hybridization Solution	Clontech	Cat#636831
Chemicals, Peptides, and Recombinant Proteins		
(+)-Mk-801 hydrogen maleate	Sigma	Cat#M107
MG-132	Sigma	Cat#M7449
Nocodazole	Sigma	Cat#SML 1665
pLenti puro HA-Ubiquitin	Addgene	Cat#74218-LV
Actinomycin D	Sigma	Cat#A1410
Percol	Sigma	Cat#P1644
Critical Commercial Assays		
Phusion High Fidelity PCR Mastermix	NEB	Cat#M0531S
Nextflex qRNA-Seq Kit v2	Bioo-Scientific	Cat#5130-11

Click-iT Cell Reaction Buffer Kit	Life technologies	Cat#C10269
ViewRNA ISH kit	Affymetrix	Cat#QVC001
Quantitect Reverse Transcription Kit	Qiagen	Cat#205311
Cy5 Mono-Reactive Dye Pack	GE Healthcare Life Sciences	Cat#PA25001
USB Poly(A) Tail-Length Assay Kit	Affymetrix	Cat#76455
Deposited Data		
RNA-Seq	This paper	GEO: GSE88777
Experimental Models: Organisms/Strains		
C57BL/6 wild-type mice	Jackson Labs	
Recombinant DNA		
pll3.7-Syn lentiviral Vector	Gift from M. Sheng	N/A
psPAX2	Gift from Didier Trono	Addgene plasmid#12260
pAAV-U6-GFP Expression Vector	Cell BioLabs	Cat#VPK413
pMD2.G	Gift from Didier Trono	Addgene plasmid#12259
Sequence-based Reagents		
See Table 2.2 for a list of oligos		
Software and Algorithms		
Tophat2	(Kim et al., 2013)	http://ccb.jhu.edu/software/tophat/index.shtml
RSEM	(Li and Dewey, 2011)	http://deweylab.github.io/RSEM/
Bowtie2	(Langmead and Salzberg, 2012)	http://bowtie-bio.sourceforge.net/bowtie2/index.shtml
Samtools	(Li et al., 2009)	http://samtools.sourceforge.net/

WebGestalt Analysis Toolkit	(Zhang et al., 2005)	http://www.webgestalt.org/
ImageJ	(Schneider et al., 2012)	https://imagej.nih.gov/ij/

Table 2.2. Sequence Based reagents

CNOT7 shRNA1: GGATCTGACTCACTGCTTA
CNOT7 shRNA2: GGAGAATACCCTCCAGGAA
CNOT8 shRNA: GAGGAGGAAGGGATCGATA
mutCNOT7 F: GTTGCTATGGCCACCGAGTTTCC
mutCNOT7 R: GGAAACTCGGTGGCCATAGCAAC
Uchl1 RNAse H primer: CGAAACACTTGGCTCTATCT
Uchl1 mRNA Forward: AGATAGAGCCAAGTGTTTCG, Reverse: GTTCACTGGAAAGGGCATT
Cdkl2 mRNA Forward: TAAACCAAATCAGCCTCCTC, Reverse: AAAGCTCTCAGTTCAGGAAG
Shisa6 mRNA Forward: TTCACCGTCTACATCACTTG, Reverse: TATACTGACGATCACCTGGA
SNCA mRNA Forward: CAAGTGACAAATGTTGGAGG, Reverse: TCAGGCTCATAGTCTTGGTA
Uchl1 pre-mRNA Reverse: TTTGAGGGGAACAGATCAAG
Cdkl2 premRNA Forward: ACTGCGGCATGAAAATTTGG, Reverse: GGGTGTCCATTGTGTACCCTT
Shisa6 premRNA Reverse: TGACTTAGAAGGGGAGAGGT
SNCA premRNA Reverse: CACATGAAGTATCAACAAGCA
Angel1 mRNA Forward: AGGACTATAGGCACCATCCA, Reverse: AGCTTGAGAGTTCCATCTCG
Angel2 mRNA Forward: TATCTAAACGAAGAAACATCAAG, Reverse: GTCTGTAGAGGTGAGAGTTATCCT
CNOT6 mRNA Forward: TCAAGACGGAAAAATTCACT, Reverse: TTGTTTTTCTGTTCCCAG
CNOT6L mRNA Forward: AGCTGCTTATAGTGGCAA, Reverse: ACTCCACCGTTGCTTAAATA
CNOT7 mRNA Forward: TTCTTTGTGAAGGGGTCAAA, Reverse: ACCTTTGAGATTTTTGCAGC
CNOT8 mRNA Forward: GTTCTTTCATATCCTGAATCTTTT, Reverse: AATACTGTCCTCAAAGAATAGCTC
Nocturnin mRNA Forward: CGGAGTACTTGGTGTCAACT, Reverse: TCCTCTCTTCCCATTTGAGC
Pan2 mRNA Forward: GATATGCAGGAGCTGGAAGT, Reverse: GTTCTTCCCGGTTTTATCCT
PARN mRNA Forward: AGTGTCCTGTGCTGTTTCGT, Reverse: TGCTTGGAATCTGTGTGGTCA

Quantification and Statistical Analysis

Statistical analyses for Differential gene expression was performed using R (R

Core Team, 2016) as described above with a p-value cutoff of 0.01. Statistical

details of each experiment is provided in the figure legends for that experiment.

Student's t-test was used to determine the significance for all figures except

Figure 2.4A, 2.6A, 2.6C, 2.6D, and 2.7B where the ANOVA test was used to determine if any significance was present and the t-test was used to identify where the significance lied. Significance was defined as a p-value < 0.05. On all figures error bars represent the standard error of the mean and *p≤0.05, **p≤0.01, ***p≤0.001.

Data and Software Availability

The RNA sequencing data reported in this chapter can be accessed with accession number GEO: GSE88777.

Author Contributions

RLM and JDR designed the experiments. RLM performed all the experiments except for those involving RNA-IP, stereotactic injections and animal behaviors, which were performed by FM. RLM and JDR wrote the chapter.

Acknowledgments

CHAPTER III

Distinct Characteristics in the 3'UTR and Coding Region of CNOT7 Neuronal Targets

Rhonda L. McFleder and Joel D. Richter

Program in Molecular Medicine, University of Massachusetts Medical School, Worcester, Ma 01605, USA

Abstract

Previously, we identified CNOT7 as an essential regulator of mRNA localization to dendrites, synaptic plasticity, and higher cognitive function. How CNOT7 targeted specific mRNAs to fulfill this role, however, remained unclear. Here we identify unique characteristics of CNOT7 neuronal targets that may serve to recruit it to mRNAs. We identified several unique motifs enriched in the 3'UTR of mRNAs whose poly(A) tail is governed by CNOT7. One of which is the targeting element for MBNL1, an RNA-binding protein known to regulate mRNA localization. In addition to containing motifs, the 3'UTRs of a subset of CNOT7 targets were also unique in their size. The coding region of CNOT7 targets contained yet another distinguishing characteristic, which was differential codon usage. We found that CNOT7 targets could be separated into two distinct populations: one enriched with optimal codons and one enriched with non-optimal codons. The direction in which CNOT7 regulated the poly(A) tails of these two populations appeared to correlate with their codon usage, indicating that this feature may determine CNOT7 function. Taken together, these data indicate that both codon usage and elements within the 3'UTR distinguish CNOT7 targets from the rest of the neuronal population, and may represent defining characteristics of the dendritic transcriptome.

Introduction

The CNOT complex is a large, heterogeneous, nine-subunit complex that at any one time contains two of four deadenylases: CNOT6, CNOT6L, CNOT7, and CNOT8 (Lau et al., 2009). Of these four, CNOT7 and CNOT8 are thought to be the major deadenylases in eukaryotes; responsible for initiating decay for the majority of mRNAs in the cell (Schwede et al., 2008). In neurons, CNOT7 plays a more specific role to regulate only 100 mRNAs. These mRNAs require CNOT7 to localize them to dendrites where they undergo stimulation-induced local translation. Despite its small number of targets, CNOT7's role in neurons is vital, as its depletion impairs synaptic plasticity and normal cognitive function. Identifying the features that target CNOT7 to specific neuronal mRNAs should provide insight into the dendritic RNA microenvironment and disorders resulting from its disruption.

Although responsible for varying aspects of mRNA regulation, the CNOT complex lacks a required RNA-binding domain and therefore must partner with RNA-binding proteins to carry out its functions (Doidge et al., 2012b). Several interacting RNA-binding proteins have been identified including: Pumilio (Goldstrohm et al., 2006, Miller and Olivas, 2011), Nanos (Kadyrova et al., 2007, Raisch et al., 2016, Suzuki et al., 2012), and Tob1 (Horiuchi et al., 2009). Most of these interactions are directly with the scaffolding protein, CNOT1, although some direct interactions with CNOT7 have been described (Horiuchi et al., 2009, Stupfler et al., 2016). It is reasonable to assume that an RNA binding protein

mediates CNOT7's specialized function in neurons, and is therefore essential for local translation. One candidate is Cytoplasmic Polyadenylation Element Binding protein (CPEB). CPEB recruits a poly(A) polymerase, Gld2, to mRNAs containing the CPE sequence (UUUUUAU) and activates their polyadenylation and local translation in response to synaptic activity (Udagawa et al., 2012, Huang et al., 2002, Wu et al., 1998). Prior to synaptic activity, CPEB is presumed to repress translation through the recruitment of a deadenylase that has yet to be identified (Richter, 2007, Udagawa et al., 2012). In addition to the two proteins playing similar roles in neurons, CNOT7 and CPEB are also known to directly interact in HeLa cells (Ogami et al., 2014). Taken together, it seems possible that CPEB could recruit CNOT7 to neuronal mRNAs in order to govern local translation.

Codon usage is another feature recently attributed to targeting CNOT7 to mRNAs (Mishima and Tomari, 2016). There are 64 different codons and only 20 different amino acids, allowing several codons to code for the same amino acid. Surprisingly, these synonymous codons are not utilized equally, thus creating an intriguing phenomenon not fully understood (Presnyak et al., 2015, Plotkin and Kudla, 2011). What is known is that certain synonymous codons are enriched in highly expressed genes (Presnyak et al., 2015). It is thought that this increased demand is met with an increased supply of specific tRNAs; thus creating an optimal environment for decoding these codons (Dittmar et al., 2006, Presnyak et al., 2015). In the developing zebrafish zygote, CNOT7 deadenylates maternal mRNAs enriched in non-optimal codons, those rarely used and for whom the

recognizing tRNA is of low abundance, to initiate their decay. Degradation of these mRNAs is vital for zygote development and dependent on the length of their 3'UTR (Mishima and Tomari, 2016). This interplay between different regions of the mRNA to specify CNOT7 function, may extend beyond the developing zebrafish and into neurons.

Here we describe unique characteristics of CNOT7 targets in neurons. First we validate our previous finding that CNOT7 bidirectionally regulates the poly(A) tails of two distinct populations of neuronal mRNAs. One population gains a poly(A) tail following CNOT7 depletion while the other loses its poly(A) tail. Both populations share enrichment for a common CUG repeat motif that may serve to target CNOT7 to the mRNAs. However, they diverge on the basis of 3'UTR length and codon usage. Opposite from the developing zebrafish, mRNAs that gain a poly(A) tail following CNOT7 depletion are enriched with optimal codons. Their counterparts, mRNAs that lose their poly(A) tail following CNOT7 depletion, are not only enriched with non-optimal codons but also possess significantly long 3'UTRs. Together these findings provide insight into the features specializing CNOT7 function in neurons, allowing it to regulate local translation and neuronal function.

Results

CNOT7 positively regulates the poly(A) tails of a subset of mRNAs
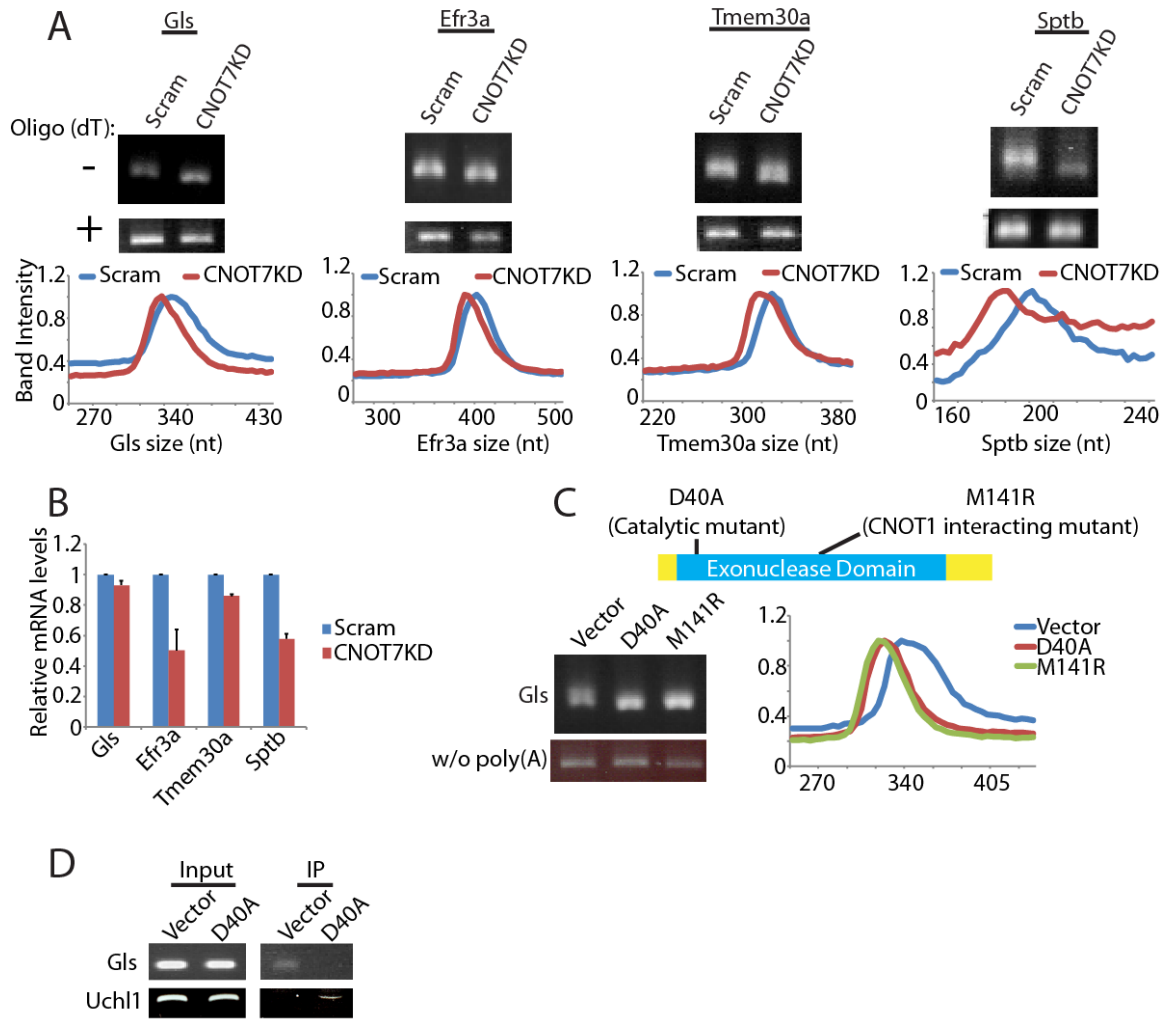
Figure 3.1 CNOT7 positively regulates the poly(A) tails of specific mRNAs. (A) PAT assay of Gls, Efr3a, Tmem30a, and Sptb mRNAs in the presence (bottom image) or absence (top image) of oligo(dT)-mediated RNAse H cleavage of their poly(A) tails. Relative quantification of the polyadenylated bands are represented below the respective gel images. (B) Histogram represents the average relative mRNA levels Gls, Efr3a, Tmem30a, and Sptb from two sets of either control (Scram) or CNOT7KD neurons. (C) Top diagram represents the CNOT7 protein with the exonuclease domain colored in blue and the placement of the two different mutations utilized. Bottom is a PAT assay image and quantification of Gls RNA with or without a poly(A) tail in vector, D40A mutant CNOT7, or M141 mutant CNOT7 expressing cells. (D) PCR of GLS and Uchl1 before (input) or after (IP) a formaldehyde cross-linked IP of FLAG from either empty vector or D40A mutant CNOT7-expressing cells.

Previously, we identified ~100 mRNAs that experienced changes in their poly(A)

and/or stability following CNOT7KD in cultured hippocampal neurons; of these,

~30% had decreased poly(A) tail length (Figure 2.8A). We first sought to validate

these changes in four mRNAs identified by sequencing: Glutaminase (Gls),

EFR3 Homolog A (Efr3a), Transmembrane Protein 30a (Tmem30a), and

Spectrin Beta (Sptb) using a Poly(A) Tail-Length Assay (PAT Assay). All four

mRNAs experienced a dramatic decrease in size following CNOT7KD. This

decrease was due to changes in poly(A) tail length as evidenced by the

observation that when the poly(A) tail is removed by oligo(dT) mediated RNAse

H cleavage, the size of these mRNAs are similar before and after CNOT7KD

(Figure 3.1A). These mRNAs also experienced a decrease in their steady-state

levels, which was likely due to decreased stability resulting from shortened

poly(A) tails (Figure 3.1B). We next utilized two different CNOT7 mutants to test

whether regulation of these mRNAs was dependent on the enzyme's catalytic

activity (a D40A mutant is enzymatically inactive) ((Viswanathan et al., 2004) or

its presence in the CNOT complex (M141R mutant prevents association with the

CNOT scaffolding protein, CNOT1) (Petit et al., 2012). Following lentivirus

transduction into neurons, both of these mutants caused a similar decrease in

the poly(A) tail of Gls, indicating that deadenylase activity and presence in the

CNOT complex is important for the control of poly(A) length by CNOT7 (Figure

3.1C). To test whether CNOT7 directly interacts with these mRNAs, we

performed a formaldehyde crosslinking RNA-Immunoprecipitation of FLAG-

tagged mutant CNOT7 (D40A) transduced into HEK cells, which were used instead of neurons to obtain sufficient starting material for the experiment. Uchl1 mRNA, which has lengthened poly(A) tail following CNOT7KD, co-immunoprecipitated with FLAG-CNOT7, suggesting it is a direct target of the deadenylase (Fig 3.1D). Gls mRNA, however was not present in the pulled down samples (Figure 3.1D). This negative result does not completely rule out the possibility that these mRNAs are direct targets of CNOT7, because it was performed in HEK cells where CNOT7 may not regulate these mRNAs in a similar manner.

CNOT7 target RNAs contain unique features in their 3'UTR
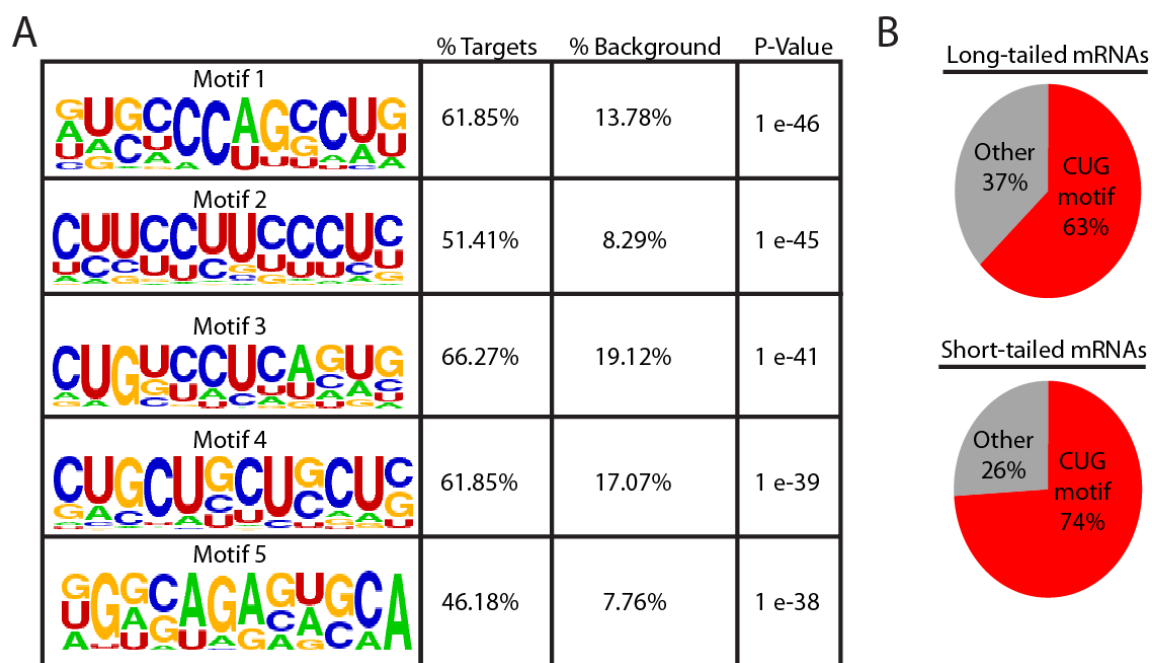
Figure 3.2 CNOT7 targets are enriched with a CUG repeat motif. (A) Top five significantly enriched motifs identified using HOMER (Heinz et al., 2010) in the 3'UTR of all genes whose poly(A) tail is regulated by CNOT7. Percent of targets, percent of background mRNAs, and the p-

value (calculated using the KS-test) for each motif is indicated. (B) Pie charts display the percent of long-tailed (up) genes and short-tailed (down) genes containing the CUG repeat (motif 4).

To test if CPEB directs CNOT7 to its targets, we analyzed their 3'UTR for enrichment of the CPE motif (UUUUUAU). We found no significant enrichment of this motif and we also could not confirm a direct interaction of these two proteins in neurons (data not shown). We next analyzed their 3' UTRs for any significantly enriched motifs (Heinz et al., 2010). We were unable to identify any significantly enriched motif in mRNAs that either gained (long-tailed mRNAs) or lost (short-tailed mRNAs) poly(A) tail following CNOT7KD. When analyzed together, however, 18 significantly enriched motifs were identified, which we surmise is due to enhanced statistical power. Figure 3.2A shows the top five significantly enriched motifs, which were present in 45-66% of CNOT7 regulated mRNAs compared to 7-19% in total cellular mRNAs. We found the CUG repeat motif (motif 4) to be very compelling because it is known to be enriched in mRNAs localized to distal neurites (Taliaferro et al., 2016). Sixty-one percent of all mRNAs that experienced a change in their poly(A) tail following CNOT7KD contained a CUG repeat motif in their 3'UTR (Figure 3.2A, Motif 4). This motif was present at similar rates in long-tailed and short-tailed mRNAs suggesting it may be a common feature that recruits CNOT7 to these mRNAs (Figure 3.2B).
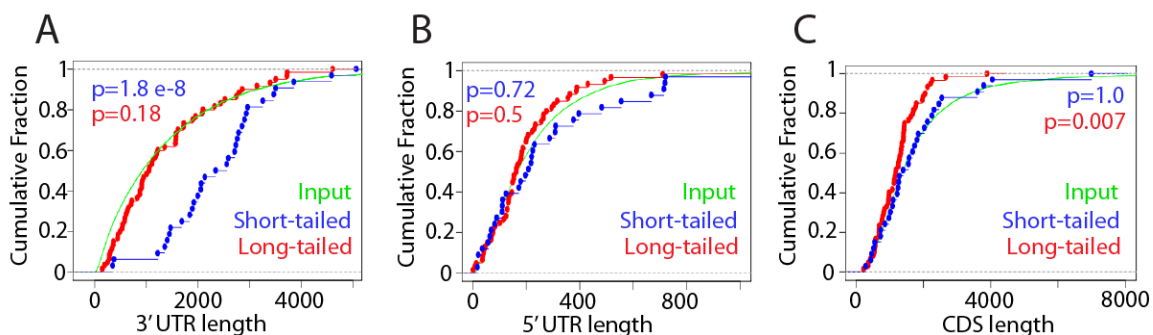
Figure 3.3 mRNAs positively regulated by CNOT7 have long 3'UTRs. (A) Cumulative distribution curve of either the 3'UTR (A), 5'UTR (B), or Coding region (C) lengths of either Input (green), Short-tailed (blue), and Long-tailed (red) genes identified following CNOT7KD. P-values were calculated using the KS-test and compare the short or long-tailed samples to input.

A further analysis of the 3'UTR of these gene sets revealed that the median length of the short-tailed 3'UTRs was over twice as long as that of the input mRNAs (2450nt vs 926nt). This stark and highly significant difference in 3'UTR length (Kolmogorov-Smirnov (KS test) p-value = 1.8 e-8) was specific to the short-tailed mRNAs as the 3'UTR length of long-tailed mRNAs was virtually identical to that of input mRNAs (1057nt vs 926nt) (Figure 3.3A). These short-tailed mRNAs had no difference in 5'UTR or coding region length, suggesting that 3'UTR length specifically could determine or otherwise influence CNOT7 regulation of poly(A) tails (Figure 3.3B & C).

CNOT7 targets have differential codon usage
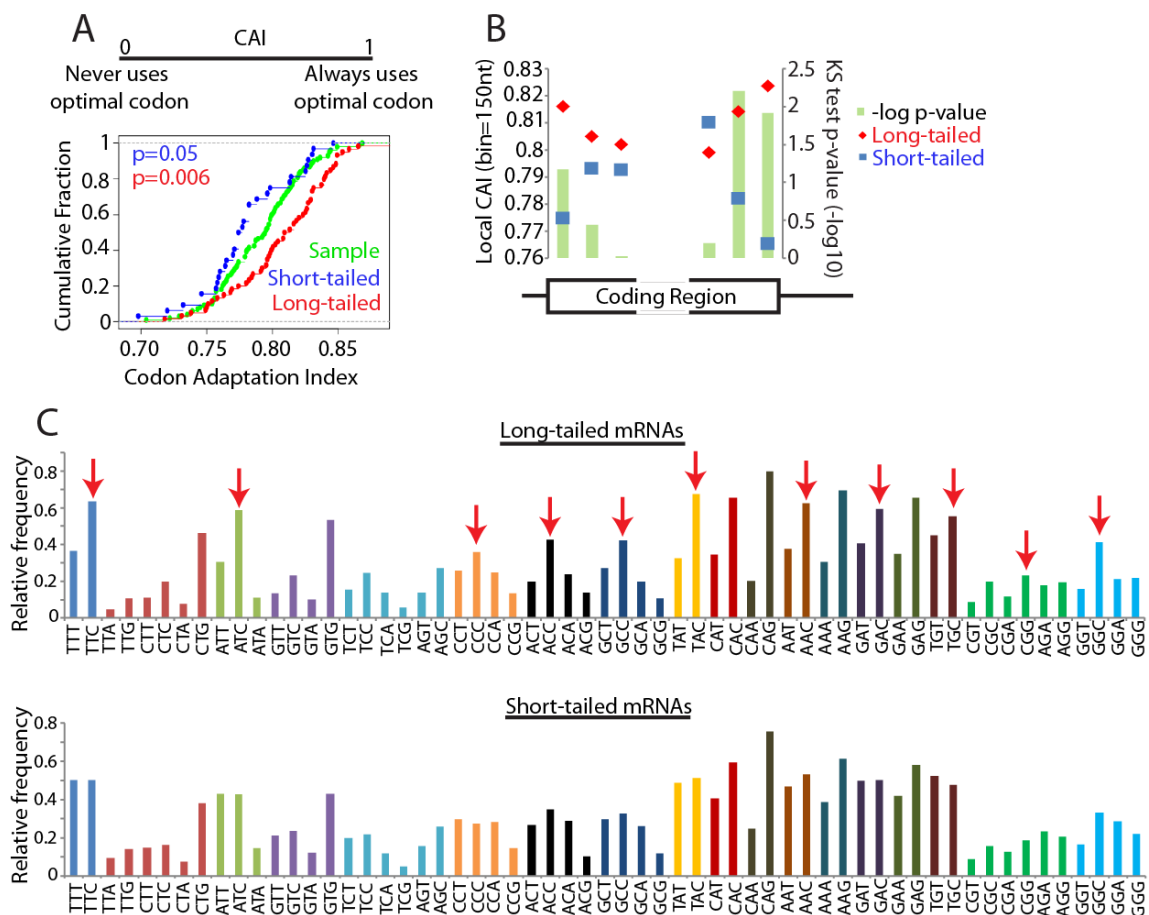
Figure 3.4 Long or short-tailed mRNAs have differential codon usage. (A) Cumulative distribution curve of the Codon Adaptation Index of either a randomly sampled set of 100 genes that don't change upon CNOT7KD, the long-tailed, or short-tailed differentially expressed genes following CNOT7KD. P-values were calculated using the KS-test and compare the short or long-tailed samples to the randomly sampled gene set. (B) Local Codon Adaptation index of long-tailed (red) or short-tailed (blue) genes identified following CNOT7KD. The coding sequence of each mRNA population was binned every 150nt from the beginning of the open reading frame (ORF) (first three data points) and from the end of the ORF (last three data points) and the median codon adaptation index is plotted for each bin. P-values were calculated using the KS-test and compare the short-tailed to the long-tailed populations. The negative log of 10 of the p-values is plotted with the green bars. (C) Histogram represents the frequency of each codon for each amino acid in the long-tailed (top) or short-tailed (bottom) mRNAs. Synonomous codons are grouped by color with each color representing a different amino acid in the following order: Phenylalanine, Leucine, Isoleucine, Valine, Serine, Proline, Threonine, Alanine, Tyrosine, Histidine, Glutamine, Asparagine, Lysine, Aspartic Acid, Glutamic Acid, Cysteine, Arginine, and Glycine. Red arrows indicate enhanced preference of a given synonomous codon in the long-tailed mRNAs compared to short-tailed.

Unequal usage of synonymous codons is a phenomenon observed throughout

the evolutionary tree (Plotkin and Kudla, 2011). "Optimal" codons are enriched in

highly expressed genes and recognized by relatively abundant tRNAs, while their

synonymous counterparts are therefore "non-optimal" (Zhou et al., 2009b). In the

developing zebrafish, mRNAs abundant in non-optimal codons are targeted for

CNOT7-mediated deadenylation and decay (Mishima and Tomari, 2016). To

assess whether this was the case in neurons, we calculated the codon

adaptation index (CAI), an index ranging from 0 to 1, with 1 signifying that the

gene always uses optimal codons and 0 signifying that the gene never uses

optimal codons (Puigbo et al., 2008) (Figure 3.4A top), for the long-tailed, short-

tailed, and a randomly selected set of 100 mRNAs. We found that CNOT7 target

mRNAs had dramatically different codon usages, with the long-tailed mRNAs

being enriched with more optimal codons and the short-tailed mRNAs being

enriched with non-optimal codons (Figure 3.4A). Placement of optimal or non-

optimal codons within the coding sequence has also been shown to be important

for determining mRNA stability in other biological conditions (Mishima and

Tomari, 2016, Radhakrishnan et al., 2016). To analyze the location of these

codons in CNOT7 neuronal targets, we binned the coding sequences every 150

bases and calculated the local CAI. We found that the largest difference in codon

usage between the long-tailed and short-tailed mRNAs was clustered at the 3'

end of these mRNAs (Figure 3.4B). These data indicate that codon usage,

particularly at the 3' end of mRNAs, may dictate CNOT7 regulation of its target

mRNAs. mRNAs that must be translated at similar times tend to prefer specific codons for a given amino acid. This shared codon preference is thought to aid in the translation of these mRNAs by allowing more tRNA reuse and recycling (Begley et al., 2007, Frenkel-Morgenstern et al., 2012, Presnyak et al., 2015). Further analysis of the coding regions of CNOT7 target mRNAs revealed that the long-tailed but not the short-tailed mRNAs tend to preferentially use one specific synonomous codon for most amino acids (Figure 3.4C arrows). These data suggest that the long-tailed mRNAs represent a group of mRNAs whose translation is activated simultaneously possibly in response to stimulation-induced CNOT7 depletion.

Discussion

Here we identify several characteristic unique to CNOT7 neuronal targets. Over 60% of CNOT7 targets contained a CUG repeat motif, similar to that recognized by the MBNL family of proteins, in their 3'UTR. This seemed to be the only element these mRNAs had in common, as they differed dramatically in the length of their 3'UTRs and codon usage. The population of mRNAs whose poly(A) tail is somehow lengthened by CNOT7, contained exceptionally long 3'UTRs and were enriched with non-optimal codons. While the population of mRNAs whose poly(A) tail is shortened by CNOT7, contained average size 3'UTRs and were enriched with optimal codons. This data suggest that codon

usage and 3'UTR length may dictate the direction in which CNOT7 regulates its targets.

We began this study with the goal of identifying the deadenylase functioning with CPEB to maintain dendritic poly(A) tails, our data suggest however that CNOT7 is not that deadenylase. First, despite an interaction being described in Human Embryonic Kidney (HEK) cells, we could not co-immunoprecipitate CNOT7 and CPEB in cultured hippocampal neurons (Ogami et al., 2014). This discrepancy could be attributed to the different approaches used. The study in HEK cells ectopically expressed tagged versions of both CPEB and CNOT7 which could result in non-specific interactions, while we ectopically expressed tagged-CPEB and probed for its interaction with endogenous CNOT7 (Ogami et al., 2014). Other evidence suggesting these proteins do not function together in neurons, is the lack of enrichment of the CPE motif in CNOT7 targets. Taken together, our data suggest that CNOT7 is not the sole deadenylase functioning in dendrites and that CPEB recruits another deadenylase to maintain the poly(A) tail of its targets.

The most likely deadenylase functioning with CPEB is PARN. The two were found to co-localize in the same complex within dendritic spines of hippocampal neurons (Udagawa et al., 2012). PARN knockdown had no effect on dendritic poly(A) and synaptic plasticity, however this could be due to insufficient depletion of PARN. Follow-up experiments, perhaps with a better

depletion of PARN should be performed to address this issue (Udagawa et al., 2012).

Identification of enrichment of the CUG repeat motif, indicates that the MBNL family of proteins may mediate CNOT7 function in neurons. MBNL1 and 2 have recently been demonstrated to regulate the neurite localization of mRNAs (Taliaferro et al., 2016). As translation repression is often tightly linked to localization (Kleiman et al., 1993), these proteins may carry out this function by targeting CNOT7 to mRNAs to repress their translation and allow for transport. Indeed, MBNL1 is known to repress translation of mRNAs and has been shown to interact with CNOT7 in other cell types (Lau et al., 2009, Masuda et al., 2012). Future work should focus on elucidating if the CUG motif and MBNL1 are essential for CNOT7 regulation of mRNA localization in neurons.

Identifying a subset of CNOT7 putative targets with exceptionally long 3'UTRs was an interesting yet unexpected finding. The implications of these long 3'UTRs is unclear at this time, however one can imagine that it may contain more cis-elements which are recognized by trans-acting factors that regulate mRNAs. Although this was not true for CUG repeat motifs, these long 3'UTR mRNAs did contain an increased amount of miRNA binding sites compared to other CNOT7 targets. Indeed miRNAs are known to regulate local translation in dendrites (Gu et al., 2015, Rajasethupathy et al., 2009), and are thought to perform this function by recruiting other inhibitory factors including the CNOT complex (Zekri

et al., 2013, Fabian et al., 2011, Braun et al., 2011). We could not identify

enrichment for sequences specific to a particular family of miRNAs, suggesting

that CNOT7 may function with the general RISC machinery to regulate several

different populations of dendritic mRNAs. Further research is necessary to test if

these long 3'UTRs are necessary for enhanced recruitment of CNOT7 and if this

recruitment is mediated through miRNAs.

3'UTR length and codon usage was recently identified as attributes that

direct CNOT7-mediated deadenylation in zebrafish (Mishima and Tomari, 2016).

Specifically, mRNAs with short 3'UTRs and non-optimal codon enrichment were

deadenylated by CNOT7 in the developing zebrafish. In yeast, it is also true that

non-optimal codons target mRNAs for deadenylation and decay (Presnyak et al.,

2015). Our data, however, suggest that in neurons the opposite occurs. mRNAs

enriched with optimal codons are targeted for CNOT7-mediated deadenylation.

These mRNAs also share a specific codon preference, suggesting codon usage

may be a feature that groups these mRNAs translationally to ensure their

seamless translation in response to stimulation.

The enrichment of non-optimal codons does not appear to lead to

deadenylation and decay in neurons as have been described in other cell types,

and in fact the opposite occurs where these mRNAs are actually polyadenylated

(Presnyak et al., 2015). This phenomenon may be similar to what was recently

described in Zebrafish, where a long 3'UTR, no matter the sequence, conferred

protection to mRNAs enriched with non-optimal codons (Mishima and Tomari, 2016). These data indicate that a unique codon usage environment may be present in dendrites and may serve as another layer of local translation regulation.

Materials and Methods

Hippocampal Neuron Culture and Drug Treatments

Hippocampal neurons were cultured and maintained exactly as previously described (Huang and Richter, 2007).

shRNA design, Site-directed Mutagenesis, and Lentivirus production

Plasmids and lentiviruses were made using standard procedures with custom designed oligonucleotides described below. To generate mRNA-specific shRNAs, a CNOT7-specific oligonucleotides (GGATCTGACTCACTGCTTA) was annealed and ligated into the pll3.7-Syn vector. For ectopic expression assays, full length mouse CNOT7 was ligated into the FUGW lentiviral vector. Site-directed mutagenesis of CNOT7 was carried out using the Phusion High-Fidelity PCR Mastermix (NEB) and two specific primers (D40A:GTTGCTATGGCCACCGAGTTTCC, GGAAACTCGGTGGCCATAGCAAC; M141R: GCAGGACTTCGGACTTCAGGAGTG, CACTCCTGAAGTCCGAAGAAGTTCTGC) with an annealing temperature of 60˚

and an extension time of five minutes. Viral plasmids in addition to an envelope and empty backbone packaging vector (pMD2.G and psPAX2) were transfected into HEK293T cells using calcium phosphate precipitation and the virus containing media collected three days later. Neurons were infected with virus at DIV 13-15.

RNA Collection and RT- PCR

All RNA was extracted using Trizol (Life Technologies). The Quantitect Reverse Transcription Kit (Qiagen) was then used to synthesize cDNA. All primer sets were tested by comparing the PCR product after at least three different number of amplification cycles to identify which cycle number was in the linear range and should therefore be used for experiments.

PAT Assay

PAT assay was performed as described elsewhere (Shin et al., 2017). A 5' phosphorylated, 3' Amino Modified adaptor anchor primer (5Phos/CGCGGCCGCGGAGCTCGC/3AmMo) was ligated onto 3.5 μg of RNA in a 25 μL reaction with T4 RNA ligase 1. The entire 25 μL reaction was used for a 40 μL RT reaction using SSIII and an anti-adaptor (GCGAGCTCCGCGGCCGCG). Two milliliters of the RT reaction was then used to perform PCR using a common reverse primer (CGAGCTCCGCGGCCGCGTTTTT) and a forward primer specific to the RNA of interest 200-300 bases upstream of the 3' end. Forty cycles of amplification was

used with an annealing temperature of 59° for all mRNAs except Tmem30a

where an annealing temperature of 57° was used. As a control, the poly(A) tail

was cleaved off using RNASe H and an oligo dT(18)-mer prior to adaptor ligation.

mRNA was separated on a 2 % agarose gel and size was determined using

ImageJ.

Protein/RNA Immunoprecipitation

For protein/RNA immunoprecipitation, HEK293T cells transduced with lentivirus

expressing mtCNOT7-FLAG or empty plasmid were cross-linked with 0.5%

formaldehyde for 10 minutes at room temperature. The formaldehyde cross-

linking was stopped by adding 125 mM glycine pH 7.0 for 5 minutes at room

temperature. Cells were washed twice with ice-cold PBS, resuspended in RIPA

buffer (50 mM Tris-HCl p 7.5, 1 % (v/v) NP-40, 0.5 % (w/v) sodium deoxycholate,

0.1 % (w/v) SDS, 1 mM EDTA, 150 mM NaCl, cocktail of protease inhibitors and

RNase OUT), and disrupted by sonication on ice 4 times for 15 seconds with

amplitude 7. The insoluble fraction was removed by centrifugation at 16,000 x g

for 10 minutes at 4°C and the supernatant was pre-cleared with anti-mouse IgG

Dynabeads for one hour at 4°C supplemented with 200 μg of tRNA and 40 μg/mL

of salmon sperm DNA. Subsequently, the pre-cleared extract was incubated with

5 μg of anti-FLAG antibody overnight a 4°C. The antibody-bound complexes

were recovered using anti-mouse IgG Dynabeads, previously blocked with 0.5 %

BSA, 0.1 mg/mL tRNA and 0.1 mg/mL glycogen, and washed 5 times with RIPA

buffer supplemented with 1 M urea. The cross-linking was reversed by resuspending the beads in 130 uL of reversal buffer (50 mM Tris-HCl pH 6.8, 5 mM EDTA, 10 mM DTT and 1 % SDS) and incubating at 70˚C for 2 hours. The RNA was then extracted with Trizol and used for cDNA synthesis followed by RT-PCR.

Motif enrichment and length analysis

The 3' UTR, 5'UTR, or coding sequence of the most abundant isoform of all differentially expressed genes, or all genes with > 5 counts (Input), was obtained using Ensembl's Biomart website (http://www.ensembl.org/biomart). Six, eight, or ten nucleotide long common motifs in the 3'UTRs were then analyzed using HOMER (Heinz et al., 2010). R was used to plot the cumulative distribution of the lengths of the different parts of the genes and to perform the Kolmogorov-Smirnov test (KS-test) between either the long-tailed or short-tailed genes and the input genes (R Core Team, 2016).

Codon usage analysis

Codon adaptation index (CAI) and the relative frequency of each codon was obtained for the coding sequence of the most abundant isoform of either the long-tailed or short-tailed differentially expressed genes using the CAIcai server (Puigbo et al., 2008). We acquired the mouse codon usage table required to calculate the CAI from the codon usage database (Nakamura et al., 2000). The total input list of genes was too large for the server, so we therefore utilized a

random sample of 100 genes as a control. Cumulative distribution and KS-test was calculated as described above. To obtain the local CAI, the first and last 450 nt of the coding sequence of the differentially expressed genes were binned every 150 nt and the CAI was calculated for each bin.

Author Contributions

RLM and JDR designed the experiments. RLM performed all the experiments. RLM and JDR wrote the manuscript

Acknowledgments

CHAPTER IV

Discussion and Conclusions

Rhonda L. McFleder

Program in Molecular Medicine, University of Massachusetts Medical School,

Worcester, Ma 01605, USA

Summary

Here we identify CNOT7 as an essential regulator of the dynamic mRNA microenvironment in dendrites. Through shRNA-mediated depletion of CNOT7, we show that CNOT7 is responsible for localizing mRNAs to the dendrites of hippocampal neurons *in-vitro* and *in-vivo*. Following stimulation, CNOT7 is degraded resulting in an immediate increase in dendritic poly(A) due to elongation of its target's poly(A) tails. After prolonged depletion of CNOT7, these polyadenylated targets have reduced dendritic localization resulting in decreased dendritic poly(A), which would in turn shut down local translation (Figure 4.1). When this stimulation-induced drop in CNOT7 is prevented, the biphasic changes in dendritic poly(A) do not occur and synaptic plasticity is inhibited. Mice depleted of CNOT7 demonstrate defects in protein synthesis dependent learning assays; demonstrating the importance of this enzyme for normal cognitive function. Using thermal elution from a poly(U) column and deep sequencing, we identified mRNAs that incurred changes in their poly(A) tail length following CNOT7KD and are therefore direct or indirect targets of CNOT7. Most of these mRNAs experienced an expected increase in their poly(A) tail following knockdown, however a substantial portion experienced a decrease in their poly(A) tail. Both groups were enriched for a common CUG repeat motif in their 3'UTRs, which may serve as a targeting element for CNOT7. However, they differed in their 3' UTR lengths and codon usage, indicating these may be defining features that dictate the function of CNOT7 in neurons.
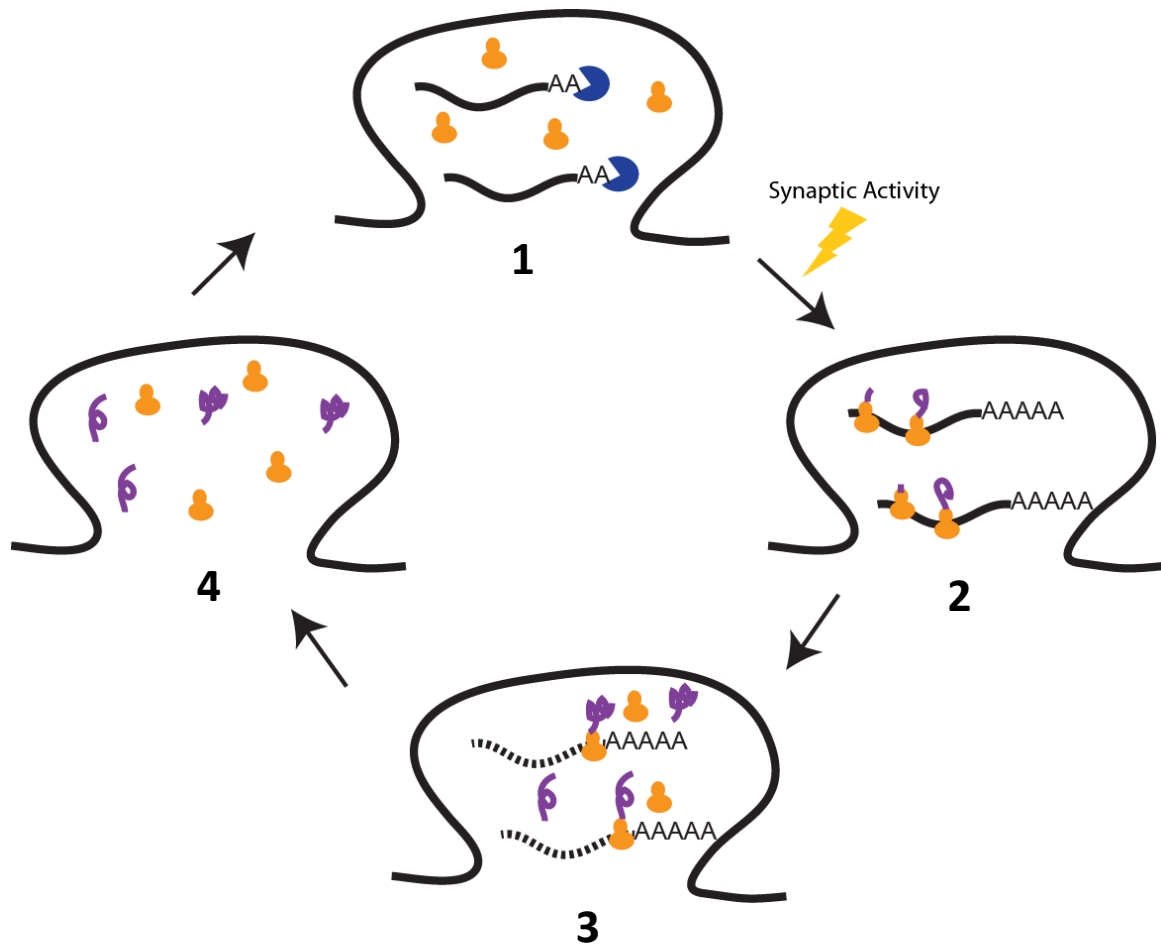
Figure 4.1: Model of CNOT7 function at synapses. Our data suggest that CNOT7 deadenylates mRNAs to repress their translation and allow their localization to post-synaptic sites (1). Immediately following synaptic activity, CNOT7 is degraded resulting in polyadenylation and likely translation of its targets (2). The dendritic mRNAs are likely degraded following their translation (3), which would result in the decrease in dendritic poly(A) we observe within twenty minutes following stimulation, and would serve to turn local translation back off (4). CNOT7 protein is likely replenished at even later time points allowing it to target newly synthesized mRNAs to post-synaptic sites where they are poised for activity-dependent local translation (1).

CNOT7 Reduction

One critical event that underlies CNOT7-regulation of dendritic poly(A) tail length is its reduction within 20 minutes following glycine-induced LTP. Given that its half-life is greater than 6 hours under normal conditions (Cano et al.,

2015), this stimulation-induced reduction is likely due primarily to CNOT7

degradation. The mechanism underlying such destruction would therefore be

vital for local translation and synaptic plasticity. One system already known to

regulate the dendritic proteome is the ubiquitin proteasome system (UPS)

(Alvarez-Castelao and Schuman, 2015). This system utilizes a multi-step process

to ligate a 76 amino acid polypeptide, ubiquitin, onto the lysine residues of

proteins to target them for degradation by the proteasome (Hershko and

Ciechanover, 1998, Ciechanover, 2005). The ubiquitination step in this process is

capable of responding to changes in cellular environment such as synaptic

activity, where the amount of ubiquitin-conjugated proteins doubles in the post-

synaptic compartment (Ehlers, 2003). CNOT7 may be one such protein

experiencing stimulation-induced ubiquitination, activating its degradation.

Visualization of ubiquitinated CNOT7 at different time points following stimulation

would address if this ligation is increased. However, identification of the lysine

residues important for such ubiquitination, possibly using point mutants, is

necessary to test if such an increase results in degradation, as CNOT7

ubiquitination has also been linked to activation of the protein (Cano et al., 2015).

Four lysine residues have already been identified as being essential for CNOT7

ubiquitination in HEK cells (K196, K200, K203, and K206) (Cano et al., 2015),

and could provide a starting point for understanding the role of the UPS in

CNOT7 function.

If increased ubiquitination underlies the stimulation-induced destruction of CNOT7, the question remains as to how it is targeted for this process. There are three enzymes necessary to tag proteins with ubiquitin: the ubiquitin-activating enzyme, E1; the ubiquitin-conjugating enzyme, E2; and the ubiquitin-ligase, E3 (Hershko and Ciechanover, 1998). Of the three enzymes, the E3 ligase provides the specificity to target particular proteins for degradation (Wells et al., 1998). There are hundreds of E3 ligases encoded by the mouse genome that could potentially target CNOT7 (Tai and Schuman, 2008). One obvious candidate is the E3 ligase member of the CNOT complex, CNOT4 (Albert et al., 2002). Little is known of the importance of CNOT4, however in humans its interaction with the complex is not stable and may be regulated based on cellular conditions (Lau et al., 2009). Synaptic plasticity may represent such a condition where CNOT4 interaction with the complex is increased, thereby inducing ubiquitination and subsequent degradation of CNOT7.

Another potential candidate is the RNA binding E3 ligase, Mex3c. Mex3c is highly expressed in brain and testis compared to other tissues in mice (Jiao et al., 2012), and specifically, its neuronal expression is vital for white adipose tissue deposition (Han et al., 2014). In other cell types, Mex3c has been demonstrated to regulate the stability of different mRNAs (Li et al., 2016, Cano et al., 2012), and its ectopic expression increases polyadenylated mRNA in HEK293t cells (Cano et al., 2012). The stability of one mRNA, HLA-A1, is regulated by Mex3c via its ubiquitination of CNOT7 (Cano et al., 2015). This

ubiquitination did not appear to destabilize CNOT7 but rather regulated its enzymatic activity (Cajigas et al., 2012). Regardless the outcome of Mex3c-mediated ubiquitination, if it targets CNOT7 similarly in hippocampal neurons, this interaction would be vital for synaptic plasticity and learning.

The UPS is not the only mechanism for degrading cytosolic proteins, this function is also carried out by lysosomes (Levine and Klionsky, 2004). Intracellular contents can either be delivered to the lysosome via a double-layered membrane (i.e. autophagy), or the lysosome can directly invaginate cellular contents (Glick et al., 2010). Disruptions in the lysosome's ability to degrade substrates impair neuronal function due to the development of protein aggregates (Settembre et al., 2008). Although traditionally thought of as an indiscriminate process, there is evidence for selective autophagy (Xie and Klionsky, 2007). Even in neurons, selective autophagy of the E3 ligase, Highwire, is essential for synapse development (Shen and Ganetzky, 2009). If CNOT7 is not degraded via the UPS, lysosomal mediated degradation is possible and should be investigated. The presence of ubiquitinated CNOT7 does not exclude the possibility of lysosome-mediated degradation, as ubiquitin also signals degradation via the lysosome (Kirkin et al., 2009, Komatsu et al., 2007) (Pankiv et al., 2007).

Although destruction certainly occurs, data from other labs suggest that CNOT7 may also undergo reduced translation in response to synaptic activity

(Cho et al., 2015, Schanzenbacher et al., 2016). One lab performed ribosome profiling from the hippocampus of mice following contextual fear conditioning, an assay for long term memory. Ribosome profiling is a specialized sequencing method to identify mRNAs bound by ribosomes. This method is used as a proxy for translation, with the more ribosomes bound signifying higher translation of a given mRNA (McGlincy and Ingolia, 2017). Within 5 minutes following learning, the relative ribosome density on CNOT7 decreased significantly by 14% (Cho et al., 2015). This 14% reduction in CNOT7 translation is not nearly as dramatic as the 50% reduction we observed. One must keep in mind, however, that we were measuring CNOT7 in hippocampal neurons whereas they were measuring translation in the intact hippocampus which contains a variety of cell types that express CNOT7 but may not respond to activity (Cho et al., 2015). Ribosome profiling, specifically in hippocampal neurons, may demonstrate a greater contribution of translation to the stimulation-induced reduction of CNOT7.

Other data suggesting reduced translation of CNOT7 in response to synaptic activity comes from the Schuman lab, using bio-orthogonal non-canonical tagging (BONCAT) (Schanzenbacher et al., 2016). BONCAT utilizes a methionine analog, azidohomoalanine (AHA), to tag newly synthesized proteins. The tagged proteins are then isolated using affinity purification and identified with Mass Spectrometry (Dieterich et al., 2006). They used this method to identify proteins in cultured hippocampal neurons synthesized within 24 hours following homeostatic scaling. Homeostatic scaling is adjustment of the strength of the

synapse in response to changes in firing rates or intensity of synaptic input, and is a form of synaptic plasticity (Schanzenbacher et al., 2016). Levels of newly synthesized CNOT7 were reduced 74% and 28% following synaptic up and down scaling respectively. Because of their long time period, 24 hours, it is unclear whether this decrease represents reduced transcription, reduced translation, or faster degradation of newly synthesized CNOT7 (Schanzenbacher et al., 2016). What is clear from these experiments and our data is that the neuron reduces CNOT7 in response to changes in synaptic activity and learning. Elucidating the relative contributions of translation and degradation to stimulation-induced reduction of CNOT7, would provide further insight into the intertwining mechanisms regulating local translation

Codon Usage

Not all synonymous codons are created equally, and it is well known that certain codons are used more frequently than others (Presnyak et al., 2015, Plotkin and Kudla, 2011). Interestingly, this codon usage bias is more prominent in highly expressed genes, suggesting it may represent some sort of adaptation to benefit their expression (Plotkin and Kudla, 2011). One prominent theory is that the codon usage of these genes adapted to match differences in tRNA isoform abundance, and therefore increase the translational efficiency of these genes (Plotkin and Kudla, 2011). In support of this hypothesis, the tRNA abundance in several organisms match beautifully with the corresponding codon

usage, making these codons "optimal" for translation (Dittmar et al., 2006, Presnyak et al., 2015). We found that in neurons, mRNAs deadenylated by CNOT7 are significantly enriched with optimal codons. This is in contrast to what was recently found in the developing zebrafish where non-optimal codons signaled deadenylation (Mishima and Tomari, 2016, Weill et al., 2012). This discrepancy may be explained by the different consequences of CNOT7-mediated deadenylation in these two systems. In the developing zebrafish zygote, CNOT7 targets maternal mRNAs for degradation (Mishima and Tomari, 2016); whereas in dendrites, deadenylation serves to silence mRNAs in anticipation of stimulation when their swift translation is required. One feature that dictates translation speed is codon optimality (Yu et al., 2015, Weinberg et al., 2016, Presnyak et al., 2015). Increased use of optimal codons results in decreased stalling of ribosomes, as demonstrated by ribosome profiling, possibly due to an increased abundance of the tRNAs recognizing such codons (Dittmar et al., 2006, Presnyak et al., 2015). Enriching dendritic mRNAs with optimal codons may aid in their speedy translation in response to synaptic activity. Another feature of these mRNAs that may enable efficient translation is their codon preference. We found that the mRNAs deadenylated by CNOT7 tend to share the same codon preference for each amino acid. This phenomenon is traditionally associated with mRNAs that must be translated simultaneously, such as DNA damage response genes and cell cycle genes, and leads to faster translation possibly due to tRNA reuse (Begley et al., 2007, Frenkel-Morgenstern

et al., 2012, Presnyak et al., 2015). It is likely that optimal codons do not target

CNOT7 to these mRNAs, but is rather a shared feature that poises them for

instantaneous, stimulation-induced translation.
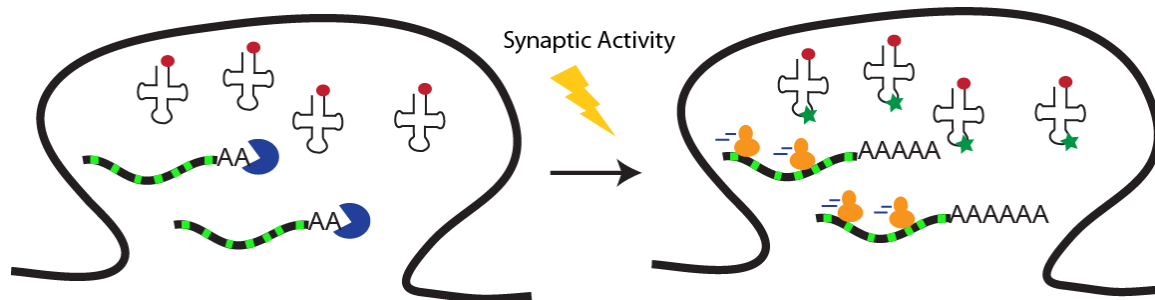
Figure 4.2: Codon usage bias can aid in efficient translation. In naïve synapses, CNOT7 represses translation of specific mRNAs localized to post-synaptic sites. In response to synaptic activity, changes in tRNA modifications (green stars) and/or localization can change the local codon optimality resulting in speedy translation of the newly un-repressed CNOT7 targets, enriched with specific codons (green boxes).

"Optimal" or "non-optimal" codons are defined based on the assumption

that codon usage in the cell is fixed. Codon optimality, however, is hinged on

tRNAs that incur changes in their abundance, modifications, and localization

making this a very dynamic process. There are over 50 different modifications in

eukaryotes that confer changes to tRNA folding, stability and translation

efficiency (Novoa and Ribas de Pouplana, 2012)

(http://mods.rna.albany.edu/home). One such modification, methylation at the

wobble position of tRNA$^{\text{Leu(}\underline{\text{C}}\text{AA)}}$, increases the binding of the anticodon with the

UUG codon. In yeast, this methylation is increased in response to oxidative

stress, resulting in increased translation of critical stress response genes who

preferentially utilize the UUG codon (Chan et al., 2012). This is just one example

of a modification of tRNAs in response to a specific stimulus (Begley et al., 2007,

Patil et al., 2012, Novoa and Ribas de Pouplana, 2012). It would be interesting to

test if synaptic activity increases specific tRNA modifications, resulting in

increased translation of CNOT7 targets who share similar codon preferences

(Figure 4.2). Such modifications and codon preferences would likely be vital for

synaptic plasticity and normal neuronal function. This idea is plausible, as

mutations in genes encoding tRNA modification enzymes have been linked to

neurological disorders in humans (Torres et al., 2014).

Using fluorescent in-situ hybridizations (FISH), tRNAs have been shown to

be present in dendrites (Tiedge and Brosius, 1996), however, it is unclear if this

population of tRNAs is different from that in the soma. Preferential localization of

tRNAs occurs in the mitochondria (Kapushoc et al., 2002, Salinas et al., 2012)

and similar mechanisms could dictate the tRNA population in dendrites. FISH for

specific tRNAs or immunocytochemistry for their modifying enzymes could

potentially reveal a local codon usage environment in dendrites that is capable of

responding to stimulation (Figure 4.2).

It is well known that non-optimal codons target mRNAs for degradation

(Radhakrishnan et al., 2016, Mishima and Tomari, 2016, Presnyak et al., 2015).

This codon-mediated degradation is dependent on translation and is probably

due to ribosomes moving slowly due to decreased levels of the tRNAs

recognizing these codons. These slow ribosomes are detected by proteins, such as Ddx6, which recruit the degradation machinery (Mishima and Tomari, 2016, Radhakrishnan et al., 2016). We identified a subset of neuronal mRNAs, enriched with non-optimal codons, which are protected from deadenylation and degradation by CNOT7. This protection is dependent on CNOT7 being present in the CNOT complex and on its enzymatic activity (Figure 3.1C). This perplexing phenomenon may be explained by our proposed neuronal function of CNOT7: translation repression. If CNOT7 represses translation by shortening the poly(A) tail, the mRNA is potentially not circularized and the ribosome is not recruited (Figure 4.3). Upon CNOT7 depletion, however, the poly(A) tail lengthens possibly recruiting more Poly(A) Binding Protein (PABP) which stabilizes the eIF4F complex on the 5' cap of the mRNA likely resulting in circularization of the mRNA and recruitment of ribosomes (Wells et al., 1998). These newly loaded ribosomes may stall over non-optimal codons, resulting in deadenylation and decay of the mRNA (Figure 4.3). For this hypothesis to be valid, the deadenylation following CNOT7-depletion must be dependent on translation, non-optimal codons, and increased stalled ribosomes. One could test this with several different reporter mRNAs whose translation is inhibited (via a stem loop inserted before the coding region), or whose codon usage is modulated. Northern blot analysis of these different reporters, as well as a non-mutated control, following polysome fractionation can then be performed to test for differential ribosome density and therefore differential stalling of the ribosome. These data also suggest that

another deadenylase is functioning with the degradation machinery to target neuronal mRNAs enriched with non-optimal codons. This deadenylase is likely one of the enzymes already shown to function in the brain. For example the deadenylase PARN is present in the hippocampal CA1 neuropil as well as synaptosomes from mouse forebrain (Udagawa 2012)(Cajigas et al., 2012). PARN also forms a complex in cultured hippocampal neurons with CPEB and Gld2, both regulators of local translation. The fact that depletion of PARN in mice hippocampi does not result in altered LTP, similar to depletion of other members of the CPEB complex, does not rule out the possibility that PARN is a regulator of local translation as these results could be due to inadequate depletion of PARN (Udagawa, 2012). Another deadenylase, PAN2, may also be a candidate for regulating neuronal mRNAs. In a recent study, PAN2 in conjunction with FUS was identified to regulate the translation of GluA1, an AMPA receptor subunit essential for synaptic plasticity (Udagawa 2015). Moreover, depletion of FUS in the hippocampus resulted in impaired synaptic transmission and social interaction. It remains unclear if PAN2 carries out these functions locally in dendrites in response to synaptic activity, which could be an important distinction between CNOT7's and PAN2's functions in the hippocampus. Either one of these enzymes could be responsible for targeting non-optimal codons in the brain and should therefore be followed up, possibly using double knockdown approaches with both CNOT7 and one of the deadenylases and observing poly(A) tail length of non-optimal mRNAs.
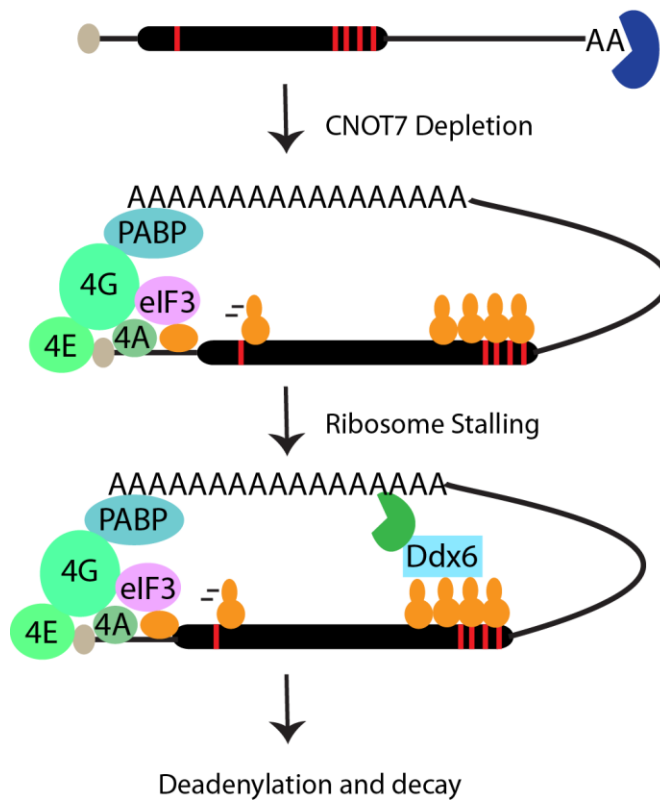
Figure 4.3: **Model for deadenylation induced by CNOT7 depletion**. CNOT7 represses translation of mRNAs through deadenylation. Upon CNOT7 depletion, Poly(A) Binding Protein (PABP) binds to the newly elongated poly(A) tail and stabilizes the eIF4F complex (4E, 4G, & 4A) onto the 5' cap. eIF3 binds the eIF4F complex and recruits the ribosome leading to translation of the mRNA (Weill et al., 2012) (Wells et al., 1998). The presence of non-optimal codons results in stalling of the ribosome, which signals Ddx6 and the decay machinery (Radhakrishnan et al., 2016, Plotkin and Kudla, 2011).

In zebrafish, a long 3'UTR, irrespective of the actual sequence, confers protection to mRNAs enriched with non-optimal codons (Mishima and Tomari, 2016). In addition to non-optimal codons, the CNOT7-protected mRNAs also have exceptionally long 3'UTRs. It would be interesting to test whether the long 3'UTR is essential for CNOT7-mediated protection, by designing mutant reporters with varying 3'UTR lengths and observing their poly(A) tail size in wildtype neurons. It is difficult to reason why a long 3' UTR could bestow protection on mRNAs. Mishima et al postulated a distance model, where the non-optimal codons target the degradation machinery to the coding region of the mRNA, however, because of the large distance between the degradation machinery and the poly(A), deadenylation is slow and

the mRNA is stable (Presnyak et al., 2015). Loss of CNOT7 would result in immediate lengthening of the poly(A) tail and encourage circularization of the mRNA (Wells et al., 1998), bringing the poly(A) and the decay machinery together; resulting in deadenylation and degradation of the mRNA (Figure 4.3).

One can imagine several scenarios where tight, negative regulation of mRNAs would be beneficial to the neurons. First, in dendrites, it is hypothesized that only a burst of translation is necessary in response to stimulation (Wu et al., 2016, Giorgi et al., 2007, di Penta et al., 2009). Some mRNAs such as arc, undergo the pioneer round of translation in dendrites and are degraded soon thereafter (Giorgi et al., 2007). The use of non-optimal codons may be one mechanism to ensure only a burst of translation before these mRNAs are targeted for degradation (Figure 4.3). One could test this by measuring the mRNA levels and their protein products following stimulation. Second, as described earlier, changes in tRNA modifications and/or localization can change the definition of "optimal codon" (Novoa and Ribas de Pouplana, 2012). Perhaps CNOT7 is repressing the translation of these mRNAs to protect them from codon-mediated degradation. Translation can then be activated, following stimulation or after localization, when their codon usage is considered optimal (Figure 4.2). Regardless of the reason for tight regulation of these mRNAs, the fact that this phenomenon is conserved between zebrafish zygotes and mouse neurons suggests that this is an evolutionally important characteristic of CNOT7 targets.

mRNA localization

In addition to its translational repression function, CNOT7 appears to also play a vital role in dendritic localization of mRNAs. It is not alone in this dual function as several translational repressors also mediate their targets localization. For example, ectopic expression of a mutant CPEB, which cannot interact with molecular motors, inhibits dendritic transport of its targets in rat hippocampal neurons (Huang et al., 2003). Another RNA-binding protein, ZBP1, represses the local translation of β-actin mRNA while also controlling its localization in hippocampal neurons (Huttelmaier et al., 2005). It is possible that dendritic localization of mRNA is merely a result of their translational silencing, as even a chemical translation inhibitor results in dendritic localization of mRNAs previously confined to the soma (Kleiman et al., 1993). One could test this hypothesis by inhibiting the translation of a CNOT7 target in CNOT7KD cells and testing if this restores its dendritic localization. Tightly linking translational inhibition to mRNA transport is beneficial to neurons as it prevents spurious translation of targets and ensures their activity-dependent local translation.

Not all translational repressors exhibit this dual function of silencing and transport. Knockout mice of FMRP, a well-known repressor of local translation, exhibit normal localization of some of FMRP targets (Steward et al., 1998), indicating these two vital roles do not always go hand in hand. Even for CNOT7, a mutation that abrogates its enzymatic activity does not produce as dramatic of

an effect on mRNA localization as its knockdown (Figure 2.2I); indicating translation repression is not the sole dictator of CNOT7-mediated localization. Protein:protein interactions may also mediate this function, as several CNOT7-associated proteins have known roles in mRNA localization (Lau et al., 2009). One such protein is the Muscleblind-like isoform 1 protein, MBNL1. This protein is an RNA-binding protein that binds CUG repeats and regulates splicing of mRNAs (Osborne and Thornton, 2006). MBNL1 has been linked to Myotonic Muscular Dystrophy (MMD), where a CUG repeat expansion sequesters the protein leading to mis-splicing of several of its targets (Osborne and Thornton, 2006). This loss of function of MBNL1 is likely crucial to the development of the MMD, as MBNL1 knockout mice recapitulate several of the disease's phenotypes (Kanadia et al., 2003). Although most work focuses on the splicing function of MBNL1, it also functions in the cytoplasm to regulate mRNA stability and localization (Masuda et al., 2012, Wang et al., 2012). Specifically in neurons, MBNL1 localizes mRNAs with CUGCUG motifs, similar to the motif enriched in CNOT7 targets, to neurites, enriching these mRNAs in this region of the neuron (Taliaferro et al., 2016). Although it has yet to be shown, it is thought that MBNL1 mediates the localization of its targets by binding directly to the cytoskeleton (Wang et al., 2012). It is possible that MBNL1 targets CNOT7 to mRNAs containing the CUG repeat motif to silence them during transport and ensure local translation of these mRNAs. This interaction would be crucial for synaptic plasticity and may connect CNOT7 to the pathophysiology of MMD.

For a subset of CNOT7 targets, dendritic localization may be dictated by their exceptionally long 3'UTRs. This region of the mRNA contains most of the elements that dictate localization (Andreassi and Riccio, 2009), and it is likely that longer 3'UTRs would contain more of these signals and therefore exhibit more localization. This assumption cannot be applied to all neurons, but at least in dorsal root ganglia neurons, longer 3'UTRs are preferentially localized to neurites (Taliaferro et al., 2016). Data from the Schuman lab identified ~30% of these mRNAs enriched in CA1 hippocampal dendrites and/or axons; one of which, SNCA, we were able to validate via FISH in dendrites of cultured neurons (Figure 2.10A) (Cajigas et al., 2012). This CA1 dendritic enrichment is not different from CNOT7 targets with shorter 3'UTRs, however the Schuman lab was very conservative in which mRNAs they defined as dendritic. They removed any mRNAs enriched in glia cells, interneurons, blood vessels, mitochondria, and ones that code for nuclear proteins based on published literature. This filtering removed ~70% of neuropil-localized mRNAs and would miss any mRNAs expressed in both neuronal and non-neuronal cells, making it likely that this list is not all encompassing (Cajigas et al., 2012). Utilizing reporter mRNAs with varying length 3'UTRs would help address if this characteristic dictates localization. Further characterization of these 3'UTRs would then be necessary to determine which elements are responsible for this localization.

miRNA-targeting elements may be examples of such features essential for dendritic localization of CNOT7 targets containing long 3'UTRs. miRNAs and

components of the RISC machinery have been identified as being enriched in the neurites of hippocampal neurons and in synaptic-enriched fractions (Kye et al., 2007, Pichardo-Casas et al., 2012, Lugli et al., 2005, Bicker et al., 2013). These components appear to be responsible for both the dendritic transport of their targets and for translation regulation in response to synaptic activity and learning and memory (Ashraf et al., 2006, Vetere et al., 2014, Sambandan et al., 2017). The exact mechanism by which the RISC machinery carry out these functions is unclear, however it is likely mediated through recruitment of translation repressors, such as the CNOT complex (Braun et al., 2011). The long 3'UTR targets of CNOT7 contain an increased amount of miRNA targeting sequences suggesting increased recruitment of miRNA and possibly CNOT7. Future work is necessary to test if the miRNA targeting sequences in the long 3'UTRs are responsible for their dendritic localization and CNOT7-mediated poly(A) tail regulation.

Concluding Remarks

This work provided the first link of CNOT7 to neuronal function, through its regulation of polyadenylation and localization of dendritic mRNAs. This role is vital for normal cognitive function in mice and may have a relevance to autistic disorders as the CNOT7KD mice exhibited phenotypes classically shown in autistic mouse models such as increased anxiety, impaired learning and memory, and impaired nest building (Restivo et al., 2005, Ding et al., 2014, Kwon

et al., 2006). We initiated this study in hopes of identifying a regulator of local translation that could potentially have implications in autistic disorders; however, it is likely that CNOT7 could be at the center of a wide variety of neurological disorders including myotonic dystrophy (as mentioned above) and Huntington's disease. Huntington's disease is an autosomal dominant disorder resulting from a CAG repeat expansion in the first exon of the huntingtin gene (1993). A complex movement disorder is the hallmark of this disease, however patients also suffer from behavioral and cognitive decline (Reilmann et al., 2014). Although toxic mutant protein accumulation is thought to underlie the neuronal dysfunction in this disease, neurotoxicity is still present when translation of the mutant mRNA is inhibited, indicating a toxic RNA gain-of-function (Banez-Coronel et al., 2012). Based on our sequencing data, the poly(A) tail of huntingtin is modulated by CNOT7; it also contains an exceptionally long 3'UTR and non-optimal codon enrichment, characteristics we found were associated with CNOT7 targets. It would be interesting to test if CNOT7 is sequestered by the mutant huntingtin gene, and if this sequestering is mediated by MBNL1. Indeed, both CAG and CUG repeats are capable of sequestering MBNL1, and studies have demonstrated that MBNL1 binds directly to huntingtin (Sun et al., 2015, Kino et al., 2015, Mykowska et al., 2011). Huntington's disease brains also demonstrate extensive alternative splicing compared to normal brains, a hallmark of MBNL1 dysfunction (Labadorf and Myers, 2015, Neueder et al., 2017). Taken together these data suggest that the CAG repeat expansion could theoretically sequester

MBNL1 in Huntington's patients, which could potentially affect CNOT7's function and contribute to disease. Now that we have demonstrated the essential role of CNOT7 in neurons, it is imperative to elucidate further how CNOT7 carries out these functions and its relevance to neurological disorders.

BIBLIOGRAPHY

1993. A novel gene containing a trinucleotide repeat that is expanded and unstable on Huntington's disease chromosomes. The Huntington's Disease Collaborative Research Group. *Cell,* 72**,** 971-83.

ALARCON, J. M., HODGMAN, R., THEIS, M., HUANG, Y. S., KANDEL, E. R. & RICHTER, J. D. 2004. Selective modulation of some forms of schaffer collateral-CA1 synaptic plasticity in mice with a disruption of the CPEB-1 gene. *Learn Mem,* 11**,** 318-27.

ALBERT, T. K., HANZAWA, H., LEGTENBERG, Y. I., DE RUWE, M. J., VAN DEN HEUVEL, F. A., COLLART, M. A., BOELENS, R. & TIMMERS, H. T. 2002. Identification of a ubiquitin-protein ligase subunit within the CCR4-NOT transcription repressor complex. *EMBO J,* 21**,** 355-64.

ALVAREZ-CASTELAO, B. & SCHUMAN, E. M. 2015. The Regulation of Synaptic Protein Turnover. *J Biol Chem,* 290**,** 28623-30.

ANDREASSI, C. & RICCIO, A. 2009. To localize or not to localize: mRNA fate is in 3'UTR ends. *Trends Cell Biol,* 19**,** 465-74.

ARTINIAN, J., DE JAEGER, X., FELLINI, L., DE SAINT BLANQUAT, P. & ROULLET, P. 2007. Reactivation with a simple exposure to the experimental environment is sufficient to induce reconsolidation requiring protein synthesis in the hippocampal CA3 region in mice. *Hippocampus,* 17**,** 181-91.

ASHRAF, S. I., MCLOON, A. L., SCLARSIC, S. M. & KUNES, S. 2006. Synaptic protein synthesis associated with memory is regulated by the RISC pathway in Drosophila. *Cell,* 124**,** 191-205.

ASLAM, A., MITTAL, S., KOCH, F., ANDRAU, J. C. & WINKLER, G. S. 2009. The Ccr4-NOT deadenylase subunits CNOT7 and CNOT8 have overlapping roles and modulate cell proliferation. *Mol Biol Cell,* 20**,** 3840-50.

BAGGS, J. E. & GREEN, C. B. 2003. Nocturnin, a deadenylase in Xenopus laevis retina: a mechanism for posttranscriptional control of circadian-related mRNA. *Curr Biol,* 13**,** 189-98.

BAILEY, C. H. & CHEN, M. 1988a. Long-term memory in Aplysia modulates the total number of varicosities of single identified sensory neurons. *Proc Natl Acad Sci U S A,* 85**,** 2373-7.

BAILEY, C. H. & CHEN, M. 1988b. Long-term sensitization in Aplysia increases the number of presynaptic contacts onto the identified gill motor neuron L7. *Proc Natl Acad Sci U S A,* 85**,** 9356-9.

BANEZ-CORONEL, M., PORTA, S., KAGERBAUER, B., MATEU-HUERTAS, E., PANTANO, L., FERRER, I., GUZMAN, M., ESTIVILL, X. & MARTI, E. 2012. A pathogenic mechanism in Huntington's disease involves small CAG-repeated RNAs with neurotoxic activity. *PLoS Genet,* 8**,** e1002481.

BARKOFF, A., BALLANTYNE, S. & WICKENS, M. 1998. Meiotic maturation in Xenopus requires polyadenylation of multiple mRNAs. *EMBO J,* 17**,** 3168-75.

BAWANKAR, P., LOH, B., WOHLBOLD, L., SCHMIDT, S. & IZAURRALDE, E. 2013. NOT10 and C2orf29/NOT11 form a conserved module of the CCR4-NOT complex that docks onto the NOT1 N-terminal domain. *RNA Biol,* 10**,** 228-44.

BEGLEY, U., DYAVAIAH, M., PATIL, A., ROONEY, J. P., DIRENZO, D., YOUNG, C. M., CONKLIN, D. S., ZITOMER, R. S. & BEGLEY, T. J. 2007. Trm9-catalyzed tRNA modifications link translation to the DNA damage response. *Mol Cell,* 28**,** 860-70.

BEILHARZ, T. H. & PREISS, T. 2007. Widespread use of poly(A) tail length control to accentuate expression of the yeast transcriptome. *RNA,* 13**,** 982-97.

BENNETTO, L., PENNINGTON, B. F. & ROGERS, S. J. 1996. Intact and impaired memory functions in autism. *Child Dev,* 67**,** 1816-35.

BERGER-SWEENEY, J., ZEARFOSS, N. R. & RICHTER, J. D. 2006. Reduced extinction of hippocampal-dependent memories in CPEB knockout mice. *Learn Mem,* 13**,** 4-7.

BHATTACHARYA, A., KAPHZAN, H., ALVAREZ-DIEPPA, A. C., MURPHY, J. P., PIERRE, P. & KLANN, E. 2012. Genetic removal of p70 S6 kinase 1 corrects molecular, synaptic, and behavioral phenotypes in fragile X syndrome mice. *Neuron,* 76**,** 325-37.

BICKER, S., KHUDAYBERDIEV, S., WEISS, K., ZOCHER, K., BAUMEISTER, S. & SCHRATT, G. 2013. The DEAH-box helicase DHX36 mediates dendritic localization of the neuronal precursor-microRNA-134. *Genes Dev,* 27**,** 991-6.

BLISS, T. V. & LOMO, T. 1973. Long-lasting potentiation of synaptic transmission in the dentate area of the anaesthetized rabbit following stimulation of the perforant path. *J Physiol,* 232**,** 331-56.

BOLAND, A., CHEN, Y., RAISCH, T., JONAS, S., KUZUOGLU-OZTURK, D., WOHLBOLD, L., WEICHENRIEDER, O. & IZAURRALDE, E. 2013. Structure and assembly of the NOT module of the human CCR4-NOT complex. *Nat Struct Mol Biol,* 20**,** 1289-97.

BONISCH, C., TEMME, C., MORITZ, B. & WAHLE, E. 2007. Degradation of hsp70 and other mRNAs in Drosophila via the 5' 3' pathway and its regulation by heat shock. *J Biol Chem,* 282**,** 21818-28.

BOURTCHOULADZE, R., ABEL, T., BERMAN, N., GORDON, R., LAPIDUS, K. & KANDEL, E. R. 1998. Different training procedures recruit either one or two critical periods for contextual memory consolidation, each of which requires protein synthesis and PKA. *Learn Mem,* 5**,** 365-74.

BRADSHAW, K., EMPTAGE, N. & BLISS, T. 2003a. A role for dendritic protein synthesis in hippocampal late LTP. *European Journal of Neuroscience***,** 3150-52.

BRADSHAW, K. D., EMPTAGE, N. J. & BLISS, T. V. 2003b. A role for dendritic protein synthesis in hippocampal late LTP. *Eur J Neurosci,* 18**,** 3150-2.

BRANDON, J. G. & COSS, R. G. 1982. Rapid dendritic spine stem shortening during one-trial learning: the honeybee's first orientation flight. *Brain Res,* 252**,** 51-61.

BRAUN, J. E., HUNTZINGER, E., FAUSER, M. & IZAURRALDE, E. 2011. GW182 proteins directly recruit cytoplasmic deadenylase complexes to miRNA targets. *Mol Cell,* 44**,** 120-33.

BROOK, J. D., MCCURRACH, M. E., HARLEY, H. G., BUCKLER, A. J., CHURCH, D., ABURATANI, H., HUNTER, K., STANTON, V. P., THIRION, J. P., HUDSON, T. & ET AL. 1992. Molecular basis of myotonic dystrophy: expansion of a trinucleotide (CTG) repeat at the 3' end of a transcript encoding a protein kinase family member. *Cell,* 69**,** 385.

BROWN, C. E., TARUN, S. Z., JR., BOECK, R. & SACHS, A. B. 1996. PAN3 encodes a subunit of the Pab1p-dependent poly(A) nuclease in Saccharomyces cerevisiae. *Mol Cell Biol,* 16**,** 5744-53.

BUTLER, M. G., DASOUKI, M. J., ZHOU, X. P., TALEBIZADEH, Z., BROWN, M., TAKAHASHI, T. N., MILES, J. H., WANG, C. H., STRATTON, R., PILARSKI, R. & ENG, C. 2005. Subset of

individuals with autism spectrum disorders and extreme macrocephaly associated with germline PTEN tumour suppressor gene mutations. *J Med Genet,* 42**,** 318-21.

BUTTERS, N., WOLFE, J., MARTONE, M., GRANHOLM, E. & CERMAK, L. S. 1985. Memory disorders associated with Huntington's disease: verbal recall, verbal recognition and procedural memory. *Neuropsychologia,* 23**,** 729-43.

BUXBAUM, A. R., HAIMOVICH, G. & SINGER, R. H. 2015. In the right place at the right time: visualizing and understanding mRNA localization. *Nat Rev Mol Cell Biol,* 16**,** 95-109.

BUXBAUM, A. R., WU, B. & SINGER, R. H. 2014. Single beta-actin mRNA detection in neurons reveals a mechanism for regulating its translatability. *Science,* 343**,** 419-22.

CAJIGAS, I. J., TUSHEV, G., WILL, T. J., TOM DIECK, S., FUERST, N. & SCHUMAN, E. M. 2012. The local transcriptome in the synaptic neuropil revealed by deep sequencing and high-resolution imaging. *Neuron,* 74**,** 453-66.

CANO, F., BYE, H., DUNCAN, L. M., BUCHET-POYAU, K., BILLAUD, M., WILLS, M. R. & LEHNER, P. J. 2012. The RNA-binding E3 ubiquitin ligase MEX-3C links ubiquitination with MHC-I mRNA degradation. *EMBO J,* 31**,** 3596-606.

CANO, F., RAPITEANU, R., SEBASTIAAN WINKLER, G. & LEHNER, P. J. 2015. A non-proteolytic role for ubiquitin in deadenylation of MHC-I mRNA by the RNA-binding E3-ligase MEX-3C. *Nat Commun,* 6**,** 8670.

CEJAS, P., CAVAZZA, A., YANDAVA, C. N., MORENO, V., HORST, D., MORENO-RUBIO, J., BURGOS, E., MENDIOLA, M., TAING, L., GOEL, A., FELIU, J. & SHIVDASANI, R. A. 2017. Transcriptional Regulator CNOT3 Defines an Aggressive Colorectal Cancer Subtype. *Cancer Res,* 77**,** 766-779.

CHAN, C. T., PANG, Y. L., DENG, W., BABU, I. R., DYAVAIAH, M., BEGLEY, T. J. & DEDON, P. C. 2012. Reprogramming of tRNA modifications controls the oxidative stress response by codon-biased translation of proteins. *Nat Commun,* 3**,** 937.

CHEN, C., ITO, K., TAKAHASHI, A., WANG, G., SUZUKI, T., NAKAZAWA, T., YAMAMOTO, T. & YOKOYAMA, K. 2011. Distinct expression patterns of the subunits of the CCR4-NOT deadenylase complex during neural development. *Biochem Biophys Res Commun,* 411**,** 360-4.

CHEN, C. Y., ZHENG, D., XIA, Z. & SHYU, A. B. 2009. Ago-TNRC6 triggers microRNA-mediated decay by promoting two deadenylation steps. *Nat Struct Mol Biol,* 16**,** 1160-6.

CHEN, Y., BOLAND, A., KUZUOGLU-OZTURK, D., BAWANKAR, P., LOH, B., CHANG, C. T., WEICHENRIEDER, O. & IZAURRALDE, E. 2014. A DDX6-CNOT1 complex and W-binding pockets in CNOT9 reveal direct links between miRNA target recognition and silencing. *Mol Cell,* 54**,** 737-50.

CHO, J., YU, N. K., CHOI, J. H., SIM, S. E., KANG, S. J., KWAK, C., LEE, S. W., KIM, J. I., CHOI, D. I., KIM, V. N. & KAANG, B. K. 2015. Multiple repressive mechanisms in the hippocampus during memory formation. *Science,* 350**,** 82-7.

CID-ARREGUI, A., PARTON, R. G., SIMONS, K. & DOTTI, C. G. 1995. Nocodazole-dependent transport, and brefeldin A--sensitive processing and sorting, of newly synthesized membrane proteins in cultured neurons. *J Neurosci,* 15**,** 4259-69.

CIECHANOVER, A. 2005. Intracellular protein degradation: from a vague idea, through the lysosome and the ubiquitin-proteasome system, and onto human diseases and drug targeting (Nobel lecture). *Angew Chem Int Ed Engl,* 44**,** 5944-67.

CLARKE, J. R., CAMMAROTA, M., GRUART, A., IZQUIERDO, I. & DELGADO-GARCIA, J. M. 2010. Plastic modifications induced by object recognition memory processing. *Proc Natl Acad Sci U S A,* 107**,** 2652-7.

COSTA-MATTIOLI, M., SOSSIN, W. S., KLANN, E. & SONENBERG, N. 2009. Translational control of long-lasting synaptic plasticity and memory. *Neuron,* 61**,** 10-26.

DARNELL, R. B. 2013. RNA protein interaction in neurons. *Annu Rev Neurosci,* 36**,** 243-70.

DE GREGORIO, E., PREISS, T. & HENTZE, M. W. 1999. Translation driven by an eIF4G core domain in vivo. *EMBO J,* 18**,** 4865-74.

DEACON, R. M. 2006. Assessing nest building in mice. *Nat Protoc,* 1**,** 1117-9.

DEO, R. C., BONANNO, J. B., SONENBERG, N. & BURLEY, S. K. 1999. Recognition of polyadenylate RNA by the poly(A)-binding protein. *Cell,* 98**,** 835-45.

DI PENTA, A., MERCALDO, V., FLORENZANO, F., MUNCK, S., CIOTTI, M. T., ZALFA, F., MERCANTI, D., MOLINARI, M., BAGNI, C. & ACHSEL, T. 2009. Dendritic LSm1/CBP80-mRNPs mark the early steps of transport commitment and translational control. *J Cell Biol,* 184**,** 423-35.

DIETERICH, D. C., LINK, A. J., GRAUMANN, J., TIRRELL, D. A. & SCHUMAN, E. M. 2006. Selective identification of newly synthesized proteins in mammalian cells using bioorthogonal noncanonical amino acid tagging (BONCAT). *Proc Natl Acad Sci U S A,* 103**,** 9482-7.

DIETRICH, D. C., HODAS, J. J. L., GOUZER, G., SHADRIN, I. Y., NGO, J. T., TRILLER, A., TIRRELL, D. A. & SCHUMAN, E. M. 2010. In situ visualization and dynamics of newly synthesized proteins in rat hippocampal neurons. *Nature Neuroscience***,** 897-905.

DING, Q., SETHNA, F. & WANG, H. 2014. Behavioral analysis of male and female Fmr1 knockout mice on C57BL/6 background. *Behav Brain Res,* 271**,** 72-8.

DITTMAR, K. A., GOODENBOUR, J. M. & PAN, T. 2006. Tissue-specific differences in human transfer RNA expression. *PLoS Genet,* 2**,** e221.

DOIDGE, R., MITTAL, S., ASLAM, A. & WINKLER, G. S. 2012a. The anti-proliferative activity of BTG/TOB proteins is mediated via the Caf1a (CNOT7) and Caf1b (CNOT8) deadenylase subunits of the Ccr4-not complex. *PLoS One,* 7**,** e51331.

DOIDGE, R., MITTAL, S., ASLAM, A. & WINKLER, G. S. 2012b. Deadenylation of cytoplasmic mRNA by the mammalian Ccr4-Not complex. *Biochem Soc Trans,* 40**,** 896-901.

DOYERE, V. & LAROCHE, S. 1992. Linear relationship between the maintenance of hippocampal long-term potentiation and retention of an associative memory. *Hippocampus,* 2**,** 39-48.

DU, L. & RICHTER, J. D. 2005. Activity-Dependent polyadenylation in neurons. *RNA***,** 1340-1347.

DUBNAU, J., CHIANG, A. S., GRADY, L., BARDITCH, J., GOSSWEILER, S., MCNEIL, J., SMITH, P., BULDOC, F., SCOTT, R., CERTA, U., BROGER, C. & TULLY, T. 2003. The staufen/pumilio pathway is involved in Drosophila long-term memory. *Curr Biol,* 13**,** 286-96.

EHLERS, M. D. 2003. Activity level controls postsynaptic composition and signaling via the ubiquitin-proteasome system. *Nat Neurosci,* 6**,** 231-42.

EHNINGER, D., HAN, S., SHILYANSKY, C., ZHOU, Y., LI, W., KWIATKOWSKI, D. J., RAMESH, V. & SILVA, A. J. 2008. Reversal of learning deficits in a Tsc2+/- mouse model of tuberous sclerosis. *Nat Med,* 14**,** 843-8.

EOM, T., ZHANG, C., WANG, H., LAY, K., FAK, J., NOEBELS, J. L. & DARNELL, R. B. 2013. NOVA-dependent regulation of cryptic NMD exons controls synaptic protein levels after seizure. *Elife,* 2**,** e00178.

EZZEDDINE, N., CHANG, T. C., ZHU, W., YAMASHITA, A., CHEN, C. Y., ZHONG, Z., YAMASHITA, Y., ZHENG, D. & SHYU, A. B. 2007. Human TOB, an antiproliferative transcription factor, is a

poly(A)-binding protein-dependent positive regulator of cytoplasmic mRNA deadenylation. *Mol Cell Biol,* 27**,** 7791-801.

FABIAN, M. R., CIEPLAK, M. K., FRANK, F., MORITA, M., GREEN, J., SRIKUMAR, T., NAGAR, B., YAMAMOTO, T., RAUGHT, B., DUCHAINE, T. F. & SONENBERG, N. 2011. miRNA-mediated deadenylation is orchestrated by GW182 through two conserved motifs that interact with CCR4-NOT. *Nat Struct Mol Biol,* 18**,** 1211-7.

FABIAN, M. R., FRANK, F., ROUYA, C., SIDDIQUI, N., LAI, W. S., KARETNIKOV, A., BLACKSHEAR, P. J., NAGAR, B. & SONENBERG, N. 2013. Structural basis for the recruitment of the human CCR4-NOT deadenylase complex by tristetraprolin. *Nat Struct Mol Biol,* 20**,** 735-9.

FABIAN, M. R., MATHONNET, G., SUNDERMEIER, T., MATHYS, H., ZIPPRICH, J. T., SVITKIN, Y. V., RIVAS, F., JINEK, M., WOHLSCHLEGEL, J., DOUDNA, J. A., CHEN, C. Y., SHYU, A. B., YATES, J. R., 3RD, HANNON, G. J., FILIPOWICZ, W., DUCHAINE, T. F. & SONENBERG, N. 2009. Mammalian miRNA RISC recruits CAF1 and PABP to affect PABP-dependent deadenylation. *Mol Cell,* 35**,** 868-80.

FARAJI, F., HU, Y., YANG, H. H., LEE, M. P., WINKLER, G. S., HAFNER, M. & HUNTER, K. W. 2016. Post-transcriptional Control of Tumor Cell Autonomous Metastatic Potential by CCR4-NOT Deadenylase CNOT7. *PLoS Genet,* 12**,** e1005820.

FARBER, V., ERBEN, E., SHARMA, S., STOECKLIN, G. & CLAYTON, C. 2013. Trypanosome CNOT10 is essential for the integrity of the NOT deadenylase complex and for degradation of many mRNAs. *Nucleic Acids Res,* 41**,** 1211-22.

FAZELI, M. S., CORBET, J., DUNN, M. J., DOLPHIN, A. C. & BLISS, T. V. 1993. Changes in protein synthesis accompanying long-term potentiation in the dentate gyrus in vivo. *J Neurosci,* 13**,** 1346-53.

FRENKEL-MORGENSTERN, M., DANON, T., CHRISTIAN, T., IGARASHI, T., COHEN, L., HOU, Y. M. & JENSEN, L. J. 2012. Genes adopt non-optimal codon usage to generate cell cycle-dependent oscillations in protein levels. *Mol Syst Biol,* 8**,** 572.

GILMARTIN, G. M. 2005. Eukaryotic mRNA 3' processing: a common means to different ends. *Genes Dev,* 19**,** 2517-21.

GINGRAS, A. C., RAUGHT, B., GYGI, S. P., NIEDZWIECKA, A., MIRON, M., BURLEY, S. K., POLAKIEWICZ, R. D., WYSLOUCH-CIESZYNSKA, A., AEBERSOLD, R. & SONENBERG, N. 2001. Hierarchical phosphorylation of the translation inhibitor 4E-BP1. *Genes Dev,* 15**,** 2852-64.

GIORGI, C., YEO, G. W., STONE, M. E., KATZ, D. B., BURGE, C., TURRIGIANO, G. & MOORE, M. J. 2007. The EJC factor eIF4AIII modulates synaptic strength and neuronal protein expression. *Cell,* 130**,** 179-91.

GKOGKAS, C. G., KHOUTORSKY, A., CAO, R., JAFARNEJAD, S. M., PRAGER-KHOUTORSKY, M., GIANNAKAS, N., KAMINARI, A., FRAGKOULI, A., NADER, K., PRICE, T. J., KONICEK, B. W., GRAFF, J. R., TZINIA, A. K., LACAILLE, J. C. & SONENBERG, N. 2014. Pharmacogenetic inhibition of eIF4E-dependent Mmp9 mRNA translation reverses fragile X syndrome-like phenotypes. *Cell Rep,* 9**,** 1742-55.

GLICK, D., BARTH, S. & MACLEOD, K. F. 2010. Autophagy: cellular and molecular mechanisms. *J Pathol,* 221**,** 3-12.

GOFFIN, A., HOEFSLOOT, L. H., BOSGOED, E., SWILLEN, A. & FRYNS, J. P. 2001. PTEN mutation in a family with Cowden syndrome and autism. *Am J Med Genet,* 105**,** 521-4.

GOLDSTROHM, A. C., HOOK, B. A., SEAY, D. J. & WICKENS, M. 2006. PUF proteins bind Pop2p to regulate messenger RNAs. *Nat Struct Mol Biol,* 13**,** 533-9.

GOLDSTROHM, A. C., SEAY, D. J., HOOK, B. A. & WICKENS, M. 2007. PUF protein-mediated deadenylation is catalyzed by Ccr4p. *J Biol Chem,* 282**,** 109-14.

GONG, B., CAO, Z., ZHENG, P., VITOLO, O. V., LIU, S., STANISZEWSKI, A., MOOLMAN, D., ZHANG, H., SHELANSKI, M. & ARANCIO, O. 2006. Ubiquitin hydrolase Uch-L1 rescues beta-amyloid-induced decreases in synaptic function and contextual memory. *Cell,* 126**,** 775-88.

GOODWIN, M., MOHAN, A., BATRA, R., LEE, K. Y., CHARIZANIS, K., FERNANDEZ GOMEZ, F. J., EDDARKAOUI, S., SERGEANT, N., BUEE, L., KIMURA, T., CLARK, H. B., DALTON, J., TAKAMURA, K., WEYN-VANHENTENRYCK, S. M., ZHANG, C., REID, T., RANUM, L. P., DAY, J. W. & SWANSON, M. S. 2015. MBNL Sequestration by Toxic RNAs and RNA Misprocessing in the Myotonic Dystrophy Brain. *Cell Rep,* 12**,** 1159-68.

GOSSELIN, P., MARTINEAU, Y., MORALES, J., CZJZEK, M., GLIPPA, V., GAUFFENY, I., MORIN, E., LE CORGUILLE, G., PYRONNET, S., CORMIER, P. & COSSON, B. 2013. Tracking a refined eIF4E-binding motif reveals Angel1 as a new partner of eIF4E. *Nucleic Acids Res,* 41**,** 7783-92.

GRIFO, J. A., TAHARA, S. M., MORGAN, M. A., SHATKIN, A. J. & MERRICK, W. C. 1983. New initiation factor activity required for globin mRNA translation. *J Biol Chem,* 258**,** 5804-10.

GRUART, A., MUNOZ, M. D. & DELGADO-GARCIA, J. M. 2006. Involvement of the CA3-CA1 synapse in the acquisition of associative learning in behaving mice. *J Neurosci,* 26**,** 1077-87.

GU, Q. H., YU, D., HU, Z., LIU, X., YANG, Y., LUO, Y., ZHU, J. & LI, Z. 2015. miR-26a and miR-384-5p are required for LTP maintenance and spine enlargement. *Nat Commun,* 6**,** 6789.

HAGHIGHAT, A., MADER, S., PAUSE, A. & SONENBERG, N. 1995. Repression of cap-dependent translation by 4E-binding protein 1: competition with p220 for binding to eukaryotic initiation factor-4E. *EMBO J,* 14**,** 5701-9.

HAN, C., JIAO, Y., ZHAO, Q. & LU, B. 2014. Mex3c mutation reduces adiposity partially through increasing physical activity. *J Endocrinol,* 221**,** 457-68.

HEESOM, K. J. & DENTON, R. M. 1999. Dissociation of the eukaryotic initiation factor-4E/4E-BP1 complex involves phosphorylation of 4E-BP1 by an mTOR-associated kinase. *FEBS Lett,* 457**,** 489-93.

HEGDE, A. N. 2016. Proteolysis, synaptic plasticity and memory. *Neurobiol Learn Mem*.

HEGDE, A. N., INOKUCHI, K., PEI, W., CASADIO, A., GHIRARDI, M., CHAIN, D. G., MARTIN, K. C., KANDEL, E. R. & SCHWARTZ, J. H. 1997. Ubiquitin C-terminal hydrolase is an immediate-early gene essential for long-term facilitation in Aplysia. *Cell,* 89**,** 115-26.

HEINZ, S., BENNER, C., SPANN, N., BERTOLINO, E., LIN, Y. C., LASLO, P., CHENG, J. X., MURRE, C., SINGH, H. & GLASS, C. K. 2010. Simple combinations of lineage-determining transcription factors prime cis-regulatory elements required for macrophage and B cell identities. *Mol Cell,* 38**,** 576-89.

HERSHKO, A. & CIECHANOVER, A. 1998. The ubiquitin system. *Annu Rev Biochem,* 67**,** 425-79.

HILGERS, V., TEIXEIRA, D. & PARKER, R. 2006. Translation-independent inhibition of mRNA deadenylation during stress in Saccharomyces cerevisiae. *RNA,* 12**,** 1835-45.

HORIUCHI, M., TAKEUCHI, K., NODA, N., MUROYA, N., SUZUKI, T., NAKAMURA, T., KAWAMURA-TSUZUKU, J., TAKAHASI, K., YAMAMOTO, T. & INAGAKI, F. 2009. Structural basis for the antiproliferative activity of the Tob-hCaf1 complex. *J Biol Chem,* 284**,** 13244-55.

HOSODA, N., FUNAKOSHI, Y., HIRASAWA, M., YAMAGISHI, R., ASANO, Y., MIYAGAWA, R., OGAMI, K., TSUJIMOTO, M. & HOSHINO, S. 2011. Anti-proliferative protein Tob negatively regulates CPEB3 target by recruiting Caf1 deadenylase. *EMBO J,* 30**,** 1311-23.

HUANG, J., IKEUCHI, Y., MALUMBRES, M. & BONNI, A. 2015. A Cdh1-APC/FMRP Ubiquitin Signaling Link Drives mGluR-Dependent Synaptic Plasticity in the Mammalian Brain. *Neuron,* 86**,** 726-39.

HUANG, Y.-S. & RICHTER, J. D. 2007. Analysis of mRNA Translation in Cultured Hippocanmpal Neurons. *Methods in Enzymology***,** 143-162.

HUANG, Y. S., CARSON, J. H., BARBARESE, E. & RICHTER, J. D. 2003. Facilitation of dendritic mRNA transport by CPEB. *Genes Dev,* 17**,** 638-53.

HUANG, Y. S., JUNG, M. Y., SARKISSIAN, M. & RICHTER, J. D. 2002. N-methyl-D-aspartate receptor signaling results in Aurora kinase-catalyzed CPEB phosphorylation and alpha CaMKII mRNA polyadenylation at synapses. *EMBO J,* 21**,** 2139-48.

HUBER, K. M., KAYSER, M. S. & BEAR, M. F. 2000. Role for rapid dendritic protein synthesis in hippocampal mGluR-dependent long-term depression. *Science,* 288**,** 1254-7.

HUBER KM, K. M., AND BEAR MF 2000. Role for rapid dendritic protein synthesis in hippocampal mGLUR-dependent long-term depression. *Science,* 273**,** 1254-1257.

HUTTELMAIER, S., ZENKLUSEN, D., LEDERER, M., DICTENBERG, J., LORENZ, M., MENG, X., BASSELL, G. J., CONDEELIS, J. & SINGER, R. H. 2005. Spatial regulation of beta-actin translation by Src-dependent phosphorylation of ZBP1. *Nature,* 438**,** 512-5.

INOUE, T., MORITA, M., HIJIKATA, A., FUKUDA-YUZAWA, Y., ADACHI, S., ISONO, K., IKAWA, T., KAWAMOTO, H., KOSEKI, H., NATSUME, T., FUKAO, T., OHARA, O., YAMAMOTO, T. & KUROSAKI, T. 2015. CNOT3 contributes to early B cell development by controlling Igh rearrangement and p53 mRNA stability. *J Exp Med,* 212**,** 1465-79.

ITO, K., INOUE, T., YOKOYAMA, K., MORITA, M., SUZUKI, T. & YAMAMOTO, T. 2011. CNOT2 depletion disrupts and inhibits the CCR4-NOT deadenylase complex and induces apoptotic cell death. *Genes Cells,* 16**,** 368-79.

JESTE, S. S., SAHIN, M., BOLTON, P., PLOUBIDIS, G. B. & HUMPHREY, A. 2008. Characterization of autism in young children with tuberous sclerosis complex. *J Child Neurol,* 23**,** 520-5.

JIAO, Y., BISHOP, C. E. & LU, B. 2012. Mex3c regulates insulin-like growth factor 1 (IGF1) expression and promotes postnatal growth. *Mol Biol Cell,* 23**,** 1404-13.

KADYROVA, L. Y., HABARA, Y., LEE, T. H. & WHARTON, R. P. 2007. Translational control of maternal Cyclin B mRNA by Nanos in the Drosophila germline. *Development,* 134**,** 1519-27.

KANADIA, R. N., JOHNSTONE, K. A., MANKODI, A., LUNGU, C., THORNTON, C. A., ESSON, D., TIMMERS, A. M., HAUSWIRTH, W. W. & SWANSON, M. S. 2003. A muscleblind knockout model for myotonic dystrophy. *Science,* 302**,** 1978-80.

KANDEL, E. R. 2001a. The molecular biology of memory storage: a dialog between genes and synapses. *Biosci Rep,* 21**,** 565-611.

KANDEL, E. R. 2001b. The molecular biology of memory storage: a dialogue between genes and synapses. *Science***,** 1030-8.

KANG, H. & SCHUMAN, E. M. 1996. A requirement for local protein synthesis in neurotrophin-induced hippocampal synaptic plasticity. *Science,* 273**,** 1402-6.

KANG H, S. E. 1996. A requirement for local protein synthesis in neutrophin-induced hippocampal synaptic plasticity. *Science***,** 1402-1406.

KAPUSHOC, S. T., ALFONZO, J. D. & SIMPSON, L. 2002. Differential localization of nuclear-encoded tRNAs between the cytosol and mitochondrion in Leishmania tarentolae. *RNA,* 8**,** 57-68.

KAUDERER, B. S. & KANDEL, E. R. 2000. Capture of a protein synthesis-dependent component of long-term depression. *Proc Natl Acad Sci U S A,* 97**,** 13342-7.

KELLEHER, R. J., 3RD & BEAR, M. F. 2008. The autistic neuron: troubled translation? *Cell,* 135**,** 401-6.

KIM, D., PERTEA, G., TRAPNELL, C., PIMENTEL, H., KELLEY, R. & SALZBERG, S. L. 2013. TopHat2: accurate alignment of transcriptomes in the presence of insertions, deletions and gene fusions. *Genome Biol,* 14**,** R36.

KIM, J. H. & RICHTER, J. D. 2006. Opposing polymerase-deadenylase activities regulate cytoplasmic polyadenylation. *Mol Cell,* 24**,** 173-83.

KINO, Y., WASHIZU, C., KUROSAWA, M., OMA, Y., HATTORI, N., ISHIURA, S. & NUKINA, N. 2015. Nuclear localization of MBNL1: splicing-mediated autoregulation and repression of repeat-derived aberrant proteins. *Hum Mol Genet,* 24**,** 740-56.

KIRKIN, V., MCEWAN, D. G., NOVAK, I. & DIKIC, I. 2009. A role for ubiquitin in selective autophagy. *Mol Cell,* 34**,** 259-69.

KLEIMAN, R., BANKER, G. & STEWARD, O. 1993. Inhibition of protein synthesis alters the subcellular distribution of mRNA in neurons but does not prevent dendritic transport of RNA. *Proc Natl Acad Sci U S A,* 90**,** 11192-6.

KOENIG, E. 1979. Ribosomal RNA in Mauthner axon: implications for a protein synthesizing machinery in the myelinated axon. *Brain Res,* 174**,** 95-107.

KOHRMANN, M., LUO, M., KAETHER, C., DESGROSEILLERS, L., DOTTI, C. G. & KIEBLER, M. A. 1999. Microtubule-dependent recruitment of Staufen-green fluorescent protein into large RNA-containing granules and subsequent dendritic transport in living hippocampal neurons. *Mol Biol Cell,* 10**,** 2945-53.

KOJIMA, S., GENDREAU, K. L., SHER-CHEN, E. L., GAO, P. & GREEN, C. B. 2015. Changes in poly(A) tail length dynamics from the loss of the circadian deadenylase Nocturnin. *Sci Rep,* 5**,** 17059.

KOMATSU, M., WAGURI, S., KOIKE, M., SOU, Y. S., UENO, T., HARA, T., MIZUSHIMA, N., IWATA, J., EZAKI, J., MURATA, S., HAMAZAKI, J., NISHITO, Y., IEMURA, S., NATSUME, T., YANAGAWA, T., UWAYAMA, J., WARABI, E., YOSHIDA, H., ISHII, T., KOBAYASHI, A., YAMAMOTO, M., YUE, Z., UCHIYAMA, Y., KOMINAMI, E. & TANAKA, K. 2007. Homeostatic levels of p62 control cytoplasmic inclusion body formation in autophagy-deficient mice. *Cell,* 131**,** 1149-63.

KRICHEVSKY, A. M. & KOSIK, K. S. 2001. Neuronal RNA granules: a link between RNA localization and stimulation-dependent translation. *Neuron,* 32**,** 683-96.

KRUG, M., LOSSNER, B. & OTT, T. 1984. Anisomycin blocks the late phase of long-term potentiation in the dentate gyrus of freely moving rats. *Brain Res Bull,* 13**,** 39-42.

KWON, C. H., LUIKART, B. W., POWELL, C. M., ZHOU, J., MATHENY, S. A., ZHANG, W., LI, Y., BAKER, S. J. & PARADA, L. F. 2006. Pten regulates neuronal arborization and social interaction in mice. *Neuron,* 50**,** 377-88.

KYE, M. J., LIU, T., LEVY, S. F., XU, N. L., GROVES, B. B., BONNEAU, R., LAO, K. & KOSIK, K. S. 2007. Somatodendritic microRNAs identified by laser capture and multiplex RT-PCR. *RNA,* 13**,** 1224-34.

LABADORF, A. T. & MYERS, R. H. 2015. Evidence of Extensive Alternative Splicing in Post Mortem Human Brain HTT Transcription by mRNA Sequencing. *PLoS One,* 10**,** e0141298.

LAMPHEAR, B. J., KIRCHWEGER, R., SKERN, T. & RHOADS, R. E. 1995. Mapping of functional domains in eukaryotic protein synthesis initiation factor 4G (eIF4G) with picornaviral proteases. Implications for cap-dependent and cap-independent translational initiation. *J Biol Chem,* 270**,** 21975-83.

LANGMEAD, B. & SALZBERG, S. L. 2012. Fast gapped-read alignment with Bowtie 2. *Nat Methods,* 9**,** 357-9.

LAU, N. C., KOLKMAN, A., VAN SCHAIK, F. M., MULDER, K. W., PIJNAPPEL, W. W., HECK, A. J. & TIMMERS, H. T. 2009. Human Ccr4-Not complexes contain variable deadenylase subunits. *Biochem J,* 422**,** 443-53.

LEE H, B. M., KAMEYAMA K, BEAR MF, HUGANIR RL 2000. Regulation of distinct AMPA receptor phosphorylation sites during bidirectional synaptic plasticity. *Nature***,** 955-959.

LEE, H. K., BARBAROSIE, M., KAMEYAMA, K., BEAR, M. F. & HUGANIR, R. L. 2000. Regulation of distinct AMPA receptor phosphorylation sites during bidirectional synaptic plasticity. *Nature,* 405**,** 955-9.

LEE, S. H., KWAK, C., SHIM, J., KIM, J. E., CHOI, S. L., KIM, H. F., JANG, D. J., LEE, J. A., LEE, K., LEE, C. H., LEE, Y. D., MINIACI, M. C., BAILEY, C. H., KANDEL, E. R. & KAANG, B. K. 2012. A cellular model of memory reconsolidation involves reactivation-induced destabilization and restabilization at the sensorimotor synapse in Aplysia. *Proc Natl Acad Sci U S A,* 109**,** 14200-5.

LEVINE, B. & KLIONSKY, D. J. 2004. Development by self-digestion: molecular mechanisms and biological functions of autophagy. *Dev Cell,* 6**,** 463-77.

LI, B. & DEWEY, C. N. 2011. RSEM: accurate transcript quantification from RNA-Seq data with or without a reference genome. *BMC Bioinformatics,* 12**,** 323.

LI, H., HANDSAKER, B., WYSOKER, A., FENNELL, T., RUAN, J., HOMER, N., MARTH, G., ABECASIS, G., DURBIN, R. & GENOME PROJECT DATA PROCESSING, S. 2009. The Sequence Alignment/Map format and SAMtools. *Bioinformatics,* 25**,** 2078-9.

LI, X., LI, Y., LIU, C., JIN, M. & LU, B. 2016. Oocyte-Specific Expression of Mouse MEX3C652AA in the Ovary and Its Potential Role in Regulating Maternal Fos mRNA. *Biol Reprod,* 94**,** 115.

LIM, J., LEE, M., SON, A., CHANG, H. & KIM, V. N. 2016. mTAIL-seq reveals dynamic poly(A) tail regulation in oocyte-to-embryo development. *Genes Dev,* 30**,** 1671-82.

LU, W., MAN, H., JU, W., TRIMBLE, W. S., MACDONALD, J. F. & WANG, Y. T. 2001. Activation of synaptic NMDA receptors induces membrane insertion of new AMPA receptors and LTP in cultured hippocampal neurons. *Neuron,* 29**,** 243-54.

LUGLI, G., LARSON, J., MARTONE, M. E., JONES, Y. & SMALHEISER, N. R. 2005. Dicer and eIF2c are enriched at postsynaptic densities in adult mouse brain and are modified by neuronal activity in a calpain-dependent manner. *J Neurochem,* 94**,** 896-905.

LYKKE-ANDERSEN, J. & WAGNER, E. 2005. Recruitment and activation of mRNA decay enzymes by two ARE-mediated decay activation domains in the proteins TTP and BRF-1. *Genes Dev,* 19**,** 351-61.

MANSUR, F., IVSHINA, M., GU, W., SCHAEVITZ, L., STACKPOLE, E., GUJJA, S., EDWARDS, Y. J. & RICHTER, J. D. 2016. Gld2-catalyzed 3' monoadenylation of miRNAs in the hippocampus has no detectable effect on their stability or on animal behavior. *RNA,* 22**,** 1492-9.

MARTIN, K. C., CASADIO, A., ZHU, H., YAPING, E., ROSE, J. C., CHEN, M., BAILEY, C. H. & KANDEL, E. R. 1997. Synapse-specific, long-term facilitation of aplysia sensory to motor synapses: a function for local protein synthesis in memory storage. *Cell,* 91**,** 927-38.

MARTIN, K. C. & KANDEL, E. R. 1996. Cell adhesion molecules, CREB, and the formation of new synaptic connections. *Neuron,* 17**,** 567-70.

MASUDA, A., ANDERSEN, H. S., DOKTOR, T. K., OKAMOTO, T., ITO, M., ANDRESEN, B. S. & OHNO, K. 2012. CUGBP1 and MBNL1 preferentially bind to 3' UTRs and facilitate mRNA decay. *Sci Rep,* 2**,** 209.

MATHYS, H., BASQUIN, J., OZGUR, S., CZARNOCKI-CIECIURA, M., BONNEAU, F., AARTSE, A., DZIEMBOWSKI, A., NOWOTNY, M., CONTI, E. & FILIPOWICZ, W. 2014. Structural and biochemical insights to the role of the CCR4-NOT complex and DDX6 ATPase in microRNA repression. *Mol Cell,* 54**,** 751-65.

MATSUO, N., REIJMERS, L. & MAYFORD, M. 2008. Spine-type-specific recruitment of newly synthesized AMPA receptors with learning. *Science,* 319**,** 1104-7.

MAUXION, F., PREVE, B. & SERAPHIN, B. 2013. C2ORF29/CNOT11 and CNOT10 form a new module of the CCR4-NOT complex. *RNA Biol,* 10**,** 267-76.

MCGLINCY, N. J. & INGOLIA, N. T. 2017. Transcriptome-wide measurement of translation by ribosome profiling. *Methods*.

MCGREW, L. L., DWORKIN-RASTL, E., DWORKIN, M. B. & RICHTER, J. D. 1989. Poly(A) elongation during Xenopus oocyte maturation is required for translational recruitment and is mediated by a short sequence element. *Genes Dev,* 3**,** 803-15.

MEIKLE, L., POLLIZZI, K., EGNOR, A., KRAMVIS, I., LANE, H., SAHIN, M. & KWIATKOWSKI, D. J. 2008. Response of a neuronal model of tuberous sclerosis to mammalian target of rapamycin (mTOR) inhibitors: effects on mTORC1 and Akt signaling lead to improved survival and function. *J Neurosci,* 28**,** 5422-32.

MENON, K. P., SANYAL, S., HABARA, Y., SANCHEZ, R., WHARTON, R. P., RAMASWAMI, M. & ZINN, K. 2004. The translational repressor Pumilio regulates presynaptic morphology and controls postsynaptic accumulation of translation factor eIF-4E. *Neuron,* 44**,** 663-76.

MERIANDA, T. T., LIN, A. C., LAM, J. S., VUPPALANCHI, D., WILLIS, D. E., KARIN, N., HOLT, C. E. & TWISS, J. L. 2009. A functional equivalent of endoplasmic reticulum and Golgi in axons for secretion of locally synthesized proteins. *Mol Cell Neurosci,* 40**,** 128-42.

MILLER, M. A. & OLIVAS, W. M. 2011. Roles of Puf proteins in mRNA degradation and translation. *Wiley Interdiscip Rev RNA,* 2**,** 471-92.

MILLER, S., YASUDA, M., COATS, J. K., JONES, Y., MARTONE, M. E. & MAYFORD, M. 2002. Disruption of Dendritic Translation of CaMKIIα Impairs Stabilization of Synaptic Plasticity and Memory Consolidation. *Neuron***,** 507-519.

MISHIMA, Y. & TOMARI, Y. 2016. Codon Usage and 3' UTR Length Determine Maternal mRNA Stability in Zebrafish. *Mol Cell,* 61**,** 874-85.

MITSUSHIMA, D., ISHIHARA, K., SANO, A., KESSELS, H. W. & TAKAHASHI, T. 2011. Contextual learning requires synaptic AMPA receptor delivery in the hippocampus. *Proc Natl Acad Sci U S A,* 108**,** 12503-8.

MITTAL, S., ASLAM, A., DOIDGE, R., MEDICA, R. & WINKLER, G. S. 2011. The Ccr4a (CNOT6) and Ccr4b (CNOT6L) deadenylase subunits of the human Ccr4-Not complex contribute to the prevention of cell death and senescence. *Mol Biol Cell,* 22**,** 748-58.

MOTHE-SATNEY, I., YANG, D., FADDEN, P., HAYSTEAD, T. A. & LAWRENCE, J. C., JR. 2000. Multiple mechanisms control phosphorylation of PHAS-I in five (S/T)P sites that govern translational repression. *Mol Cell Biol,* 20**,** 3558-67.

MUNROE, D. & JACOBSON, A. 1990. mRNA poly(A) tail, a 3' enhancer of translational initiation. *Mol Cell Biol,* 10**,** 3441-55.

MYKOWSKA, A., SOBCZAK, K., WOJCIECHOWSKA, M., KOZLOWSKI, P. & KRZYZOSIAK, W. J. 2011. CAG repeats mimic CUG repeats in the misregulation of alternative splicing. *Nucleic Acids Res,* 39**,** 8938-51.

NAGOSHI, E., SUGINO, K., KULA, E., OKAZAKI, E., TACHIBANA, T., NELSON, S. & ROSBASH, M. 2010. Dissecting differential gene expression within the circadian neuronal circuit of Drosophila. *Nat Neurosci,* 13**,** 60-8.

NAKAMURA, Y., GOJOBORI, T. & IKEMURA, T. 2000. Codon usage tabulated from international DNA sequence databases: status for the year 2000. *Nucleic Acids Res,* 28**,** 292.

NEUEDER, A., LANDLES, C., GHOSH, R., HOWLAND, D., MYERS, R. H., FAULL, R. L. M., TABRIZI, S. J. & BATES, G. P. 2017. The pathogenic exon 1 HTT protein is produced by incomplete splicing in Huntington's disease patients. *Sci Rep,* 7**,** 1307.

NOUSCH, M., TECHRITZ, N., HAMPEL, D., MILLONIGG, S. & ECKMANN, C. R. 2013. The Ccr4-Not deadenylase complex constitutes the main poly(A) removal activity in C. elegans. *J Cell Sci,* 126**,** 4274-85.

NOVOA, E. M. & RIBAS DE POUPLANA, L. 2012. Speeding with control: codon usage, tRNAs, and ribosomes. *Trends Genet,* 28**,** 574-81.

O'ROAK, B. J., VIVES, L., FU, W., EGERTSON, J. D., STANAWAY, I. B., PHELPS, I. G., CARVILL, G., KUMAR, A., LEE, C., ANKENMAN, K., MUNSON, J., HIATT, J. B., TURNER, E. H., LEVY, R., O'DAY, D. R., KRUMM, N., COE, B. P., MARTIN, B. K., BORENSTEIN, E., NICKERSON, D. A., MEFFORD, H. C., DOHERTY, D., AKEY, J. M., BERNIER, R., EICHLER, E. E. & SHENDURE, J. 2012. Multiplex targeted sequencing identifies recurrently mutated genes in autism spectrum disorders. *Science,* 338**,** 1619-22.

OGAMI, K., HOSODA, N., FUNAKOSHI, Y. & HOSHINO, S. 2014. Antiproliferative protein Tob directly regulates c-myc proto-oncogene expression through cytoplasmic polyadenylation element-binding protein CPEB. *Oncogene,* 33**,** 55-64.

OSBORNE, R. J. & THORNTON, C. A. 2006. RNA-dominant diseases. *Hum Mol Genet,* 15 Spec No 2**,** R162-9.

OTANI, S., MARSHALL, C. J., TATE, W. P., GODDARD, G. V. & ABRAHAM, W. C. 1989. Maintenance of long-term potentiation in rat dentate gyrus requires protein synthesis but not messenger RNA synthesis immediately post-tetanization. *Neuroscience,* 28**,** 519-26.

PANKIV, S., CLAUSEN, T. H., LAMARK, T., BRECH, A., BRUUN, J. A., OUTZEN, H., OVERVATN, A., BJORKOY, G. & JOHANSEN, T. 2007. p62/SQSTM1 binds directly to Atg8/LC3 to facilitate degradation of ubiquitinated protein aggregates by autophagy. *J Biol Chem,* 282**,** 24131-45.

PARIS, J., SWENSON, K., PIWNICA-WORMS, H. & RICHTER, J. D. 1991. Maturation-specific polyadenylation: in vitro activation by p34cdc2 and phosphorylation of a 58-kD CPE-binding protein. *Genes Dev,* 5**,** 1697-708.

PATIL, A., DYAVAIAH, M., JOSEPH, F., ROONEY, J. P., CHAN, C. T., DEDON, P. C. & BEGLEY, T. J. 2012. Increased tRNA modification and gene-specific codon usage regulate cell cycle progression during the DNA damage response. *Cell Cycle,* 11**,** 3656-65.

PETIT, A. P., WOHLBOLD, L., BAWANKAR, P., HUNTZINGER, E., SCHMIDT, S., IZAURRALDE, E. & WEICHENRIEDER, O. 2012. The structural basis for the interaction between the CAF1 nuclease and the NOT1 scaffold of the human CCR4-NOT deadenylase complex. *Nucleic Acids Res,* 40**,** 11058-72.

PIAO, X., ZHANG, X., WU, L. & BELASCO, J. G. 2010. CCR4-NOT deadenylates mRNA associated with RNA-induced silencing complexes in human cells. *Mol Cell Biol,* 30**,** 1486-94.

PICHARDO-CASAS, I., GOFF, L. A., SWERDEL, M. R., ATHIE, A., DAVILA, J., RAMOS-BROSSIER, M., LAPID-VOLOSIN, M., FRIEDMAN, W. J., HART, R. P. & VACA, L. 2012. Expression profiling of synaptic microRNAs from the adult rat brain identifies regional differences and seizure-induced dynamic modulation. *Brain Res,* 1436**,** 20-33.

PIERETTI, M., ZHANG, F. P., FU, Y. H., WARREN, S. T., OOSTRA, B. A., CASKEY, C. T. & NELSON, D. L. 1991. Absence of expression of the FMR-1 gene in fragile X syndrome. *Cell,* 66**,** 817-22.

PLOTKIN, J. B. & KUDLA, G. 2011. Synonymous but not the same: the causes and consequences of codon bias. *Nat Rev Genet,* 12**,** 32-42.

POON, M. M., CHOI, S. H., JAMIESON, C. A., GESCHWIND, D. H. & MARTIN, K. C. 2006. Identification of process-localized mRNAs from cultured rodent hippocampal neurons. *J Neurosci,* 26**,** 13390-9.

PREISS, T. & M, W. H. 2003. Starting the protein synthesis machine: eukaryotic translation initiation. *Bioessays,* 25**,** 1201-11.

PRESNYAK, V., ALHUSAINI, N., CHEN, Y. H., MARTIN, S., MORRIS, N., KLINE, N., OLSON, S., WEINBERG, D., BAKER, K. E., GRAVELEY, B. R. & COLLER, J. 2015. Codon optimality is a major determinant of mRNA stability. *Cell,* 160**,** 1111-24.

PUIGBO, P., BRAVO, I. G. & GARCIA-VALLVE, S. 2008. CAIcal: a combined set of tools to assess codon usage adaptation. *Biol Direct,* 3**,** 38.

QIN, M., KANG, J., BURLIN, T. V., JIANG, C. & SMITH, C. B. 2005. Postadolescent changes in regional cerebral protein synthesis: an in vivo study in the FMR1 null mouse. *J Neurosci,* 25**,** 5087-95.

QUEVEDO, J., VIANNA, M. R., ROESLER, R., DE-PARIS, F., IZQUIERDO, I. & ROSE, S. P. 1999. Two time windows of anisomycin-induced amnesia for inhibitory avoidance training in rats: protection from amnesia by pretraining but not pre-exposure to the task apparatus. *Learn Mem,* 6**,** 600-7.

R CORE TEAM 2016. R: A language and environment for statistical computing. R

Foundation for Statistical Computing. Vienna, Austria: R Foundation for Statistical Computing.

RADHAKRISHNAN, A., CHEN, Y. H., MARTIN, S., ALHUSAINI, N., GREEN, R. & COLLER, J. 2016. The DEAD-Box Protein Dhh1p Couples mRNA Decay and Translation by Monitoring Codon Optimality. *Cell,* 167**,** 122-132 e9.

RAISCH, T., BHANDARI, D., SABATH, K., HELMS, S., VALKOV, E., WEICHENRIEDER, O. & IZAURRALDE, E. 2016. Distinct modes of recruitment of the CCR4-NOT complex by Drosophila and vertebrate Nanos. *EMBO J,* 35**,** 974-90.

RAJASETHUPATHY, P., FIUMARA, F., SHERIDAN, R., BETEL, D., PUTHANVEETTIL, S. V., RUSSO, J. J., SANDER, C., TUSCHL, T. & KANDEL, E. 2009. Characterization of small RNAs in Aplysia reveals a role for miR-124 in constraining synaptic plasticity through CREB. *Neuron,* 63**,** 803-17.

RAY, D., KAZAN, H., COOK, K. B., WEIRAUCH, M. T., NAJAFABADI, H. S., LI, X., GUEROUSSOV, S., ALBU, M., ZHENG, H., YANG, A., NA, H., IRIMIA, M., MATZAT, L. H., DALE, R. K., SMITH, S. A., YAROSH, C. A., KELLY, S. M., NABET, B., MECENAS, D., LI, W., LAISHRAM, R. S., QIAO, M., LIPSHITZ, H. D., PIANO, F., CORBETT, A. H., CARSTENS, R. P., FREY, B. J., ANDERSON, R. A., LYNCH, K. W., PENALVA, L. O., LEI, E. P., FRASER, A. G., BLENCOWE, B. J., MORRIS, Q. D. & HUGHES, T. R. 2013. A compendium of RNA-binding motifs for decoding gene regulation. *Nature,* 499**,** 172-7.

REILMANN, R., LEAVITT, B. R. & ROSS, C. A. 2014. Diagnostic criteria for Huntington's disease based on natural history. *Mov Disord,* 29**,** 1335-41.

REISBERG, B., FERRIS, S. H., DE LEON, M. J. & CROOK, T. 1982. The Global Deterioration Scale for assessment of primary degenerative dementia. *Am J Psychiatry,* 139**,** 1136-9.

RESTIVO, L., FERRARI, F., PASSINO, E., SGOBIO, C., BOCK, J., OOSTRA, B. A., BAGNI, C. & AMMASSARI-TEULE, M. 2005. Enriched environment promotes behavioral and morphological recovery in a mouse model for the fragile X syndrome. *Proc Natl Acad Sci U S A,* 102**,** 11557-62.

RICHTER, J. D. 2007. CPEB: a life in translation. *Trends Biochem Sci,* 32**,** 279-85.

RICHTER, J. D. C. J. 2015. Pausing on Polyribosomes: Make Way for Elongation in Translational Control. *Cell,* 163**,** 8.

RODRIGUEZ-GIL, A., RITTER, O., SAUL, V. V., WILHELM, J., YANG, C. Y., GROSSCHEDL, R., IMAI, Y., KUBA, K., KRACHT, M. & SCHMITZ, M. L. 2017. The CCR4-NOT complex contributes to repression of Major Histocompatibility Complex class II transcription. *Sci Rep,* 7**,** 3547.

ROSSATO, J. I., BEVILAQUA, L. R., MYSKIW, J. C., MEDINA, J. H., IZQUIERDO, I. & CAMMAROTA, M. 2007. On the role of hippocampal protein synthesis in the consolidation and reconsolidation of object recognition memory. *Learn Mem,* 14**,** 36-46.

SALINAS, T., DUBY, F., LAROSA, V., COOSEMANS, N., BONNEFOY, N., MOTTE, P., MARECHAL-DROUARD, L. & REMACLE, C. 2012. Co-evolution of mitochondrial tRNA import and codon usage determines translational efficiency in the green alga Chlamydomonas. *PLoS Genet,* 8**,** e1002946.

SAMBANDAN, S., AKBALIK, G., KOCHEN, L., RINNE, J., KAHLSTATT, J., GLOCK, C., TUSHEV, G., ALVAREZ-CASTELAO, B., HECKEL, A. & SCHUMAN, E. M. 2017. Activity-dependent spatially localized miRNA maturation in neuronal dendrites. *Science,* 355**,** 634-637.

SARKISSIAN, M., MENDEZ, R. & RICHTER, J. D. 2004. Progesterone and insulin stimulation of CPEB-dependent polyadenylation is regulated by Aurora A and glycogen synthase kinase-3. *Genes Dev,* 18**,** 48-61.

SCHAEFFER, C., BARDONI, B., MANDEL, J. L., EHRESMANN, B., EHRESMANN, C. & MOINE, H. 2001. The fragile X mental retardation protein binds specifically to its mRNA via a purine quartet motif. *EMBO J,* 20**,** 4803-13.

SCHANZENBACHER, C. T., SAMBANDAN, S., LANGER, J. D. & SCHUMAN, E. M. 2016. Nascent Proteome Remodeling following Homeostatic Scaling at Hippocampal Synapses. *Neuron,* 92**,** 358-371.

SCHNEIDER, C. A., RASBAND, W. S. & ELICEIRI, K. W. 2012. NIH Image to ImageJ: 25 years of image analysis. *Nat Methods,* 9**,** 671-5.

SCHRATT, G. 2009. microRNAs at the synapse. *Nat Rev Neurosci,* 10**,** 842-9.

SCHWEDE, A., ELLIS, L., LUTHER, J., CARRINGTON, M., STOECKLIN, G. & CLAYTON, C. 2008. A role for Caf1 in mRNA deadenylation and decay in trypanosomes and human cells. *Nucleic Acids Res,* 36**,** 3374-88.

SCOVILLE, W. B. & MILNER, B. 1957. Loss of recent memory after bilateral hippocampal lesions. *J Neurol Neurosurg Psychiatry,* 20**,** 11-21.

SETTEMBRE, C., FRALDI, A., RUBINSZTEIN, D. C. & BALLABIO, A. 2008. Lysosomal storage diseases as disorders of autophagy. *Autophagy,* 4**,** 113-4.

SHEETS, M. D. & WICKENS, M. 1989. Two phases in the addition of a poly(A) tail. *Genes Dev,* 3**,** 1401-12.

SHEN, W. & GANETZKY, B. 2009. Autophagy promotes synapse development in Drosophila. *J Cell Biol,* 187**,** 71-9.

SHIN, J., PAEK, K. Y., IVSHINA, M., STACKPOLE, E. E. & RICHTER, J. D. 2017. Essential role for non-canonical poly(A) polymerase GLD4 in cytoplasmic polyadenylation and carbohydrate metabolism. *Nucleic Acids Res*.

SHYU, A. B., BELASCO, J. G. & GREENBERG, M. E. 1991. Two distinct destabilizing elements in the c-fos message trigger deadenylation as a first step in rapid mRNA decay. *Genes Dev,* 5**,** 221-31.

SIEMEN, H., COLAS, D., HELLER, H. C., BRUSTLE, O. & PERA, R. A. 2011. Pumilio-2 function in the mouse nervous system. *PLoS One,* 6**,** e25932.

STANTON, P. K. & SARVEY, J. M. 1984. Blockade of long-term potentiation in rat hippocampal CA1 region by inhibitors of protein synthesis. *J Neurosci,* 4**,** 3080-8.

STEWARD, O., BAKKER, C. E., WILLEMS, P. J. & OOSTRA, B. A. 1998. No evidence for disruption of normal patterns of mRNA localization in dendrites or dendritic transport of recently synthesized mRNA in FMR1 knockout mice, a model for human fragile-X mental retardation syndrome. *Neuroreport,* 9**,** 477-81.

STEWARD, O. & LEVY, W. B. 1982. Preferential localization of polyribosomes under the base of dendritic spines in granule cells of the dentate gyrus. *J Neurosci,* 2**,** 284-91.

STEWARD, O. & RIBAK, C. E. 1986. Polyribosomes associated with synaptic specializations on axon initial segments: localization of protein-synthetic machinery at inhibitory synapses. *J Neurosci,* 6**,** 3079-85.

STUPFLER, B., BIRCK, C., SERAPHIN, B. & MAUXION, F. 2016. BTG2 bridges PABPC1 RNA-binding domains and CAF1 deadenylase to control cell proliferation. *Nat Commun,* 7**,** 10811.

SUBTELNY, A. O., EICHHORN, S. W., CHEN, G. R., SIVE, H. & BARTEL, D. P. 2014. Poly(A)-tail profiling reveals an embryonic switch in translational control. *Nature,* 508**,** 66-71.

SUN, X., LI, P. P., ZHU, S., COHEN, R., MARQUE, L. O., ROSS, C. A., PULST, S. M., CHAN, H. Y., MARGOLIS, R. L. & RUDNICKI, D. D. 2015. Nuclear retention of full-length HTT RNA is mediated by splicing factors MBNL1 and U2AF65. *Sci Rep,* 5**,** 12521.

SUTTON, M. A. & SCHUMAN, E. M. 2006a. Dendritic Protein Synthesis, Synaptic Plasticity, and Memory. *Cell***,** 49-58.

SUTTON, M. A. & SCHUMAN, E. M. 2006b. Dendritic protein synthesis, synaptic plasticity, and memory. *Cell,* 127**,** 49-58.

SUTTON, M. A., TAYLOR, A. M., ITO, H. T., PHAM, A. & SCHUMAN, E. M. 2007. Postsynaptic decoding of neural activity: eEF2 as a biochemical sensor coupling miniature synaptic transmission to local protein synthesis. *Neuron,* 55**,** 648-61.

SUZUKI, A., SABA, R., MIYOSHI, K., MORITA, Y. & SAGA, Y. 2012. Interaction between NANOS2 and the CCR4-NOT deadenylation complex is essential for male germ cell development in mouse. *PLoS One,* 7**,** e33558.

SUZUKI, T., KIKUGUCHI, C., SHARMA, S., SASAKI, T., TOKUMASU, M., ADACHI, S., NATSUME, T., KANEGAE, Y. & YAMAMOTO, T. 2015. CNOT3 suppression promotes necroptosis by stabilizing mRNAs for cell death-inducing proteins. *Sci Rep,* 5**,** 14779.

SWANGER, S. A., BASSELL, G. J. & GROSS, C. 2011. High-Resolution Fluorescence In Situ Hybridization to Detect mRNAs In Neuronal Compartments In Vitro and In Vivo. *Methods Molecular Biology***,** 103-23.

TAI, H. C. & SCHUMAN, E. M. 2008. Ubiquitin, the proteasome and protein degradation in neuronal function and dysfunction. *Nat Rev Neurosci,* 9**,** 826-38.

TAKAHASHI, A., KIKUGUCHI, C., MORITA, M., SHIMODAIRA, T., TOKAI-NISHIZUMI, N., YOKOYAMA, K., OHSUGI, M., SUZUKI, T. & YAMAMOTO, T. 2012. Involvement of CNOT3 in mitotic progression through inhibition of MAD1 expression. *Biochem Biophys Res Commun,* 419**,** 268-73.

TALIAFERRO, J. M., VIDAKI, M., OLIVEIRA, R., OLSON, S., ZHAN, L., SAXENA, T., WANG, E. T., GRAVELEY, B. R., GERTLER, F. B., SWANSON, M. S. & BURGE, C. B. 2016. Distal Alternative Last Exons Localize mRNAs to Neural Projections. *Mol Cell,* 61**,** 821-33.

TARUN, S. Z., JR. & SACHS, A. B. 1995. A common function for mRNA 5' and 3' ends in translation initiation in yeast. *Genes Dev,* 9**,** 2997-3007.

TEMME, C., ZAESSINGER, S., MEYER, S., SIMONELIG, M. & WAHLE, E. 2004. A complex containing the CCR4 and CAF1 proteins is involved in mRNA deadenylation in Drosophila. *EMBO J,* 23**,** 2862-71.

TEMME, C., ZHANG, L., KREMMER, E., IHLING, C., CHARTIER, A., SINZ, A., SIMONELIG, M. & WAHLE, E. 2010. Subunits of the Drosophila CCR4-NOT complex and their roles in mRNA deadenylation. *RNA,* 16**,** 1356-70.

TIEDGE, H. & BROSIUS, J. 1996. Translational machinery in dendrites of hippocampal neurons in culture. *J Neurosci,* 16**,** 7171-81.

TORRES, A. G., BATLLE, E. & RIBAS DE POUPLANA, L. 2014. Role of tRNA modifications in human diseases. *Trends Mol Med,* 20**,** 306-14.

TUCKER, M., VALENCIA-SANCHEZ, M. A., STAPLES, R. R., CHEN, J., DENIS, C. L. & PARKER, R. 2001. The transcription factor associated Ccr4 and Caf1 proteins are components of the major cytoplasmic mRNA deadenylase in Saccharomyces cerevisiae. *Cell,* 104**,** 377-86.

UDAGAWA, T., FARNY, N. G., JAKOVCEVSKI, M., KAPHZAN, H., ALARCON, J. M., ANILKUMAR, S., IVSHINA, M., HURT, J. A., NAGAOKA, K., NALAVADI, V. C., LORENZ, L. J., BASSELL, G. J., AKBARIAN, S., CHATTARJI, S., KLANN, E. & RICHTER, J. D. 2013. Genetic and acute CPEB1 depletion ameliorate fragile X pathophysiology. *Nat Med,* 19**,** 1473-7.

UDAGAWA, T., FUJIOKA, Y., TANAKA, M., HONDA, D., YOKOI, S., RIKU, Y., IBI, D., NAGAI, T., YAMADA, K., WATANABE, H., KATSUNO, M., INADA, T., OHNO, K., SOKABE, M., OKADO,

H., ISHIGAKI, S. & SOBUE, G. 2015. FUS regulates AMPA receptor function and FTLD/ALS-associated behaviour via GluA1 mRNA stabilization. *Nat Commun,* 6**,** 7098.

UDAGAWA, T., SWANGER, S. A., TAKEUCHI, K., KIM, J. H., NALAVADI, V., SHIN, J., LORENZ, L. J., ZUKIN, R. S., BASSELL, G. J. & RICHTER, J. D. 2012. Bidirectional control of mRNA translation and synaptic plasticity by the cytoplasmic polyadenylation complex. *Mol Cell,* 47**,** 253-66.

VAN ETTEN, J., SCHAGAT, T. L., HRIT, J., WEIDMANN, C. A., BRUMBAUGH, J., COON, J. J. & GOLDSTROHM, A. C. 2012. Human Pumilio proteins recruit multiple deadenylases to efficiently repress messenger RNAs. *J Biol Chem,* 287**,** 36370-83.

VERKERK, A. J., PIERETTI, M., SUTCLIFFE, J. S., FU, Y. H., KUHL, D. P., PIZZUTI, A., REINER, O., RICHARDS, S., VICTORIA, M. F., ZHANG, F. P. & ET AL. 1991. Identification of a gene (FMR-1) containing a CGG repeat coincident with a breakpoint cluster region exhibiting length variation in fragile X syndrome. *Cell,* 65**,** 905-14.

VESSEY, J. P., SCHODERBOECK, L., GINGL, E., LUZI, E., RIEFLER, J., DI LEVA, F., KARRA, D., THOMAS, S., KIEBLER, M. A. & MACCHI, P. 2010. Mammalian Pumilio 2 regulates dendrite morphogenesis and synaptic function. *Proc Natl Acad Sci U S A,* 107**,** 3222-7.

VETERE, G., BARBATO, C., PEZZOLA, S., FRISONE, P., ACETI, M., CIOTTI, M., COGONI, C., AMMASSARI-TEULE, M. & RUBERTI, F. 2014. Selective inhibition of miR-92 in hippocampal neurons alters contextual fear memory. *Hippocampus,* 24**,** 1458-65.

VISWANATHAN, P., OHN, T., CHIANG, Y. C., CHEN, J. & DENIS, C. L. 2004. Mouse CAF1 can function as a processive deadenylase/3'-5'-exonuclease in vitro but in yeast the deadenylase function of CAF1 is not required for mRNA poly(A) removal. *J Biol Chem,* 279**,** 23988-95.

WAGNER, E., CLEMENT, S. L. & LYKKE-ANDERSEN, J. 2007. An unconventional human Ccr4-Caf1 deadenylase complex in nuclear cajal bodies. *Mol Cell Biol,* 27**,** 1686-95.

WANG, E. T., CODY, N. A., JOG, S., BIANCOLELLA, M., WANG, T. T., TREACY, D. J., LUO, S., SCHROTH, G. P., HOUSMAN, D. E., REDDY, S., LECUYER, E. & BURGE, C. B. 2012. Transcriptome-wide regulation of pre-mRNA splicing and mRNA localization by muscleblind proteins. *Cell,* 150**,** 710-24.

WANG, E. T., WARD, A. J., CHERONE, J. M., GIUDICE, J., WANG, T. T., TREACY, D. J., LAMBERT, N. J., FREESE, P., SAXENA, T., COOPER, T. A. & BURGE, C. B. 2015. Antagonistic regulation of mRNA expression and splicing by CELF and MBNL proteins. *Genome Res,* 25**,** 858-71.

WANG, P. Y., LIN, Y. M., WANG, L. H., KUO, T. Y., CHENG, S. J. & WANG, G. S. 2017. Reduced cytoplasmic MBNL1 is an early event in a brain-specific mouse model of myotonic dystrophy. *Hum Mol Genet,* 26**,** 2247-2257.

WANG, X., MCLACHLAN, J., ZAMORE, P. D. & HALL, T. M. 2002. Modular recognition of RNA by a human pumilio-homology domain. *Cell,* 110**,** 501-12.

WANISCH, K., TANG, J., MEDERER, A. & WOTJAK, C. T. 2005. Trace fear conditioning depends on NMDA receptor activation and protein synthesis within the dorsal hippocampus of mice. *Behav Brain Res,* 157**,** 63-9.

WEILL, L., BELLOC, E., BAVA, F. A. & MENDEZ, R. 2012. Translational control by changes in poly(A) tail length: recycling mRNAs. *Nat Struct Mol Biol,* 19**,** 577-85.

WEINBERG, D. E., SHAH, P., EICHHORN, S. W., HUSSMANN, J. A., PLOTKIN, J. B. & BARTEL, D. P. 2016. Improved Ribosome-Footprint and mRNA Measurements Provide Insights into Dynamics and Regulation of Yeast Translation. *Cell Rep,* 14**,** 1787-99.

WELLS, S. E., HILLNER, P. E., VALE, R. D. & SACHS, A. B. 1998. Circularization of mRNA by eukaryotic translation initiation factors. *Mol Cell,* 2**,** 135-40.

WHITLOCK, J. R., HEYNEN, A. J., SHULER, M. G. & BEAR, M. F. 2006. Learning induces long-term potentiation in the hippocampus. *Science,* 313**,** 1093-7.

WREDEN, C., VERROTTI, A. C., SCHISA, J. A., LIEBERFARB, M. E. & STRICKLAND, S. 1997. Nanos and pumilio establish embryonic polarity in Drosophila by promoting posterior deadenylation of hunchback mRNA. *Development,* 124**,** 3015-23.

WU, B., ELISCOVICH, C., YOON, Y. J. & SINGER, R. H. 2016. Translation dynamics of single mRNAs in live cells and neurons. *Science,* 352**,** 1430-5.

WU, L., WELLS, D., TAY, J., MENDIS, D., ABBOTT, M. A., BARNITT, A., QUINLAN, E., HEYNEN, A., FALLON, J. R. & RICHTER, J. D. 1998. CPEB-mediated cytoplasmic polyadenylation and the regulation of experience-dependent translation of alpha-CaMKII mRNA at synapses. *Neuron,* 21**,** 1129-39.

XIE, Z. & KLIONSKY, D. J. 2007. Autophagosome formation: core machinery and adaptations. *Nat Cell Biol,* 9**,** 1102-9.

YAMASHITA, A., CHANG, T. C., YAMASHITA, Y., ZHU, W., ZHONG, Z., CHEN, C. Y. & SHYU, A. B. 2005. Concerted action of poly(A) nucleases and decapping enzyme in mammalian mRNA turnover. *Nat Struct Mol Biol,* 12**,** 1054-63.

YAN, Y. B. 2014. Deadenylation: enzymes, regulation, and functional implications. *Wiley Interdiscip Rev RNA,* 5**,** 421-43.

YE, B., PETRITSCH, C., CLARK, I. E., GAVIS, E. R., JAN, L. Y. & JAN, Y. N. 2004. Nanos and Pumilio are essential for dendrite morphogenesis in Drosophila peripheral neurons. *Curr Biol,* 14**,** 314-21.

YU, C. H., DANG, Y., ZHOU, Z., WU, C., ZHAO, F., SACHS, M. S. & LIU, Y. 2015. Codon Usage Influences the Local Rate of Translation Elongation to Regulate Co-translational Protein Folding. *Mol Cell,* 59**,** 744-54.

YUEN, E. Y., JIANG, Q., FENG, J. & YAN, Z. 2005. Microtubule regulation of N-methyl-D-aspartate receptor channels in neurons. *J Biol Chem,* 280**,** 29420-7.

ZALFA, F., GIORGI, M., PRIMERANO, B., MORO, A., DI PENTA, A., REIS, S., OOSTRA, B. & BAGNI, C. 2003. The fragile X syndrome protein FMRP associates with BC1 RNA and regulates the translation of specific mRNAs at synapses. *Cell,* 112**,** 317-27.

ZEARFOSS, N. R., ALARCON, J. M., TRIFILIEFF, P., KANDEL, E. & RICHTER, J. D. 2008. A molecular circuit composed of CPEB-1 and c-Jun controls growth hormone-mediated synaptic plasticity in the mouse hippocampus. *J Neurosci,* 28**,** 8502-9.

ZEKRI, L., KUZUOGLU-OZTURK, D. & IZAURRALDE, E. 2013. GW182 proteins cause PABP dissociation from silenced miRNA targets in the absence of deadenylation. *EMBO J,* 32**,** 1052-65.

ZHANG, B., KIROV, S. & SNODDY, J. 2005. WebGestalt: an integrated system for exploring gene sets in various biological contexts. *Nucleic Acids Res,* 33**,** W741-8.

ZHENG, D., EZZEDDINE, N., CHEN, C. Y., ZHU, W., HE, X. & SHYU, A. B. 2008. Deadenylation is prerequisite for P-body formation and mRNA decay in mammalian cells. *J Cell Biol,* 182**,** 89-101.

ZHENG, X., DUMITRU, R., LACKFORD, B. L., FREUDENBERG, J. M., SINGH, A. P., ARCHER, T. K., JOTHI, R. & HU, G. 2012. Cnot1, Cnot2, and Cnot3 maintain mouse and human ESC identity and inhibit extraembryonic differentiation. *Stem Cells,* 30**,** 910-22.

ZHENG, X., YANG, P., LACKFORD, B., BENNETT, B. D., WANG, L., LI, H., WANG, Y., MIAO, Y., FOLEY, J. F., FARGO, D. C., JIN, Y., WILLIAMS, C. J., JOTHI, R. & HU, G. 2016. CNOT3-Dependent mRNA Deadenylation Safeguards the Pluripotent State. *Stem Cell Reports,* 7**,** 897-910.

ZHOU, B., LIU, J., REN, Z., YAO, F., MA, J., SONG, J., BENNETT, B., ZHEN, Y., WANG, L., HU, G. & HU, S. 2017. Cnot3 enhances human embryonic cardiomyocyte proliferation by promoting cell cycle inhibitor mRNA degradation. *Sci Rep,* 7**,** 1500.

ZHOU, J., BLUNDELL, J., OGAWA, S., KWON, C. H., ZHANG, W., SINTON, C., POWELL, C. M. & PARADA, L. F. 2009a. Pharmacological inhibition of mTORC1 suppresses anatomical, cellular, and behavioral abnormalities in neural-specific Pten knock-out mice. *J Neurosci,* 29**,** 1773-83.

ZHOU, T., WEEMS, M. & WILKE, C. O. 2009b. Translationally optimal codons associate with structurally sensitive sites in proteins. *Mol Biol Evol,* 26**,** 1571-80.

ZORI, R. T., MARSH, D. J., GRAHAM, G. E., MARLISS, E. B. & ENG, C. 1998. Germline PTEN mutation in a family with Cowden syndrome and Bannayan-Riley-Ruvalcaba syndrome. *Am J Med Genet,* 80**,** 399-402.

ZWARTJES, C. G., JAYNE, S., VAN DEN BERG, D. L. & TIMMERS, H. T. 2004. Repression of promoter activity by CNOT2, a subunit of the transcription regulatory Ccr4-not complex. *J Biol Chem,* 279**,** 10848-54.